

Computational Model for Anatomical and Flow Characteristic Analysis for Arteriovenous Fistulae

By

Samuel Thomas Dunn

Copyright © Samuel Thomas Dunn 2023

A Thesis Submitted to the Faculty of the

DEPARTMENT OF MECHANICAL ENGINEERING

In Partial Fulfillment of the Requirements

For the Degree of

MASTER OF SCIENCE

In the Graduate College

THE UNIVERSITY OF ARIZONA

2023

THE UNIVERSITY OF ARIZONA
GRADUATE COLLEGE

As members of the Master’s Committee, we certify that we have read the thesis prepared by: Samuel Thomas Dunn

titled: Computational Model for Anatomical and Flow Characteristic Analysis for Arteriovenous Fistulae

and recommend that it be accepted as fulfilling the thesis requirement for the Master’s Degree.

Kaveh Laksari

Kaveh Laksari

Date: May 5, 2023

Kyle Hanquist

Kyle Hanquist

Date: May 5, 2023

Eniko T Enikov

Eniko T Enikov (May 5, 2023 17:12 PDT)

Eniko T Enikov

Date: May 5, 2023

Final approval and acceptance of this thesis is contingent upon the candidate’s submission of the final copies of the thesis to the Graduate College.

I hereby certify that I have read this thesis prepared under my direction and recommend that it be accepted as fulfilling the Master’s requirement.

Kaveh Laksari

Kaveh Laksari

Thesis committee chair

Dept of Biomedical Eng, Dept Aerospace and Mechanical Eng

Date: May 5, 2023

Signature: Samuel Thomas Dunn

Samuel Thomas Dunn (May 4, 2023 20:00 PDT)

Email: samueldunn@arizona.edu

Acknowledgements:

I would like to thank the following people for their support over the course of this research and the program:

My wife Hailey, who has provided so much support and I appreciate everything you have done over the past 5 years to help make this happen.

My family who are always there for me and who provided great encouragement.

Dr. Tubaldi, who helped guide me through this process and help with this project for the past 5 years, even after joining another University. Also, Rohit and Jose for their contributions to the research.

My multiple managers, Stephanie and Danilo, that helped accommodate my work schedule and my academic pursuits.

Dr. Laksari, Dr. Hanquist, and Dr. Enikov for their flexibility and guidance through this process.

The AME Department, Staff and students, who I have had the pleasure of working through classes with.

Thank you all for the support over the years.

Contents

List of Figures:	5
List of Tables:	7
Abstract	8
Introduction	9
1. Chapter 1: Background/Current Field	11
1.1 Vascular Access Procedures	11
1.2 Arteriovenous Fistulas Flow Characteristics and Theory	19
2. Chapter 2: Imaging and Segmentation	32
2.1 Magnetic Resonance Imaging (MRI):	32
2.2 Published Manuscript:	34
3. Chapter 3: Computational Fluid Dynamics (CFD) of Arteriovenous Fistula	55
3.1 Introduction	55
3.2 Methods	57
3.3 Results	61
4. Chapter 4: Conclusion	72
4.1 Conclusions	72
4.2 Limitations and Future Work.....	74
5. Appendix:	76
6. References	93

List of Figures:

1. Figure 1: Diagram of the three forms of Hemodialysis	11
2. Figure 2: Example AV Fistula and Diagram of the fistula Components	13
3. Figure 3: Example of stenosis occurring in a Fistula.	14
4. Figure 4: Diagram of general Cardiovascular System	16
5. Figure 5: Diagram of fistula blood flow	20
6. Figure 6: Example of MRI image of the Femoral Artery and the Femoral Vein in a Yorkshire Pig	22
7. Figure 7: Example of the Volumetric Flow Rate of Fistula in a Yorkshire Pig	24
8. Figure 8: Velocity streamlines of a fistula	25
9. Figure E1: Example of Range of Yorkshire Pig Flow Rates	26
10. Figure E1: Example of WSS values	27
11. Figure 10: Example of various fistula configuration at different angles	28
12. Figure 11: Example of curved and straight fistula configurations	29
13. Fig. 2. Fistula analysis flowchart	38
14. Fig. 3. Selection of control points and regions divided by arterial analysis	41
15. Fig. 4. Steps to generate cross-sectional area	42
16. Fig. 5. Acquiring cross-sectional area from 3D models.	46
17. Fig. 6. Representation of venous cross-sectional area plotted with respect to the distance from anastomosis and correlation between proximal arterial CSA and minimum venous CSA	47
18. Fig. 7. Reconstructed 3D models of the fistulae	49
19. Figure 11: Depiction of vein subregions and the direction of blood flow	58
20. Figure 12: Fistula Flow Rates	61
21. Figure 13: A) Fistula Case 1 with Velocity Streamlines at Day 3 and Day 28	62
22. Figure 14: Hemodynamic Parameters at Day 3	65
23. Figure 15: Δ CSA vs Average OSI and the OSI of the internal Subregion	69
24. Figure A.1 Alternative Streamline angle for Case 1 Fistula at Day 3	76
25. A.2 Alternate Zoomed view of velocity streamlines for Case 1 at Day 3	77
26. Figure A.3 Alternative Streamline angle for Case 1 Fistula at Day 28.	77
27. Figure A.4 Alternative Streamline angle for Case 2 Fistula at Day 3	78
28. Figure A.5 Alternative Streamline angle for Case 2 Fistula at Day 28	78
29. Figure A.6 Alternative Streamline angle for Case 3 Fistula at Day 3	79

30. Figure A.7 Alternative Streamline angle for Case 3 Fistula at Day 28	79
31. Figure A.8 WSS Case 1 Fistula at Day 28	80
32. Figure A.9 WSS Case 2 Fistula at Day 28	81
33. Figure A.10 WSSG vs Δ CSA Case 1 Fistula at Day 3	81
34. Figure A.11 WSS vs Δ CSA Case 1 Fistula at Day 3	82
35. Figure A.12 WSSG vs Δ CSA Case 2 Fistula at Day 3	82
36. Figure A.13 WSS vs Δ CSA Case 2 Fistula at Day 3	83
37. Figure A.14 WSSG vs Δ CSA Case 3 Fistula at Day 3	83
38. Figure A.15 WSS vs Δ CSA Case 3 Fistula at Day 3	84
39. A.16 Larger View of Case 1 Fistula	84
40. A.17 Larger View of Case 2 Fistula	85
41. A.18 Larger View of Case 3 Fistula Hemodynamic Parameters	85
42. Figure A.19 WSS Heatmap Case 1 Fistula at Day 3	86
43. Figure A.20 OSI Heatmap Case 1 Fistula at Day 3	86
44. Figure A.21 WSS Heatmap Case 1 Fistula at Day 28	87
45. Figure A.22 OSI Heatmap Case 1 Fistula at Day 28	87
46. Figure A.23 WSS Heatmap Case 2 Fistula at Day 3	88
47. Figure A.24 OSI Heatmap Case 2 Fistula at Day 3	88
48. Figure A.25 WSS Heatmap Case 2 Fistula at Day 28	89
49. Figure A.26 OSI Heatmap Case 2 Fistula at Day 28	89
50. Figure A.27 WSS Heatmap Case 3 Fistula at Day 3	90
51. Figure A.28 OSI Heatmap Case 3 Fistula at Day 3	90
52. Figure A.29 WSS Heatmap Case 3 Fistula at Day 28	91
53. Figure A.30 OSI Heatmap Case 3 Fistula at Day 28	92

List of Tables:

1. Table 1. Contrast-free MRI protocol on Yorkshire cross cohort.	39
2. Table 2. Weight and MRI-derived venous functional parameters for each swine.	47
3. Table 3. Mean cross-sectional area from various AVF regions.	48
4. Table 4. Cross-sectional area and weight range relationship of non-fistulae artery.	48
5. Table 5: Fistula Data	60

Abstract

Currently, arteriovenous fistulas (typically the attachment of the radial artery to the cephalic vein and termed AVF) are the most common form of vascular access for patients enduring end-stage renal failure undergoing hemodialysis. Plagued with high failure rates, the root causes of the primary failure mode, stenosis, are still unknown. The purpose of this thesis is to (i) investigate and potentially identify hemodynamic parameters that may contribute to the onset and progression of stenosis and (ii) determine surgical configurations to promote fistula maturation in patients.

Here, a numerical method has been developed to noninvasively analyze the geometric fistula and flow parameters and, in turn, to improve the understanding of the underlying mechanisms behind fistula stenosis. This approach involves the use of non-contrast magnetic resonance (MR) imaging to generate 3D fistula models and perform computational fluid dynamic (CFD) analyses to analyze fistula hemodynamic parameters 3 days post-operation and the subsequent impact on Cross-Sectional Area (CSA) at 28 days post-operation. This study was performed on 3 fistulas created in 2 Yorkshire cross domestic swine. The vein CSA was divided into four subregions to examine how hemodynamic flow parameters vary across the same cross section.

Based on our findings, high levels of oscillatory shear index (OSI) at day 3 suggests a great risk of CSA reduction. The hemodynamic profiles vary based on the angle of attachment of the fistulas and the curvature of the vein.

The angle of attachment of the AVF and the curvature impact the uniformity of the low, Flow profiles that reduce blood recirculation in the vein and create a uniform velocity promote factors that lead to maturation, though more fistulas need to be analyzed to establish direct relationships. Characterizing the hemodynamic profiles of a several fistulas configurations could aid in the determination of factors that drive stenosis and allow for the creation of risk categories. This approach could eventually lead to higher fistula maturation rates and allow for early stratification of patient risk to enhance patient treatment.

Introduction

The kidney is an organ in the body responsible for multiple functions, such as blood filtration with the production of urine, hormone secretion and blood pressure regulation, and the regulating of the body's osmolality. The kidney filters toxins out of blood and then produces urine which allows for the excreting of the extracted toxins. Kidney hormone secretion has multiple effects on the body, such as increasing blood vessel production or the release of a hormone that raises the amount of calcium in the intestines intake. The kidney is also responsible for the water-electrolyte balance in the body through an increase in urine concentration or increase in water absorption [49].

In the United States, 786,000 people are living with end-stage renal disease. End-stage renal disease occurs when reduction of kidney function reaches a point where it no longer meets the needs of the body [16]. During chronic kidney disease, the kidney becomes less efficient in these biological processes. When end-stage kidney failure occurs and is left untreated, an individual has the potential to suffer from a multitude of symptoms and complications. The regulatory nature of the kidney leads to symptoms that are a result of underproduction or overproduction of bodily processes. Complications range from high blood pressure, swelling of the legs, diabetes, higher blood volume, and anemia[49].

Treatment falls into three categories [44]:

1. Hemodialysis
2. Peritoneal Dialysis
3. Kidney Transplant

Hemodialysis occurs by filtering a patient's blood through a machine that primarily removes the waste, salt, and fluid. Then the machine returns the blood to the patient. This process is regimented, and frequency varies with disease severity. With the most common regiment requiring three treatments a week, while a patient suffering from a severe form of the disease may need to have the procedure done multiple times a day.

Patients typically have hemodialysis performed in a clinic or hospital setting, and the procedure on average takes three to four hours when following the three day a week regimen. Daily dialysis sessions typically take 2 hours.

Hemodialysis treatment in a clinic setting consists of healthcare professionals monitoring the effectiveness of the session and to maintain patient safety. Home hemodialysis could be an option for patients, but it may not be available to patients depending on the care options provided by the dialysis

center. Home hemodialysis requires the patient to have a trained individual to care for them during the session and home dialysis requires the care provider to have the equipment available to the patient to keep in their home.

An individual undergoing hemodialysis as a treatment for end-stage kidney failure has an expected life expectancy of five to ten years. The treatment is not a cure for the disease but tends to extend the life of the patient and has the potential to improve the quality of life.

The only way to fully treat the cause of kidney failure is to receive a kidney transplant. Kidney transplantation remains the best form of kidney replacement therapy but suffers from a shortage of organs with over 90,000 patients currently on the waiting list for a kidney transplant in the US. With 71% of patients currently on dialysis and 29% with a kidney transplant, hemodialysis vascular access is the primary treatment method [16].

Though hemodialysis is the predominant form of dialysis in the United States, about 11% of dialysis patients choose peritoneal dialysis as their method of treatment. Peritoneal dialysis uses the peritoneal membrane for fluid and toxin exchange. Peritoneal dialysis provides an overall better quality of life as it can be performed at home and is a more continuous form of dialysis [16].

Instead of filtering blood, peritoneal dialysis requires a catheter to be inserted into the abdomen with a connection to the dialysis solution. Typically, the fluid dwells in the abdomen for four to six hours. This dwell time allows for internal interactions to pull waste and other fluids into the abdomen, which is then drawn out of the body through the catheter tube. Due to the length of the treatment, this is typically done at home, and over the course of the patient's night sleep.

Though peritoneal dialysis has a higher quality of life, the method of waste extraction may not work for all patients and may become less effective over time. For patients who are not able to have effective peritoneal dialysis done, hemodialysis is the primary treatment method. For patients whose peritoneal dialysis decreases in effectiveness over time and has no transplant options available, the patient is required to switch to hemodialysis as the primary mode of treatment. Both Peritoneal Dialysis and Hemodialysis require regular blood tests to confirm the effectiveness of the treatment. With the lack of available organs for transplant, this leads to 89% of dialysis patients choosing hemodialysis and the need for reliable vascular access [16].

Chapter 2 of this thesis is a published manuscript, and Chapter 3 is the drafted form of second manuscript that will be submitted for publication.

1. Chapter 1: Background/Current Field

1.1 Vascular Access Procedures

There are currently three main forms of hemodialysis vascular access [16]:

1. Arteriovenous Fistula
2. Arteriovenous Graft
3. Central Venous Catheter

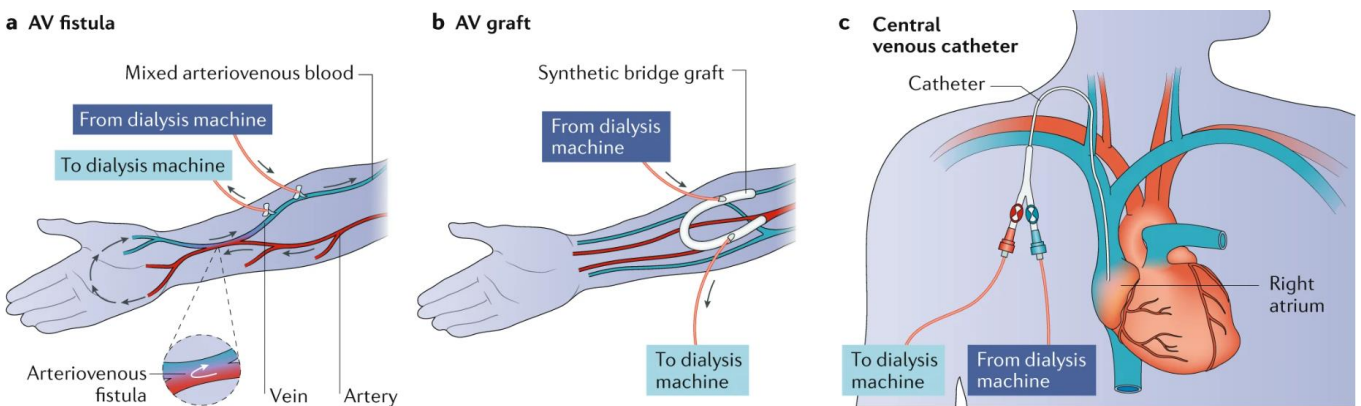


Figure 1: The three major forms of vascular access for Hemodialysis [16] a) Arteriovenous Fistula b) Arteriovenous Graft c) Central Venous Catheter

Arteriovenous Fistulas

Arteriovenous fistulas comprise a surgically created anastomosis between an artery and vein, usually in the forearm or upper arm. The connection of the artery with the vein ideally results in a high blood flow through the vein that can be used for vein cannulation. Vein cannulation refers to the catheter that is inserted into the vein for ease of vascular access. The reason the vein is used for cannulation is that it is easier to access as the vein is near the surface of the arm. The ease of access allows the caregiver to avoid needing to search for an inlet and outlet point. This increases the reliability of the vascular access to be achieved with a single jab of the needle and minimizes patient discomfort.

The first choice for a physician deciding on which vein and artery to attach the cephalic vein to the radial artery. This is typically done in the patient's non-dominant hand and is located near the forearm. The second option is to attach the cephalic vein or basilic vein to brachial artery, which is farther up the arm of the individual [44]. After the surgery, in addition to attaching the vein to the artery, the surgeon prepares the vein for cannulation. The cannulation provides a location on the arm that allows for repeated use by the attending staff to access [51]. This creates a port that has easier and quicker access for the patient, as it prevents caregiver from needing to re-find the correct vein during each appointment. As with any exposed wounds there is a risk of infection [16].

Arteriovenous Fistulas are the preferred mode of vascular access due to a few factors. The first factor is the overall longevity of the fistula. When looking at rates of creating new access points or revisions to the surgical sites are lower at this point compare to procedures using arteriovenous grafts [16]. In comparison to AVGs, there are lower rates of infection and reduced mortality rate. These aspects combine to reduce the cost to the individual as they are able to avoid hospital visits and the cost of additional surgeries [1], [2], [3], [4].

For a standard fistula, the time it takes to fully mature for use in hemodialysis is not fully agreed upon. Different regions of the world define maturity at different time points. Despite the differences in the definition of maturity, the meantime for reliable use is 6 months[16]. The time to first use in dialysis for a fistula can be as early as the two-month timepoint, but the stress on the fistula comes from the hemodialysis session means that the fistula could not be ready for repeated use [51]. With reliability considered being able to complete the three session a week regiment, first use may not indicate the fistula is fully matured. Thus, maturity is the fistula's ability to increase venous blood flow, an increase in diameter to support dialysis, and to withstand the strain on the structure through multiple uses. At the four-week point, a physician can typically determine whether a fistula is likely to mature. This determination can vary with the patient's age, and the various conditions they might have.

The volumetric flow rate of blood through the fistula is defined as $\frac{mL}{min}$. One of the conditions for a successful maturity of a fistula is whether it can sustain a blood output to the dialysis machine of $\geq 300 \frac{mL}{min}$ in 8 out of 12 sessions. With three sessions a week, the timeframe to consider the fistula a success takes approximately four months [16].

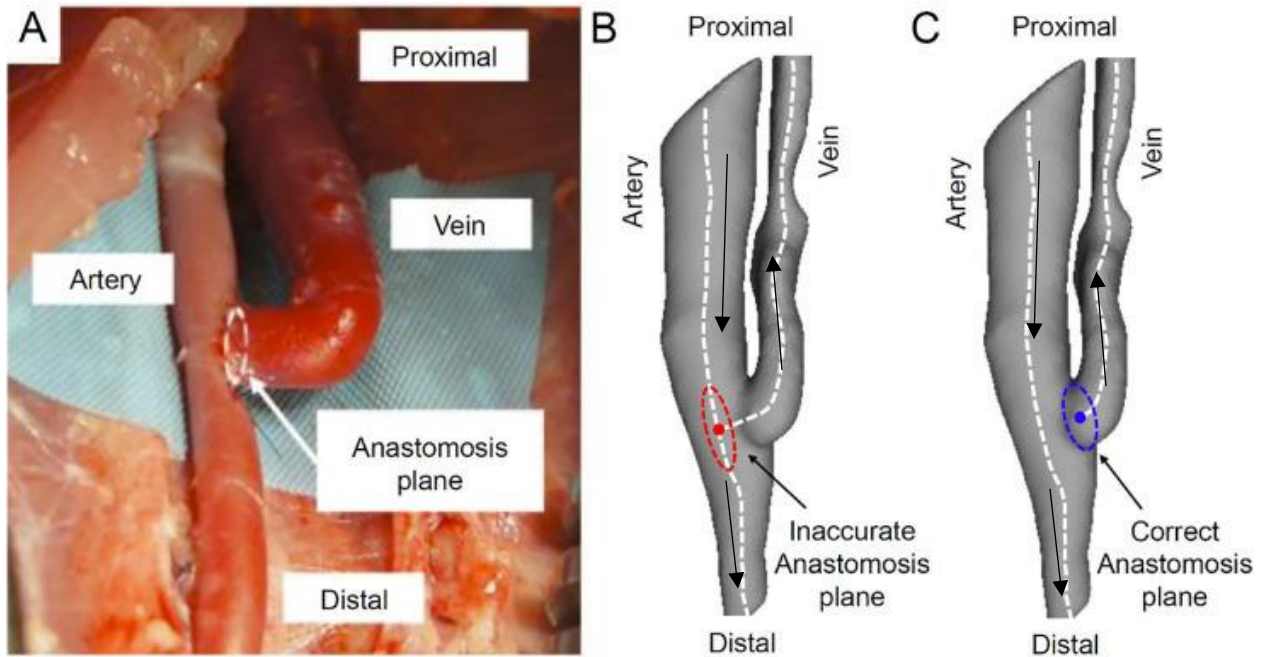


Figure 2: Sample of an AVF and the location of the anastomosis plane calculated by different post-processing techniques [45]. (A) Denotes an AVF surgery on a swine fistula. (B) Contains the centerlines acquired from current available software in fistula segmentation and the derived anastomosis plane, which is defined as the location where the bifurcation of the centerline occurs. (C) Contains the centerlines and anastomosis plane acquired from the proposed method. Note that the centerlines do not overlap, thus producing an anastomosis plane that resembles the physiological one shown in (A). The arrows in (B) and (C) indicate the direction of flow.

An arteriovenous fistula consists of four components to contextualize the fluid flow. The first component is the Proximal Artery. The Proximal Artery is the side direction the flow is coming from. Proximal in the anatomical setting refers to the orientation of an object in the body with respect to the center of the body or an attachment point. In this setting, proximal refers to the part of the artery closest to the shoulder. The Distal portion of the artery indicates the side that is farther from the shoulder and is closer to the hand. For a matured fistula, only a tiny portion of the blood flows continues through the Distal Artery [45].

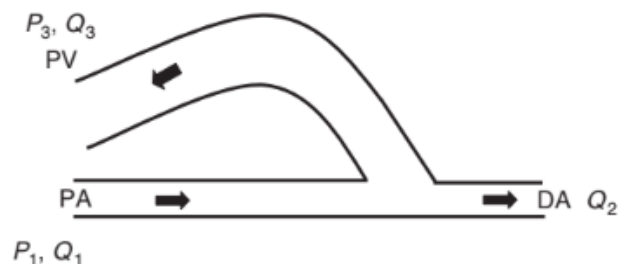


Figure 3: Example of Arteriovenous Blood Flow [46]. P represents Pressure, A represents Area, and Q represents Volumetric Flow

The vein is the vessel that is used for cannulation and has a majority of the blood flow diverted through it [46]. As low-pressure vessels connected to a high-pressure vessel in the artery, the low resistance of the vein causes the blood to flow through the vein. Over the course of the maturation process for a successful surgery, the vessel wall thickness of the vein increases, and the vein starts to resemble the characteristics of an artery. This hardier vein allows it to better stand up to the continued use of vascular access.

The fourth component (Figure 2C) is the connection point between the vein and the artery. This is called an anastomosis plane. This region is important as the reference point for where the blood flow is diverted and is used for the calculation of the angle of vein attachment [45].

Another aspect of the anastomosis region is that it is considered the region that represents the highest risk for AVF failure. The blood flow in this region of the vein is not uniform as the flow bends to follow the geometry of the vein. The closer region of the vein to the proximal artery is at higher risk of have a lower local flow velocity and mass flow rate compared to the average of the vein, while the outer region is likely to have a higher local flow velocity and mass flow rate compared to the average of the vein [43]. Only about 40% of arteriovenous fistulas are able to mature to the point of being able to be used for hemodialysis without any intervention [8]. The extended time to determine the success of a surgery mixed with a high failure can create delays in being able to begin treatments, or additional surgical interventions to hopefully induce maturation, or have the patient to use a different method of vascular access that is not as effective [5,6]. Even with successful fistula, 70–86% of the time it requires two or three interventions per patient in year one to aid in fistula function [16].

Bleeding is an issue that may occur which increases the risk of blood clots or a decrease in the volume of blood flow if the bleeding is serious enough. With frequent use of dialysis needles, there is a risk that frequent use may lead to bleeding. This is called needle stick injury [42]. When using needles, there is a risk of unintended puncturing of vein walls which can cause additional clotting factors to be introduced. In conjunction with bleeding, there is a thrombosis risk. Thrombosis is a blood clot that blocks a vessel. The blood clot that can travel through the bloodstream can potentially cause blockages or a fatal heart condition. In addition to thrombosis, there is a risk of heart failure due to the increase strain on the heart due to the need for higher blood output [16].

In addition, the fistula has a risk of aneurysm formation in the arm. In an aneurysm, the vessel wall weakens and can bulge. With this bulge in the vein or artery, blood can be caught in the pocket and grow. If left untreated, an aneurysm can burst and cause many adverse side-effects. The rates of aneurysm formation in fistulas vary from 43% to 60%, and this depends significantly on how a physician or region determines what should be considered an aneurysm [16]. For most aneurysms, the fistula remains functional, and the aneurysm remains stable. For the cases where it is stable, dialysis can continue without any interventions. Although in those cases, the physical disfiguration of the fistula may lead to pain or distress due to cosmetic aspect. The rate of fistula aneurysm rupture ranges from 0.8% to 5.6% [16]. Since a rupture can be fatal, the risk is high for a patient if there is a rupture, but the occurrences are relatively low. These high-risk aneurysms require intervention to prevent those negative outcomes.

Moreover, the fistula side-effects may lead to the patient developing steal syndrome. Steal syndrome is when diverted blood flow prevents enough blood from reaching a region of the body or a tissue. In arteriovenous fistulas, the region of the body is usually the hand. This results in the condition of ischemic hand. If a tissue is ischemic, there is not enough oxygenated blood reaching that tissue [42]. If left untreated, not having enough blood can lead to necrosis, hypoxia, or paralysis of the limb. Arteriovenous fistula that fails to mature is considered to have multifactorial clinical problems that contribute to the failure. A diverse range of factors like race, sex, comorbidities (cardiovascular disease, peripheral artery disease, diabetes, hypertension) have been associated with lower or higher maturation rates [9].

The clinical definition of arteriovenous fistula failures stenosis occurring at the region closest to the anastomosis region and is known technically as peri-anastomotic venous segment stenosis. [10] When the vessel diameter is excessively reduced as a result of inward remodeling and neointimal hyperplasia, regular cannulation is compromised and blood flow for hemodialysis is insufficient [15], [16], [17]. The single region of maximal stenosis (minimal venous CSA) is the marker of fistula non-maturity, other fistula configuration-related features such as vein curvature and fistula angle have been shown to affect blood flow and diameter of the vein [4].

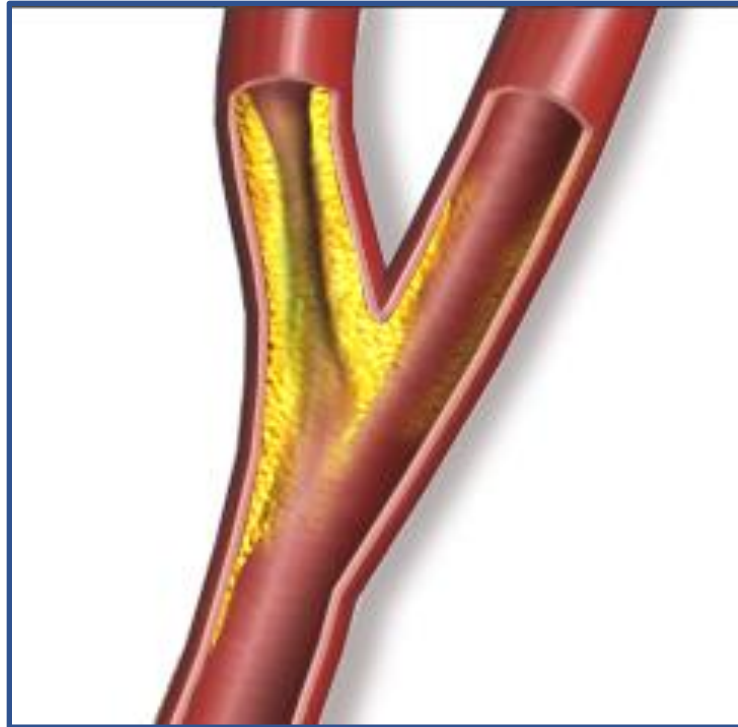


Figure 4: Example of stenosis occurring in a Fistula.

Once a fistula has matured, there is still a risk of stenosis occurring after successful hemodialysis. Extended use of the fistula in hemodialysis can lead to injury to cannulation site. This can prompt stenosis in the vein and require surgical intervention to allow for continued use [16].

Continued hemodialysis can lead to the presence of venous valves, which provides a health risk to the patient and reduces the blood flow through the vein. This reduced blood flow leads to more time intensive treatments.

The long-term impact of non-laminar flow through the vein can lead to stenosis to occur over time. As noted earlier, the vein properties change due to the increased flow and with successful hemodialysis, the flow dynamic may trigger stenosis. With the flow effecting physical stresses, this leads to a potential change in gene expression that can drive changes in the vein. Those changes can help to maintain the fistula or drive the changes that could result in stenosis [43].

While waiting for the fistula to be suitable for vascular access, Tunneled Dialysis Catheter is used for access and extended use can lead to very significant morbidity, mortality, and economic cost [45].

With the failure rate for arteriovenous fistula, there is a financial, physical, and emotional cost when the patient undergoes treatments or interventions to maintain hemodialysis functionality. Every time there

is an intervention, there is an individual that undergoes a surgical procedure and the medical cost that entails. As a result, it is important to be able to identify factors in fistula maturation that can minimize failures and limit patient stress.

Arteriovenous Graft

Arteriovenous grafts are the second main form of dialysis vascular access. The graft is comprised of a tube made of synthetic material that is typically expanded polytetrafluoroethylene (ePTFE) [16]. The synthetic material typically connects the radial artery and the cephalic vein to increase blood flow in the vein, which is the same as the intended purpose an arteriovenous fistula. The graft provides a target for cannulation and the graft itself is the point of vascular access [16].

In contrast to arteriovenous fistulas, arteriovenous grafts are typically determined to be matured and able to be used successfully at three to four weeks after surgery. Despite the faster maturation time, the grafts typically see stenosis at the graft vein anastomosis site which can result in 1-year primary patency rates as low as 23% [7]. This rate is approximately half of a fistula's success rate. Whenever synthetic material is introduced to the body, there is the risk of immune response and clotting due to material being foreign. This leads to clotting at the anastomosis regions of the graft in either the vein or artery, leading to closure of the graft and then require intervention to re-open the blood flow through the graft again.

Arteriovenous grafts also have a significantly higher rate of infectious complications when compared to fistulas, occurring twice as often in grafts. Additionally, fatal infections occur more often in patients who have grafts than those with fistulas [16].

In addition to the risk previously stated, arteriovenous grafts still have the same risk as fistulas. These risks being steal syndrome, bleed and thrombosis, and aneurysms. Despite the higher number of negative outcomes compared to fistulas, patients with smaller veins or arteries may require an arteriovenous graft to be able to have reliable vascular access [42].

Synthetic grafts have potential for significant improvement in the future. Newer graft material can allow for hemodialysis within three days and for successful graft there are fewer intervention when compared to fistula intervention [16].

Tunneled Dialysis Catheter

Dialysis catheters are the current method to provide immediate vascular access for hemodialysis. The point of access for the dialysis catheter is the jugular vein [42]. They have the potential to be used for short-term or long-term use. Catheters for short-term use tend to be stiffer materials and are used as a bridge treatment method until a fistula or a graft is available for use. Long-term use tends to be made of more flexible materials and termed Tunneled Dialysis Catheters (TDC). Tunneled Dialysis Catheters are fed through the venous system before terminating in the Right Atrium of the heart. This method of treatment is considered to have many potential complications and it should only consider to be a “last resort” treatment [16].

One of the major issues with tunneled dialysis catheters is that there is a high rate of infection compared to fistulas and this leads to an increase of hospitalizations [52]. These infectious incidents create the need for intravenous antibiotic treatments and can often be fatal.

The rate of failure for Tunneled Catheters is high due to fibrin sheath formation or the occurrence of thrombosis. A fibrin sheath is a thin film of protein that grows over the catheter and can block the opening of it. The fibrin sheet can develop as quickly as a week and is a common failure mode. It can prevent blood flow through the catheter [16]. As a result, thrombosis is a possible consequence due to the clotting along the catheter. This is a common occurrence and requires frequent interventions to maintain functionality and prevent adverse patient consequences. The failure rate of Tunneled Dialysis Catheters is 91% for the first year and approximately half are removed within that timeframe [45].

Central Venous Stenosis is a common complication as well. This is the narrowing of the vein and requires angioplasty to treat. On top of the risk of thrombosis, the complication can cause reduced flow rates for other forms of hemodialysis that are used after TDC use is stopped [16].

1.2 Arteriovenous Fistulas Flow Characteristics and Theory

Cardiovascular System

The cardiovascular system serves two primary functions. The first being to deliver oxygenated blood through the body and the second being the return of the deoxygenated blood to the heart and lungs to be re-oxygenated. In addition to the delivery of oxygen to the body, blood carries nutrients to the different organ systems and carries away the waste those systems generate. This system is made up of the heart and the blood vessels that branch out through the body [54].

The heart acts as the pump for the body and is divided into four chambers. There are the Right Atrium, the Right Ventricle, the Left Atrium, the Left Ventricle. The Right Atrium carries deoxygenated blood to the Right Ventricle, which then pumps the blood to the pulmonary artery. The pulmonary artery then pumps the blood into the lungs to be re-oxygenated and to remove carbon dioxide. The blood is then returned to the Left Atrium. The Left Atrium carries the re-oxygenated blood into the Left Ventricle. The Left Ventricle then pumps the oxygenated blood into systemic circuit to deliver the oxygenated blood to the various organs and eventually returns to the Right Atrium to complete the circuit [54]. The pumping of the heart involves the contracting of the Ventricles to increase the pressure and push out the blood. The Ventricle then retracts to allow for the chamber to refill again. This is termed the cardiac cycle [54]. When the heart contracts, the highest pressure is generated and is termed the systolic pressure. The resting period is considered diastolic pressure. This results in blood flow that can pulsatile.

The two major blood vessel category types in the cardiovascular system are the artery and the vein. An artery is a high-pressure vessel in the body that is responsible for the delivery of oxygenated blood throughout the body. The exceptions to the delivery of oxygenated blood by an artery is the pulmonary artery which carries blood to the lungs to be oxygenated, while the umbilical artery carries deoxygenated blood from a fetus to the mother.

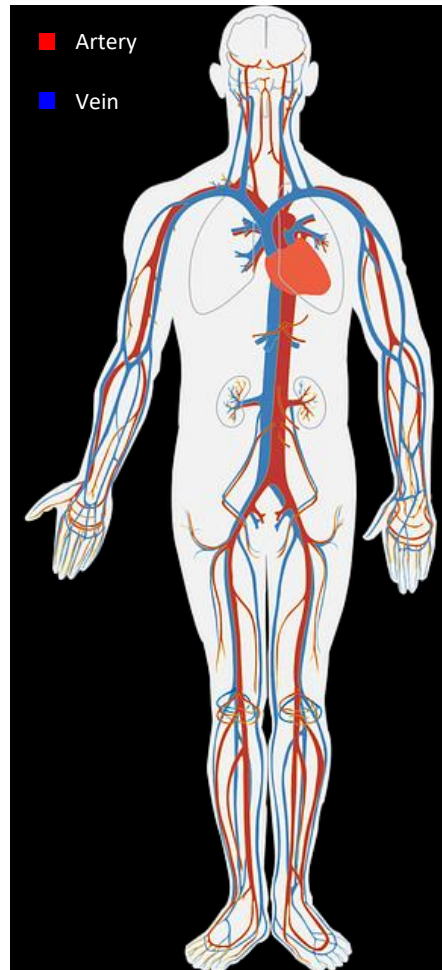


Figure 5: Depiction of the cardiovascular system

Systolic is the point in the cardiac cycle with the arterial highest blood pressure. Diastolic is the point in the cycle with the lowest arterial blood pressure. An artery follows the cardiac cycle, having its highest pressure at when the cardiac cycle is at systolic pressure and its lowest pressure at the diastolic pressure. The artery is the highest-pressure vessel in the localized region of the circulatory system. Due to the high-pressure, the arteries have thicker vessel walls when compared to veins. With the cardiac cycle creating a pulsatile flow, the artery is responsible for controlling the local blood flow [50].

The artery has a fill volume that allows for the blood flow to either end of the artery to create a continuous flow. The artery contracts and relaxes, relying on the pressure difference to push the appropriate amount of blood to the various organs. This creates a constant flow when the blood reaches the various organs. The arteries that can be potentially used for an arteriovenous fistula are the radial artery and the brachial artery [45].

Veins are the low-pressure vessel that carries deoxygenated blood back to the heart. The vein tends to have flexible vessel walls to accommodate blood volume and is considered the capacitance vessel as a majority on individuals' blood is present in the veins at any given moment. In general, a vein blood flow is relatively constant, but under the flow conditions of a fistula, it experiences a pulsatile flow [53]. The two veins that are typically used in arteriovenous fistulas are superficial veins. Superficial veins are not paired with an artery and carry a lower volume of blood compared to deep veins, as deep veins are paired with an artery. Superficial veins are able to be removed surgically, if necessary, as in the case of varicose veins. Due to this feature, the cephalic vein and basilic vein are good candidates for fistulas. Stenosis of the vein in this scenario does not lead to adverse effects on a patient aside from requiring a new surgery to continue hemodialysis [16]. Due to the use of superficial veins, the vein typically has a smaller cross-sectional area compared to the artery.

Animal Models

Across the field of medicine, animal models are used to better understand disease states without risking the health of people. Different animals have different levels of protection due to displays of intelligence and there is a requirement of having experiments on the animal be necessary. One of the major benefits to animal studies is seeing how the biological systems over time act on the fistula. For single timepoints, ex vivo studies can be performed, but the effects of the immune responses or the biological response to the mechanical changes due to the fistula help to understand long-term effects.

There are two animal models used to compare human fistulas. They are mice and pigs. Mice are easier to achieve regulatory approval for and are cheaper to use, which allows a faster time to study completion. Multiple studies have examined fistula configuration in mice. Though the relative sizes of arteries and veins are much smaller than in humans, the effects of the fistula configuration can be studied to examine how those configurations affect the flow properties [50].

Pigs are considered to have similar cardiovascular systems to humans and as a result are a prime candidate for fistula studies. A key aspect is that the size of the heart and the way it functions is

anatomically similar. As a result, the hemodynamic properties are similar to a human as well and have led pigs to be used in numerous cardiac related studies over the decades. Mechanically, pig arteries and human arteries behave similarly, but they are still not identical. Porcine arteries generally have a smaller internal diameter than human ones but are more flexible and have significantly larger circumferential strain maximums. This relationship allows for informed comparisons with human configurations but doesn't allow for direct one-to-one conclusions. Another aspect to consider for pig to human cardiovascular comparisons is that pigs have a faster growth rate. This means temporal studies need to consider the age of the pig and the impacts growth has on the system. This requires studies with multiple animals to have similarly aged pigs to avoid needing to control for age factors [46]. For arteriovenous fistula studies in pigs, the femoral artery is connected to a vein to create the structure. This causes the fistula to have a higher volumetric flow rate when compared to an expected human AVF.

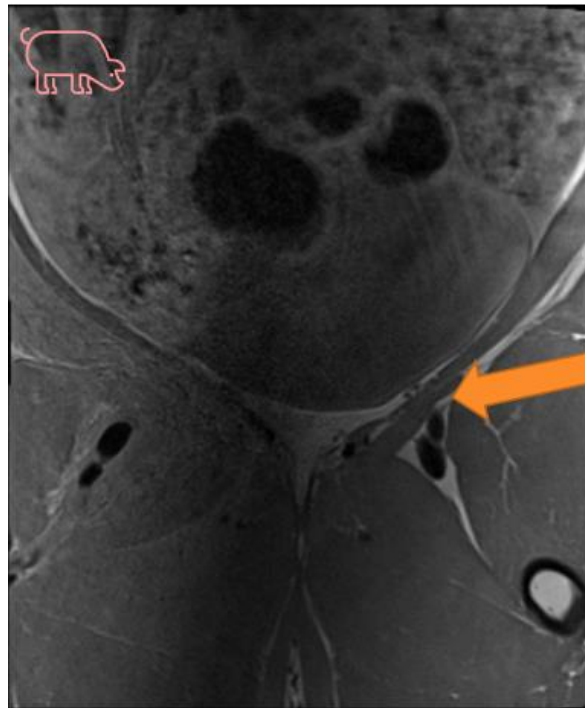


Figure 7: Example of MRI image of the Femoral Artery and the Femoral Vein in a Yorkshire Pig. The arrow depicts the Left Fistula

Though there is a significant monetary cost for animal purchasing, care, and treatment to go along with the increased level of regulatory approval necessary.

Flow Characteristics

Blood is a viscoelastic and non-Newtonian fluid. The size difference between the arteriovenous fistula and the blood cells allows for the neglect of the non-Newtonian flow characteristic, blood flow can be described using the incompressible Navier-Stokes equations. Studies have shown simulations accounting for the non-Newtonian aspects of flow have negligible changes to results, validating the incompressible assumption [47, 48]. The higher velocity blood flow moving through the venous segment produces higher overall shear values, which reduces the scale of differences between the Newtonian and non-Newtonian models for blood flow. For blood moving through a blood vessel, the Hagen-Poiseuille equation is one formulation to provide a calculation for the mean wall shear stress as [40]:

$$\tau_w = 4 * \mu \frac{Q}{\pi r^3} \quad (1)$$

Where r is the radius of the inner wall of the blood vessel, μ is the viscosity, and Q is the volumetric flow rate. With higher flow rates and a larger vessel inner wall radius, the small changes in viscosity due to non-Newtonian models can be neglected. For narrow vessels or where significant stenosis has occurred, blood would need to be considered non-Newtonian to provide accurate examinations of the blood flow. For the purposes of this study, the simulation examines an early timepoint where the large vessel assumption remains valid.

Navier-Stokes in its incompressible form is the flow equation used Computational Fluid Dynamics (CFD) for fistula modeling.

The x-component of the Navier-Stoke Equation for incompressible flow is defined as:

$$\rho \frac{\partial u}{\partial t} + \rho u \frac{\partial u}{\partial x} + v \frac{\partial u}{\partial y} + w \frac{\partial u}{\partial z} = -\frac{\partial P}{\partial x} + \mu \left(\frac{\partial^2 u}{\partial x^2} + \frac{\partial^2 u}{\partial y^2} + \frac{\partial^2 u}{\partial z^2} \right) \quad (2)$$

The density, ρ , of blood for a person is $1050 \frac{kg}{m^3}$, the viscosity, μ , is approximately $.0035 \frac{kg}{m*s}$, and x is the distance in the coordinate plane. These assumptions for the deriving of the wall shear stress and other derived flow characteristics.

Blood flow through the vein is laminar, while the artery is pulsatile. With the connection of the vein and the artery, the flow through the vein becomes more pulsatile. Though pulsatile flow is assumed to be laminar, the anastomosis connection disrupts the flow as the flow deflection is significant and the normal arterial pressure differential is changed. The flow disruption results in the blood having a transition to turbulent flow near the anastomosis region [48].

As stated previously, this pressure difference led to a majority of the blood flowing through vein and only small flow through the Distal artery.

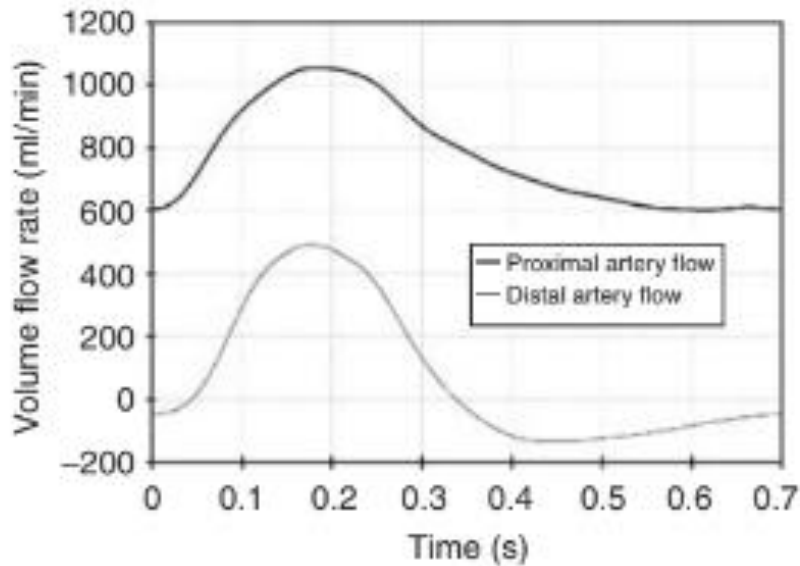


Figure 8: Example of the Volumetric Flow Rate of Fistula in a Yorkshire Pig [46]. The values represent the volumes flowing through the proximal artery and exiting the distal artery. The remaining blood flows through the vein.

The average blood flow through a fistula typically ranges between $700 \frac{ml}{min}$ and $1400 \frac{ml}{min}$. When a fistula is first attached, the volumetric flow rate maintains the shape of the cardiac cycle with the primary difference that the distal and proximal ends of the artery no longer have equal fluid volumes travelling through it [46]. For mature fistulas, the shape of the flow rate can vary drastically. Some fistulas will maintain the shape of the cardiac cycle while others will more closely resemble a vein with constant flow rate and only have minor changes with the different points in the cycle. For the fistula's vein that stenosis has occurred in or developing, the difference in volume following through the distal and proximal end of the artery gradually decreases until the vein closes and the flow only is through the artery. The velocity of the blood is defined as the following with the unit scales for the fistula [40]:

$$u = \frac{Q}{A} \quad (3)$$

Where for u is the velocity in $\frac{cm}{s}$, A is the cross-sectional area in cm^2 , and Q is the volumetric flow rate in $\frac{ml}{min}$.

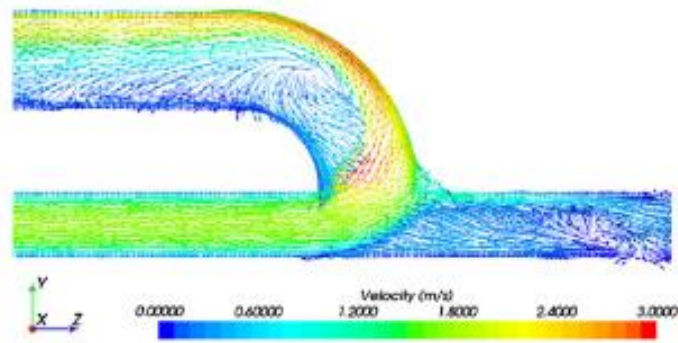


Figure 9: Example of a velocity profile in a fistula [42].

With the smaller vein area compared to the artery, the flow is accelerated. This creates flow conditions for the vein that are significantly different than normal flow conditions a vein experiences. For a patient whose fistula matured, in contrast with reducing the cross-sectional area during stenosis, the vein cross-sectional area can grow which is desired outcome when the goal is to maintain flow through the vessel [42].

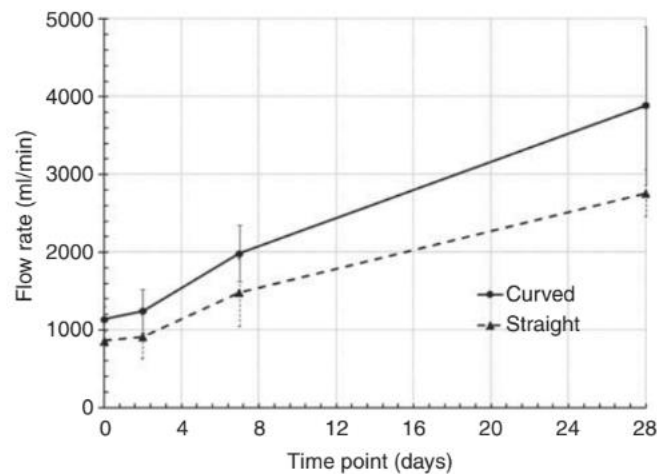


Figure E1: Range of Flow Rates in Yorkshire Pigs [4]

In the CFDs executed for each fistula, the flow rates are within the expected range of a Yorkshire Pig. There are three hemodynamic parameters that are thought to impact fistula maturation, but without agreement on how they might affect the process.

Wall Shear Stress (WSS)

Wall Shear Stress (WSS) is the frictional force generated from the fluid near the wall. For fluid flow, the WSS is defined as [40]:

$$\tau_w = \mu \left(\frac{\partial u}{\partial y} \right) \quad (4)$$

Where τ_w is the shear stress at the wall. For modelling of fistula blood flow, the no-slip condition is considered valid at the walls of the fistula. This is the calculation used in simulations of the wall shear stress.

WSS is thought to have an impact on fistula maturation and stenosis, but how its role in fistula maturation is uncertain. High WSS has been seen in fistulas that matured, and in fistulas that didn't mature. The same was observed in fistulas that have low WSS. This leaves an undetermined range of WSS between the extremes that promote maturation. The importance for this application being that the WSS is affected by large range of factors and as the radius increases, the shear stress is going to decrease. As the flow is typically moving from larger vessel to a smaller vessel, there are significant increases in the WSS [46].

The units used for WSS in the body are $\frac{\text{dynes}}{\text{cm}^2}$. A dyne is a force the units are $\frac{\text{g*cm}}{\text{s}^2}$, as it is based on the force necessary to accelerate 1 gram. 1 Pascal is equal to $10 \frac{\text{dynes}}{\text{cm}^2}$.

The WSS for a large artery range from 10 to 70 $\frac{\text{dynes}}{\text{cm}^2}$ and a vein typically has the WSS range of 1-5 $\frac{\text{dynes}}{\text{cm}^2}$ [40]. Once the arterial flow is introduced to the vein, the change in cross-sectional causes a large increase in the mean Wall Shear Stress for vein. The dramatic increase in mechanical stress is likely one of the reasons for failed maturations. To this point there is no agreement on how WSS affects fistula maturation, except that it does have an impact. Studies point to low WSS being correlated with stenosis, while other studies have seen high WSS occur in cases where fistulas fail to mature. This drives the need to look at multiple flow factors to find maturation trends. This does leave the likelihood that there is a middle range of optimal WSS but that has yet to be determined [53]. Variety between individuals makes thresholding difficult and no upper or lower range has been determined. It is hypothesized that high WSS effects gene expression of the cells in the vein's wall that trigger stenosis by creating a surface that triggers thrombosis but has not been shown yet [46, 53].

When examining the impact of the fistula configuration on the vein and the artery, the proximal artery and the distal artery tend to have WSS values that remain consistent with what is expected of a normal artery. The Proximal artery flow conditions until it reaches the anastomosis remain see small increases but still stays in a similar range to what it was prior to the procedure. The Distal artery tends to see

lower volumes moving through it and has relatively low WSS. The entire vein region is significantly impacted by the procedure.

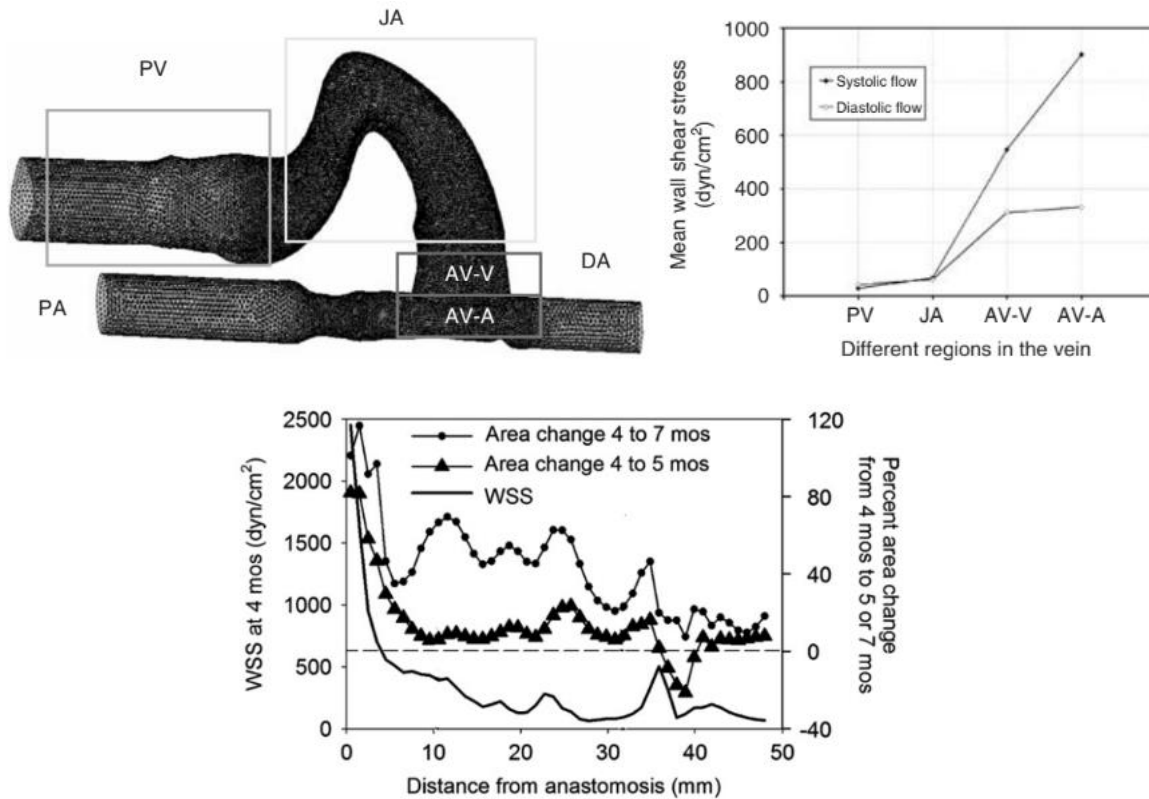


Figure E2: Example of WSS values at 42 days after surgery [37] and example WSS 4 months after surgery [56].

The WSS generated by the CFD were within the range of the WSS generated using the same CFD protocol, with the overall WSS in this study being higher due to the higher flow rates of in the fistulae created for this study. For each these cases, the WSS closer to the time of surgery tend to have higher values and is consistent with the CFD results of the study performed [56].

Oscillatory Stress Index (OSI)

The second hemodynamic parameter that is thought to impact fistula maturation is Oscillatory Shear Index (OSI). Oscillatory Shear Index is a measurement of the directional wall shear stress normalized to the total WSS. As a result, OSI is a non-dimensional number that describes the oscillatory nature of a flow based on the WSS. The equation for OSI is [40]:

$$OSI = 0.5 \left(1 - \frac{\int \tau_w dt}{\int |\tau_w| dt} \right) \quad (5)$$

Where the t is the time domain examined. OSI is used to capture eddies in the flow and recirculation that may be occurring within a region. A high OSI value indicates that a large portion of the flow is generating a WSS that is not aligned with the total WSS and the direction of the flow. A low OSI means that the WSS of the flow is directionally aligned with the flow, and that the flow is more likely to be uniform. With the $1 - \frac{\int \tau_w dt}{\int |\tau_w| dt}$ component, 0 would mean that the flow is perfectly unidirectional as $\frac{\int \tau_w dt}{\int |\tau_w| dt} \rightarrow 1$. While $\frac{\int \tau_w dt}{\int |\tau_w| dt} \rightarrow 0$ would mean that the τ_w directionally sum to 0 and implies that the flow is re-circulating, and that leaves the maximum possible OSI value as 0.5.

The generally held assumption is that low OSI improves the likelihood of fistula maturation while having high OSI is assumed to be associated with stenosis. Despite these assumptions, this relationship has yet to be shown to this point. Similarly to the WSS, there is an assumed impact on gene expression if the OSI is high. The general assumption is that low OSI promotes maturation while high OSI promotes stenosis, but no studies have been able to show that to this point [48].

When examining the impact of the fistula configuration on the vein and the artery, the proximal artery tends to see little changes in OSI until the flow reaches the anastomosis plane. The region directly after the anastomosis plane of the distal artery typically will see an increase but the flow becomes more uniform as it moves to the end of the Distal artery. The region that will see high levels of OSI is the region of the vein closest to the anastomosis plane. As the flow moves further down the vein, the flow generally becomes more uniform. This marks the anastomosis plane as a primary region of interest [45].

Wall Shear Stress Gradient (WSSG)

The Wall Shear Stress Gradient (WSSG) is the direction derivative of the WSS. As a result, the units used are $\frac{\text{dynes}}{\text{cm}^3}$. The Wall Shear Stress Gradient (WSSG) is the third analyzed parameter that is thought to be impactful but has not had a directional link towards either outcome to this point. WSSG is defined as:

$$WSSG = \sqrt{\left(\frac{\partial \tau_{w,x}}{\partial x}\right)^2 + \left(\frac{\partial \tau_{w,y}}{\partial y}\right)^2 + \left(\frac{\partial \tau_{w,z}}{\partial z}\right)^2} \quad (6)$$

This constitution of the WSSG allows the comparison of the WSS changes in comparison to its neighboring regions. A higher WSSG indicates the variability of the location is large and the effect being

seen is localized. A smaller WSSG would indicate that the effect being seen is occurring over an extended area. This is useful in pointing out outliers or if only a small portion of the vein is being affected or if the WSS over the region is in the same range. Since OSI and WSSG are derived from the WSS, the effects can help show how constant the values of OSI and WSS are as the flow moves along the vein.

Fistula Configuration

Fistula configuration is known to have a significant impact on fistula maturation and failure [53]. The primary descriptor of arteriovenous fistula configuration is the angle of attachment. By using the centerline of the arterial flow and the centerline of the vein flow, an angle of attachment can be determined for the fistula. The angle is determined by using the proximal approach towards the anastomosis of the arterial centerline and is projected to the anastomosis region. The arterial centerline and the vein's centerline closest to the anastomosis plane are what is used for angle in degrees [45]. An angle of 90° means that the vein's centerline close to the anastomosis is perpendicular to the projected arterial centerline.

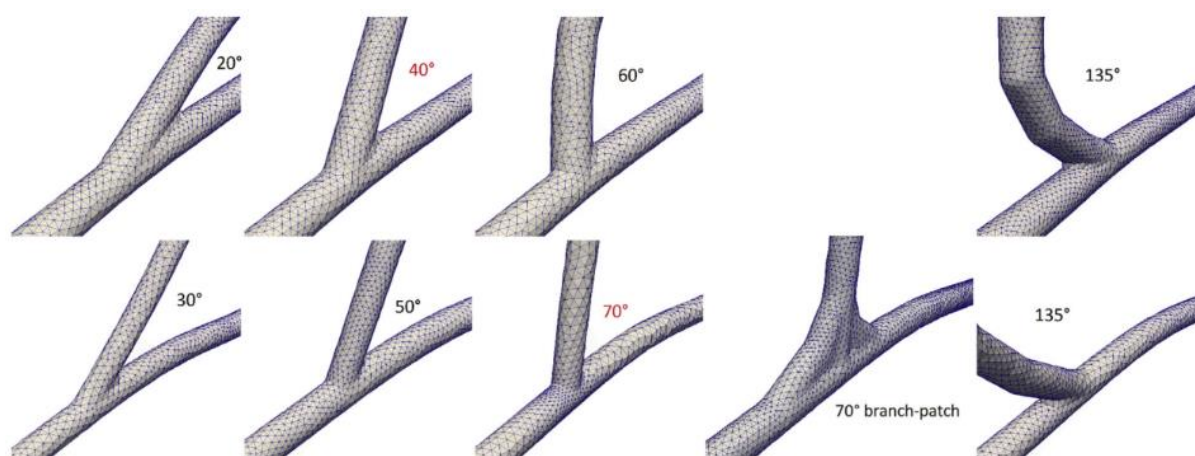


Figure 10: Example of various fistula configuration at different angles [41]

The angle significantly dictates the resultant flow and whether a fistula will mature [42].

As the fistula angle get closer to 90° , there tend to be a higher risk of arterial backflow as the blood flow will hit the bend of the vein may re-circulate. If the angle is too narrow, there is a greater pressure and WSS on the outer region that can cause irregular flow and lead to stenosis. Patients who have fistula configuration below 30° see a higher number of interventions. Additionally, once angles become $>90^\circ$,

studies tend to see higher WSS and OSI values in the vein. This leaves the general desired angle near 55° [41].

The second major aspect of fistula configuration is its curvature. The curvature represents how much bend the vein has when it is attached to the artery. In general, the artery has relatively little curvature in comparison to the vein, which is manipulated to be attached.

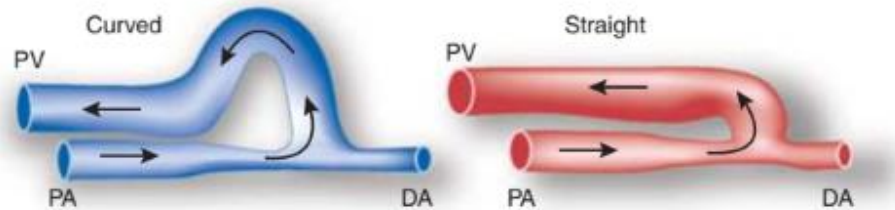


Figure 11: Example of curved and straight fistula configurations [43]

Fistulas do not have an agreed upon definition or metric to measure the curvature of a fistula, but methods generally analyze how much the centerlines of the vein curves. Centerline measurements do vary depending on the initial starting point. For this study, the centerline of the vein starts from the anastomosis plane. Fistulas with a curved geometries have been shown to alter the hemodynamics of the flow when compared to fistulas that are deemed “straight” [43,4]. The shape of the vein’s geometry affects the uniformity of the flow, with fistulas with a bent configuration creating a more uniform flow. Fistulas with a straight geometry leads uneven flows, with some region with a high flow velocity magnitude in the outer regions, and some regions with comparatively lower velocity magnitudes in inner regions. One of the key results found was how the vein wall changed over time between the orientations. Straighter fistula had a more varied WSS distribution and cell wall thickening was considered ‘eccentric’ [46], meaning the cell wall thickness change varied depending on the flow profile at that location. In curved or bent configurations, the vein wall thickened in a similar manner along the length of the vein [4]. This indicates that curved fistulas could result in more even flow distribution which may produce a higher maturation rate. Despite these studies, most patient fistulas are formed with a straight configuration. This may be due to the lack of human AVF studies and due to straight fistulas being the common configuration for fistulas since the surgery began in 1966. Additionally, patients may not have enough vein length to create fistulas and to remodel the vein for cannulation [43].

The focus of this dissertation is on the occurrence of stenosis prior to arteriovenous fistula maturation. The scope is narrowed to arteriovenous fistula flow characteristics that lead to maturation or stenosis. A fistula that does not mature will lead to multiple endovascular and surgical interventions, and eventually it reaches the point where vascular access is impossible. This leads to extra time, money, and stress for patients dealing with end-stage renal failure. The purpose of the study is to characterize these parameters in a temporal study with an initial timepoint of 3 days after initial surgery and analyze the impacts of these parameters at 28 days after surgery on the fistula. The 3 days after surgery timepoint was selected so that the fistula geometry had enough time to stabilize under the new flow conditions. The 28-day timepoint was selected as it is the first check-in point a physician can determine whether a fistula is maturing. The goal is to identify how these parameters contribute to fistula maturation or stenosis.

2. Chapter 2: Imaging and Segmentation

2.1 Magnetic Resonance Imaging (MRI):

Accurate fistula modelling is an important aspect of characterizing an in vivo AVF. Modelling of the fistula allows for the determination of the cross-sectional area throughout the vein and artery, which provides a method of tracking vein stenosis. It is important in determining the configuration angle as well. The centerlines for the artery and vein are typically found based on geometry. Improper modelling leads to incorrect area calculations and inaccurate centerlines. Thus, having a reliable method of modelling is vital. The creation of these models is done by a segmentation method, where a series of 2-D images are put together to create a 3-D image [45].

Magnetic Resonance Imaging (MRI) provides a 3-dimensional dataset that can be used to create the 2-D slices necessary for segmentation. MRIs are known to provide better image contrasting of soft tissue compared to other imaging methods like CT scanning without producing a radiation risk to the patient undergoing imaging. MRIs generate a strong magnetic field and magnetic field gradients to measure the spin of hydrogen protons to generate images based on the time the protons relax to its original spin [55]. There are two types of MRI imaging methods that are generally used, T1-weighted scans and T2-weighted scans. T1 refers to the use of a faster relaxation time and measure the time it takes for the proton in the same direction of the magnetic field. This type of sequencing is typically used to measure blood flow. T2 refers to the proton's relaxation in the transverse spin in relation to the magnetic field and is generally used for tissue imaging.

To improve contrast, there is phase-contrast MRI. In MR imaging using contrast agents, there is a fluid contrast agent that is intravenously injected to a patient to improve image quality during imaging. For patients enduring kidney failure at any stage, contrast agents can provide high levels of strain on the kidneys. Therefore, physicians tend to avoid using contrast agents for these patients. As result, this type of imaging is not an option for this method due to potential harm to patients.

Non-contrast MR imaging does not use contrast agents and is a prime candidate for high resolution imaging in this context. Non-contrast MRIs are able image swine fistula with a high enough resolution to segment and model the fistula [45]. This imaging uses the T2 sequence. For black blood sequences, the T1 sequence is used and techniques over the past decade have improved the quality of black blood imaging. Black blood refers to the color of the fast-moving blood when seen on the MR image. By imaging different phases of the black blood flow, the changes in pixel intensity allows for a conversion of

pixel intensity to volumetric flow rate [55]. For the size of the vessel analyzed, higher resolution is important and necessary to accurately extract the flow rate of the artery. The MRI technique to increase image resolution is called Controlled Aliasing in Parallel Imaging Results in Higher Acceleration (CAIPIRINHA) [26]. CAIPIRINHA is method that measures multiple slices for the same tissue at the same time. This provides a high-resolution image. For this application only one slice on either end of the artery is necessary to record the flow intensity. Thus, this technique allows for the measurement of either side of the artery, meaning that flow profile is measured over the same cardiac cycle. Additionally, the technique allows for higher resolution images in both black blood images and tissue imaging [26]. The higher resolution is also important for fistula segmentation. When creating the 3D model, the image resolution is a constraint on the accuracy. Having higher resolution allows for a closer tracing of the fistula walls and the creation of a more accurate model.

2.2 Published Manuscript:

Introduction to Manuscript

The manuscript detailed in Chapter 2.2 is centered around the creations of 6 AVFs using a porcine animal model. The focus of the manuscript is the segmentation of a fistula from a 3D model, identifying the Cross-Sectional Area (CSA) of each segment, the calculation of the centerlines starting from the anastomosis plane, and the angle of the fistula. The creation of the model from the MRI images is important due to the safety of the procedure for the patients. With the resolution of the images from the MRI, the tracing of the fistula regions can be done with reduced errors. The reduction of errors in the segmentation process is key, as errors that occur here are perpetuated through the entire procedure, as the CSA and the centerlines are dependent on accurate modelling.

The CSA is an important parameter identified in this paper as accurate CSA calculations allow for long-term changes in the fistula to be tracked, and for accurate centerline identification. Examining CSA allows two important aspects to be analyzed, whether stenosis is occurring, and/or how the hemodynamic profile at an early timepoint changes the venous CSA at a studies endpoint. This manuscript identifies the framework of inputs for the context of Computational Fluid Dynamics (CFD). Though the change in the CSA may have a multitude of factors, identifying trends with the hemodynamic profile allows for the initial steps in improving AVF surgical configurations. Accurate CSA calculations also allow for correct identification of changes in the venous wall overtime. The framework provided allows for the construction of the model from 3 planes:

1. Axial View
2. Sagittal View
3. Coronal View

The use of multiple views to segment the image improves the accuracy of the CSA, as the entire context of the vein and artery can be considered. The CSA at one time point and location on the vein can be compared at the same location on the vein and different time point, thus enabling longitudinal studies. Having accurate CSAs also allows for accurate centerline calculations, as inaccurate areas will shift the centerlines of each segment.

In addition to the value provided by accurate CSAs, the paper also examines the centerlines of the vein and artery. One of the novel aspects of the method outlined in the manuscript is that the centerline for the vein starts from the center of the anastomosis plane, and not directly from the centerline of the artery. This provides a more accurate value for the vein centerline since the arterial centerline is no

longer influencing the vein calculation. If the centerline of the vein started from the artery, then the vein centerline would shift as it moved through the artery and cause artificial changes in the vein centerline (See Figure 2 B and C). By starting from the anastomosis plane, two parameters have increased accuracy. These parameters are the curvature of the vein and the fistula angle of attachment. The change in the centerlines along the length of the vein allows the “bend” to be calculated. By determining the bend in the vein, the curvature impacts on the hemodynamic parameters can be characterized and used to understand why certain fistula configurations may be at risk of failing. The curvature determination allows for the examination of how the hemodynamic profile changes over time. The centerlines are important in fistula angle determination as well. Having an accurate centerline can shift the angle significantly. Additionally, the distance along centerline impacts the angle as well depending on the curvature. For this manuscript, the closest arterial centerline point is used for angle calculations. This arterial centerline is projected to the anastomosis plane and used to create the two lines necessary to calculate an angle. For Chapter 3, the angle calculation was adjusted to consider the leading points from the proximal artery’s centerline to account for the artery’s curvature.

My contributions to the project are as follows:

1. Segmentation of the Fistula
2. Troubleshooting of the 3D Mode Generation Protocol
 - a. Identified Failure Modes
 - b. Helped Establish Best Practices
3. Figure Generation and Data Processes

The segmentation of the vein and artery was completed by me and Jose Rosado-Toro. This work involved segmenting the vein, artery, and confirming the accurate separation of the anastomosis plane. This work included failure mode identification of the segmentation process. This involved identifying errors in the segmentation process and identifying what to avoid while segmenting the image. I also was involved in figure creation and post-processing data generation for the paper.

Publications Reference:

Rosado-Toro J., Philip R., Dunn S., Celdran-Bonafonte D., He Y., Berceli S., Roy-Chaudhury P., Tubaldi E. Functional analysis of arteriovenous fistulae in non-contrast magnetic resonance images. *Computer Methods and Programs in Biomedicine* . 2022; 222 ,106938.

Abstract

Background and Objective: Arteriovenous fistulae (AVF) are the preferred mode of hemodialysis vascular access and their successful maturation is critical to reduce patient morbidity, mortality, cost, and improve quality of life. Peri-anastomotic venous segment stenosis is the primary cause of AVF maturation failure. The objective is to develop a software protocol for the functional analysis of arteriovenous fistula.

Method: We have developed a standard protocol for the anatomical analysis of the AVF to better understand the mechanisms involved in AVF stenosis and to identify future imaging biomarkers for AVF success or failure using non-contrast magnetic resonance imaging (MRI). The 3D model of the AVF is created using a polar dynamic programming technique. Analysis has been performed on six Yorkshire cross domestic swine, but techniques can be applied into clinical settings.

Results: Differences in AVF angles and vein curvature are associated with significant variability of venous cross-sectional area suggesting that the pattern of stenosis is likely to be dependent upon hemodynamic profiles which are largely determined by AVF anatomical features and could play an important role in AVF maturation.

Conclusions: This protocol enables us to visualize and study the hemodynamic profiles indirectly allowing early stratification of patients into high and low risk groups for AVF maturation failure. High risk patients could then be targeted with an enhanced process of care or future maturation enhancing therapies resulting in a much-needed precision-medicine approach to dialysis vascular access.

1. Introduction

There are currently three main forms of hemodialysis vascular access. Arteriovenous fistulae (AVF) comprise a surgically created anastomosis between an artery and vein, usually in the forearm or upper arm which should ideally result in a high flow superficial vein that can be used for cannulation. While AVFs are the preferred mode of vascular access due to overall longevity, low rates of infection, and reduced mortality and cost [1-4], they are plagued by high early primary failure rates and unsuccessful maturation (ability to increase venous segment flow and diameter to support dialysis) [5-6]. They also have additional problems such as bleeding (often linked to the use of dialysis needles), aneurysm formation and the steal syndrome (the latter resulting in an ischemic hand). Arteriovenous grafts (AVG) are the second main form of dialysis vascular access and comprise a synthetic conduit (usually expanded polytetrafluoroethylene; ePTFE) that is connected between an artery and vein in the upper extremity and which then provides a target for successful cannulation. In contrast to AVFs, arteriovenous grafts (AVGs) can usually be used successfully at 3-4 weeks after surgery but then suffer from a reproducible stenosis at the graft vein anastomosis which can result in 1-year primary patency rates as low as 23% [7]. AVGs also have a significantly higher rate of infectious complications as compared to AVFs. Finally, tunneled dialysis catheters (TDC) can provide immediate access to the circulation for hemodialysis, but have a high incidence of infection, thrombosis and central vein stenosis and should be the vascular access of last resort.

It is also important to mention, that though hemodialysis is the predominant form of dialysis in the United States, about 11% of dialysis patients are on peritoneal dialysis which uses the peritoneal membrane for fluid and toxin exchange. Peritoneal dialysis provides an overall better quality of life as it can be performed at home and is a more continuous form of dialysis. Last but not least, kidney transplantation remains the best form of kidney replacement therapy but suffers from a shortage of organs with over 90,000 patients currently on the waiting list for a kidney transplant in the US. As described above, despite being the preferred mode of hemodialysis vascular access, only about 40% of AVFs are able to be successfully used for hemodialysis without any intervention [8].

AVF maturation failure is recognized as a multifactorial clinical problem in which a diverse range of factors like race, sex, comorbidities (cardiovascular disease, peripheral artery disease, diabetes, hypertension) have been associated with lower or higher maturation rates [9]. The main cause of AVF failures is attributed to peri-anastomotic venous segment stenosis [10] which can be quantified by generating three-dimensional (3D) models of the fistula and measuring cross-sectional area (CSA)

throughout the venous segment [11-14] as described in this manuscript. When the vessel diameter is excessively reduced as a result of inward remodeling and neointimal hyperplasia, regular cannulation is compromised and blood flow for hemodialysis is insufficient [15-17]. Even though a single region of maximal stenosis (minimal venous CSA) is the clinical marker for fistula non-maturity, other fistula configuration-related features such as vein curvature and fistula angle have been shown to affect blood flow and diameter of the vein [4]. It does need to be mentioned that AVFs can also form stenotic lesions after being successfully used for hemodialysis for some time. This could be due to cannulation injury, the presence of venous valves or the long-term impact of non-laminar flow. The main focus of this manuscript will, however, be on the early peri-anastomotic lesion which results in multiple endovascular and surgical interventions and also a prolonged period of TDC use with all of its attendant complications, resulting in a very significant morbidity, mortality and economic cost.

Open-sourced software environments, such as SimVascular [18] and CRIMSON [19], represent powerful and customizable tools to perform image-based patient-specific cardiovascular simulations. These packages provide complete pipelines for basic, translational, and clinical research and they serve as research platforms for cardiovascular modeling studies. These desktop computer programs consist of graphical user interfaces for segmenting blood vessels from medical images, building arterial and venous models, and performing CFD simulations considering the sophisticated boundary conditions typical of physiological cardiovascular models. While these vascular analysis methods are largely used for clinically-relevant vascular phenomena, AVF analyses would benefit from a specialized software due to the complexity and the uniqueness of the fistula configuration. Critical features are defined by fistula angle, vein curvature, and the identification of particular regions of interest such as the anastomosis plane (Fig. 1). In this study, we accurately identify the anastomosis plane to analyze the region close to the anastomosis which is mostly affected in case of failure. We develop our software on non-contrast MRI that yields high-resolution images [20] without the use of harmful ionizing radiation or contrast agents that may be toxic to patients with advanced renal failure [21]. From the MR images of the AVF, our software calculates the key parameters of venous and arterial CSA, together with biomarkers of AVF maturation such as vein curvature, and fistula angle (Fig. 2).

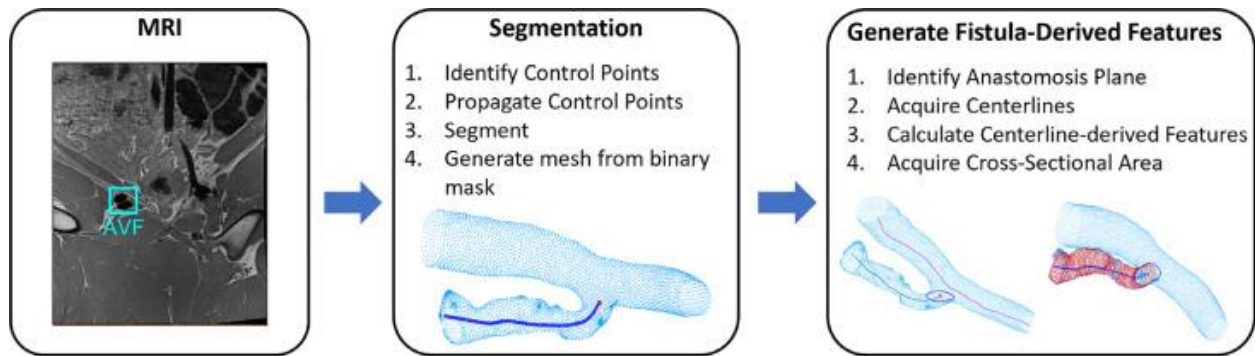


Fig. 2. **Fistula analysis flowchart.** The proposed method acquires MRIs of the fistula and then generates fistula mesh as well as fistula-derived features such as fistula angle, curvature, and cross-sectional area (CSA).

By correlating hemodynamics profiles with CSA changes, leading indicators for stenosis can be used in the future to create a functional model that would stratify patients into clinically high risk and low risk groups. While this study focused on Yorkshire cross domestic swine (*sus scrofa*), their resemblance to the human vasculature [22], [23], [24] potentially allows for rapid translation of our AVF functional analysis protocol to clinical settings.

2. Methods

2.1. Subjects and MRI-acquisition

All animal procedures conducted in this study were approved by the Institutional Animal Care and Use Committee and performed in an AAALAC accredited animal care program. Six male Yorkshire cross domestic swine (*sus scrofa*) were purchased from a USDA approved vendor and housed at the University of Arizona Animal Care Center. After a week of acclimation to the experimental facilities, AVF were surgically created [25], under general anesthesia (Isoflurane, 4% induction 1.8% maintenance) and proper surgical analgesia (Buprenorphine HCl 0.03mg/Kg), between the femoral artery and femoral vein in each of these six subjects using standard surgical techniques. Using aseptic technique and a 10 cm incision below the inguinal ligament, the femoral artery (4 mm) and vein (6 mm) were dissected bilaterally. The end of the femoral vein was then anastomosed to the side of the femoral artery, with an anastomotic length of 8-10mm, using taper double armed 6/0 polypropylene suture. Special attention was paid to ensure that there was no kinking or torsion of the completed fistula. Following demonstration of good blood flow through the venous segment, the subcutaneous tissue and skin were closed in layers using 3/0 absorbable braided sutures. Post-surgical analgesia was provided

with sustained release buprenorphine (Buprenorphine SR, 0.2mg/Kg) for 72h. Contrast-free coronal black-blood MRI sequences with spin-echo, segmented k-space, spoiled oversampling phase were acquired on the six subjects using a Siemens 3T MAGNETOM Skyra scanner at 28 days post AVF surgery. All swine were imaged in the feet-first supine position. The specific imaging parameters are in Table 1. CAIPIRINHA variation of the black blood sequence [26] was used for one subject (swine 1 in Table 1).

Table 1. Contrast-free MRI protocol on Yorkshire cross cohort.

MR Imaging Parameters	28 Days from AVF Creation					
	SWINE	SWINE	SWINE	SWINE	SWINE	SWINE
	1	2	3	4	5	6
Slice Thickness (<i>mm</i>)	0.75	0.8	0.8	0.8	0.8	0.8
In-plane Resolution (mm x mm)	0.78 × 0.78	0.78 × 0.78	0.78 × 0.78	0.78 × 0.78	0.78 × 0.78	0.78 × 0.78
Matrix Size (<i>pixels</i>)	320 × 320	320 × 266	320 × 266	320 × 266	320 × 266	320 × 266
Echo Train Length	60	60	60	60	60	60
Echo Time (<i>ms</i>)	11	22	22	22	22	22
Repetition Time (<i>ms</i>)	1400	1700	1790	1690	1710	1690

2.2. Segmentation

The proposed AVF functional analysis software was developed on archived data using MATLAB (Mathworks Inc., Natick, Massachusetts). The 3D model of the fistula is generated by joining the 3D model of the femoral vein and femoral artery. The 3D models of the vein and artery are generated by selecting a series of control points on the 2D image slices (Figure 3A). Our software divides the artery

into three regions: proximal, anastomosis, and distal (Figure 3B). The distal control point of the artery should be selected approximately 10 mm distal to the junction of the artery and the vein prior to the bifurcation of the femoral artery into the circumflex femoral artery. The proximal control point of the artery should be selected approximately 25 mm proximal to the junction of the artery and the vein prior to the junction of the external femoral artery and the internal femoral artery. The distal control point of the vein should be selected at the junction of the artery and the vein and the proximal control point of the vein should be selected approximately 25 mm proximal to the junction of the artery and the vein. Additional control points may be selected in the case of complex/non-cylindrical shapes like the vein shown in Fig. 3A. The proximal and distal control points of the arterial and venous segments is determined by following the sectioning protocol developed by Wang et al. [25]. Once the control points are selected, we use a 3D version of a dynamic programming algorithm [27] to generate the intermediate control points (marked x in Fig. 3A). The dynamic programming algorithm constrains the intermediate points to only one per image slice which simplifies the generation of the 3D model but still needs refinement to generate the centerline. Methods that do not enforce that constraint may result in erroneous intermediate control points that extend into the artery when segmenting the vein. Once the intermediate control points are obtained, we use a polar dynamic programming technique [28] to generate the outlines of the vessels of interest, namely, the femoral artery and the femoral vein. Polar dynamic programming incorporates a circular structure to the segmentation output, thus reducing the amount of manual refinement required when compared with thresholding techniques that segment the vessel based on grayscale intensity alone. To minimize the amount of manual refinement, the vein is segmented first followed by the artery. An example 2D image slice is shown in Fig. 4A. Using the segmentation mask (Fig. 4B) we generate a smooth mesh model (Fig. 4C) by first creating a mesh from a discrete 3D array followed by smoothing the mesh using the technique developed by Desbrun et al. [29]. We will then use this segmentation to generate fistula-derived features. Overall, the process for segmenting one fistula and creating the corresponding 3D models requires approximately 40 minutes (see Appendix 1).

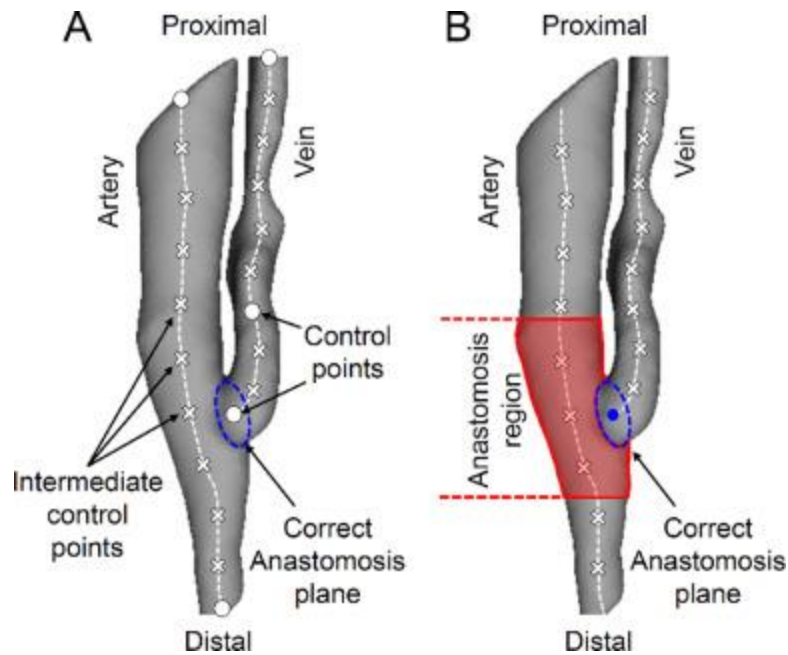


Fig. 3. **Selection of control points and regions divided by arterial analysis.** (A) The artery control points should be selected approximately 25mm proximal and 10 mm distal from the anastomosis plane. The vein control points should include the anastomosis plane and the proximal part of the vein, approximately 25mm from the anastomosis plane. Additional control points may be selected in case of complex/non-cylindrical shapes. Intermediate control points (x) will be generated from the manually selected points (filled circles). (B) Proximal region composes the region from 5mm proximal to the anastomosis to 25mm from anastomosis. Anastomosis region goes from 5mm proximal to 5mm distal and the distal region goes from 5mm to 10mm distal to the anastomosis.

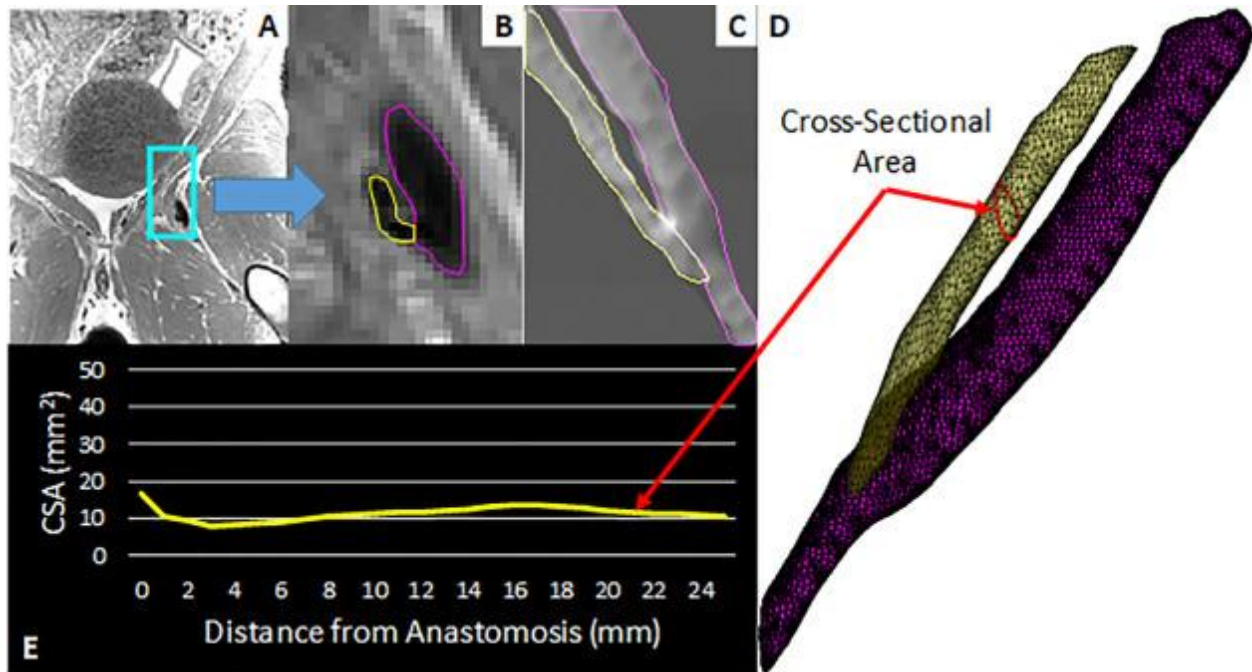


Fig. 4. **Steps to generate cross-sectional area.** (A) Black-blood (BB) MRI was performed to image lumen geometry of the fistula. (B) Segmentation of the vein (yellow) and artery (magenta) outline using polar dynamic programming (PDP). (C) Cropped version of the 3D model that will be used to estimate centerline and cross-sectional area (CSA). (D) Mesh of the fistula; the red circle is the cross-sectional area at a distance of 20 mm from the anastomosis plane. (E) The CSA plot from 0 to 25mm from the anastomosis acquired on (D).

2.3. Generating fistula-derived features

Once we have obtained the 3D models of the vein and artery, we find the anastomosis plane. The center of the anastomosis plane provides the start point for the venous segment while the venous end point is shown in Fig. 3A. The arterial control points are selected using the previous instructions. Using the start and end points, the centerline is found using a 3D fast marching algorithm [30,31]. This centerline is then used to acquire a series of AVF configuration features such as normal planes, curvature, and fistula angles. Using the centerlines and the normal planes we acquire CSA.

2.3.1. Acquiring anastomosis plane

Let's define the tuple associated with the external femoral artery coordinates in image space as: $A = [x_a, y_a, z_a]$. To transform the coordinates from image space to real world coordinates (RWC) we use (1).

$$A_c = M_T A \quad (1)$$

Where the rotation matrix (M_T) is defined as [32]:

$$M_T = \begin{bmatrix} X_x \Delta i & Y_x \Delta j & Z_x & S_x \\ X_y \Delta i & Y_y \Delta j & Z_y & S_y \\ X_z \Delta i & Y_z \Delta j & Z_z & S_z \\ 0 & 0 & 0 & 1 \end{bmatrix} \quad (2)$$

where

X_{xyz} The values from the row direction cosine of the image orientation attribute.

Δi Column pixel resolution.

Y_{xyz} The values from the column direction cosine of the Image Orientation attribute.

Δj Row pixel resolution.

Z_{xyz} $X_{xyz} \Delta i \times Y_{xyz} \Delta j$ where \times is the cross product.

S_{xyz} The image position attribute. It is the location in mm from the origin of the RWC.

If V is the tuple associated with the femoral vein in image space, then the V in the RWC (V_c) is defined as:

$$V_c = M_T V \quad (3)$$

Given the coordinates of the vein and artery in RWC, the next step is to generate 3D models. The mesh for both the artery and vein were generated using the *isosurface* function from the MATLAB programming language (Mathworks Inc, Natick, Massachusetts). The output of each 3D model is:

vertices $[x,y,z]$ coordinates pertaining to the outline of the object.

faces Relationship between the vertices. Each face forms a triangle by joining three different vertices.

Given the 3D models of the vein and artery, the anastomosis vertices tuple $A_v = [x_{av}, y_{av}, z_{av}]$ is defined as a subset of vein vertices that have a distance to the arterial vertices equal or less than 0.5mm. Using A_v we can define the anastomosis plane. A plane is defined as [33]:

$$ax + by + cz + d = 0 \quad (4)$$

Where the normal of the plane is $\hat{n} = \begin{bmatrix} a \\ b \\ c \end{bmatrix}$, and the point in the plane is $p = [x_0, y_0, z_0]$ and d is a constant associated with the plane of interest. Using A_v we define p as:

$$x_0 = \frac{1}{N} \sum_{i=0}^{N-1} x_{av_i} \quad (5)$$

$$y_0 = \frac{1}{N} \sum_{i=0}^{N-1} y_{av_i}$$

$$z_0 = \frac{1}{N} \sum_{i=0}^{N-1} z_{av_i}$$

where N is the cardinality or length of A_v . To acquire \hat{n} , first remove the mean of A_v (6).

$$\overline{A_v} = A_v - p \quad (6)$$

Next, find the single value decomposition (SVD) of the de-meant anastomosis vertices $\overline{A_v}$ (7). The SVD was acquired using the *svd* function from the MATLAB programming language (Mathworks Inc, Natick, Massachusetts).

$$[U, S, V] = svd(\overline{A_v}) \quad (7)$$

where U is a $N \times N$ matrix, S is a $N \times 3$ matrix and V is 3×3 matrix. The anastomosis plane normal (\hat{n}_a) is the third orthonormal vector of V . The third orthonormal vector is used, because the first and second orthonormal vectors correspond to the major and minor axis of the anastomosis vertices.

2.3.2. Acquiring arterial/vein-centerline based features

By defining the centerline acquired from a given object (e.g., femoral external artery, femoral vein) as a space curve, $\gamma(t) = (x(t), y(t), z(t))$, $0 \leq t \leq 1$ where the endpoints are defined as follows:

Empty Cell	Vein	Artery
$\gamma(0)$	Anastomosis Point (p)	Distal-most point
$\gamma(1)$	Proximal-most point	Proximal-most point

we can derive the following set of features such as normal plane, curvature, and fistula angle. The normal plane is defined as

$$\text{Vein } \hat{n}(t) = \begin{cases} \hat{n}_a, t = 0 \\ \frac{\gamma(t + \Delta) - \gamma(t - \Delta)}{\|\gamma(t + \Delta) - \gamma(t - \Delta)\|}, 0 < t < 1 \\ \frac{\gamma(t) - \gamma(t - \Delta)}{\|\gamma(t) - \gamma(t - \Delta)\|}, t = 1 \end{cases} \quad (1)$$

$$\text{Artery } \hat{n}(t) = \begin{cases} \frac{\gamma(t + \Delta) - \gamma(t)}{\|\gamma(t + \Delta) - \gamma(t)\|}, t = 0 \\ \frac{\gamma(t + \Delta) - \gamma(t - \Delta)}{\|\gamma(t + \Delta) - \gamma(t - \Delta)\|}, 0 < t < 1 \\ \frac{\gamma(t) - \gamma(t - \Delta)}{\|\gamma(t) - \gamma(t - \Delta)\|}, t = 1 \end{cases} \quad (2)$$

where \hat{n}_a is the normal anastomosis plane. The curvature of the object is obtained by

$$\kappa(t) = \frac{\|\gamma'(t) \times \gamma''(t)\|}{\|\gamma'(t)\|^3} \quad (3)$$

where $\gamma(t)$ is the centerline of the object we want to measure. To acquire the fistula angle, we project the arterial centerlines onto the anastomosis plane as follows

$$\alpha_p(t) = \alpha(t) - \frac{(\alpha(t) - p) \hat{n}_a}{\|\hat{n}_a\|} \hat{n}_a \quad (4)$$

where $\alpha(t)$ is the arterial centerlines, p is the middle of the anastomosis plane, \hat{n}_a is the anastomosis plane normal. From the projected arterial centerlines ($\alpha_p(t)$) we find t that minimizes the distance of $\alpha_p(t)$ to p

$$\operatorname{argmin}_{T \in \{0,1\}} |\alpha_p(T) - p| \quad (5)$$

Using T acquired from (5) we can then find the fistula angle (θ) as follows:

$$\theta = \cos^{-1} \left(\frac{(\alpha(T) - p) \cdot (\alpha(T) - \alpha(T - \Delta))}{\|\alpha(T) - p\| \|\alpha(T) - \alpha(T - \Delta)\|} \right) \quad (6)$$

where \cdot is the dot product.

2.3.3. Cross-sectional area

Using the smoothed mesh of an object³⁴, the normal arrays ($\hat{n}(t)$) and centerline ($\gamma(t)$), we find the cross-sectional area (CSA) by first finding the distance of nearby centerline points to the plane of interest. This relationship is defined by

$$d(t - \Delta) = \frac{|\hat{n}(t) \cdot (\gamma(t - \Delta) - \gamma(t))|}{|\hat{n}(t)|} \quad (7)$$

$$d(t + \Delta) = \frac{|\hat{n}(t) \cdot (\gamma(t + \Delta) - \gamma(t))|}{|\hat{n}(t)|}$$

where \cdot is the dot product.

Only vertices from the 3D models that have distances from the plane between $d(t - \Delta)$ and $d(t + \Delta)$ will be propagated into the plane described by $\hat{n}(t)$ and $\gamma(t)$ (Figure 5A). Polar dynamic programming [35] is then used to join projected vertices (Figure 5B) and morphological filling [36] is used to identify lumen region (Figure 5C). Cross-sectional area is acquired by adding lumen pixels shown in (Figure 5C).

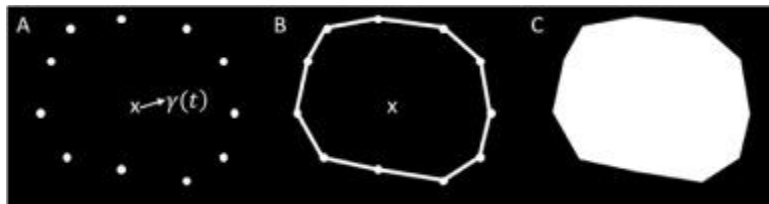


Fig. 5. **Acquiring cross-sectional area from 3D models.** (A) Projection of the vertices of the object into a plane. (B) Results of joining projected vertices using polar dynamic programming. (C) Morphological filling of closed contour; this image is used to derive cross-sectional area (CSA).

3. Results

We plot the CSA of the venous segment as a function of the distance from the anastomosis plane (Fig. 6A). This venous analysis is performed on the proximal portion of the fistula (i.e., up to 25 mm from the anastomosis) and is similar to the work performed by Wang et al. [25]. The CSA profiles can be divided into two kinds of profiles (looking at Fig. 6A from the right to the left): a) a stenosis in the region proximal to the anastomosis plane followed by a venous dilatation (swine 1, 2, 4, and 5); and b) a venous dilatation followed by a stenosis (swine 3 and 6). In some cases, we see a second venous dilatation, as seen in swine 4 at 14 mm and swine 2 at 16 mm. Stenosis regions associated with swine 1 and 5 happens within 10 mm of the anastomosis plane. Stenosis regions in swine 3 and 6 occurs 20 mm and 15 mm from anastomosis plane respectively. Clinical measurements such as minimum CSA and swine body

weight as well as fistula-derived features that quantify AVFs configuration [37,38] such as curvature (mm^{-1}) and fistula angle are quantified in Table 2. These measurements suggest that a small variability in these angles/curvatures, results in different venous CSA profiles which emphasize the importance of hemodynamics in AVF maturation.

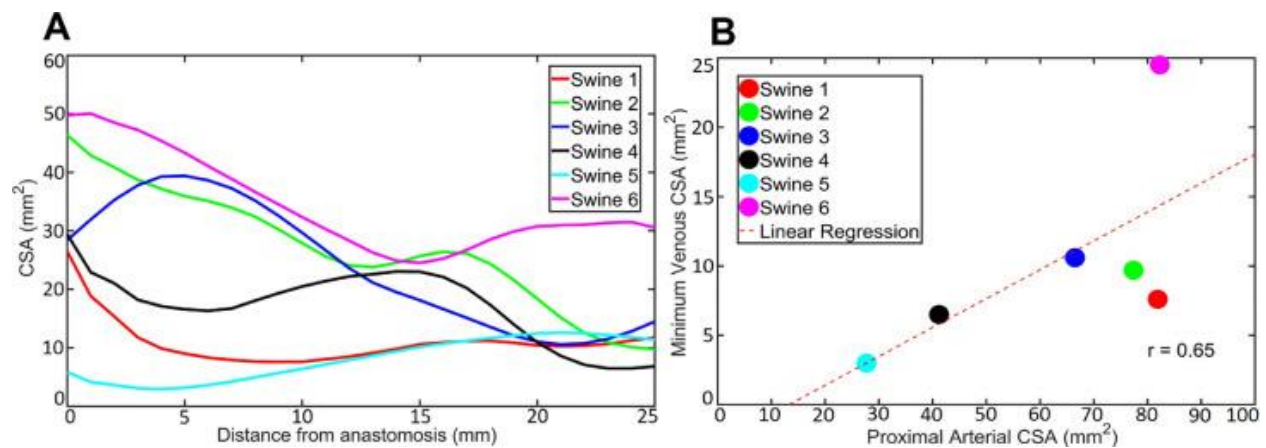


Fig. 6. Representation of venous cross-sectional area plotted with respect to the distance from anastomosis and correlation between proximal arterial CSA and minimum venous CSA. (A) The CSA of the venous segment of the AVF (mm^2) in six swine are plotted as a function of the distance from anastomosis (mm) at 0.5 mm intervals. (B) The minimum venous CSA is plotted against the CSA of the proximal arterial region along with the correlation. The correlation coefficient, r , is found to be 0.65 indicating positive correlation between these CSAs.

Table 2. Weight and MRI-derived venous functional parameters for each swine.

Functional Parameters	SWINE 1	SWINE 2	SWINE 3	SWINE 4	SWINE 5	SWINE 6
Weight (kg)	60	75.7	80	50	63.5	77.1
Min CSA (mm^2)	7.5	9.9	10.5	6.3	3	24.6
Mean Curvature (κ)	0.05	0.09	0.08	0.07	0.05	0.06
Maximum Curvature (κ_{max})	0.16	0.2	0.14	0.21	0.23	0.17
Fistula Angle ($^\circ$)	47.3	72.6	62.2	77.3	68	55.3

In view of the importance of arterial inflow, an indirect method of looking at the role of venous hemodynamics is to examine average arterial CSA and the change in the CSA proximal and distal to the

anastomosis. In our software, CSA is calculated in the three regions of the artery (i.e. proximal, anastomosis, and distal). These measurements along with the difference in CSA between the proximal and distal artery and the minimum venous CSA have been tabulated in Table 3. Swine 6 has a difference of 34.5 mm² between the average proximal and distal CSA and an average proximal CSA of 82.3 mm² and a minimum venous CSA of 24.6 mm². These high values of CSA correlate with successful AVF maturation. At the other end of the spectrum, swine 5 contains the lowest differences between proximal and distal average arterial CSA, which in turn correlates with the lowest minimum venous CSA (Table 3). Swine 5 not only has a low difference between proximal and distal average CSA, but also has an average CSA that is comparable to non-fistula external femoral arteries (shown in Table 4), unlike other fistulae in the study, demonstrating a poor luminal remodeling following fistula creation. We also plotted the correlation between the minimum venous CSA against the proximal arterial CSA (Fig. 6B) and calculated the correlation coefficient, r , which was found to be 0.65 indicating a positive correlation between the proximal arterial CSA and the minimum venous CSA. The reconstructed 3D models of the fistulas for each of the six swine are shown in Fig. 7.

Table 3. Mean cross-sectional area from various AVF regions.

Mean CSA Region (mm ²)	SWINE 1	SWINE 2	SWINE 3	SWINE 4	SWINE 5	SWINE 6
Proximal Artery	81.9	77.4	66.5	41.2	27.7	82.3
Anastomosis Plane	54.7	72.2	29.9	20.5	13.9	48.4
Distal Artery	61.6	47.2	18.5	15.9	9.2	47.8
Δ CSA	20.3	30.2	48.0	25.3	18.5	34.5
Minimum Venous CSA	7.5	9.9	10.5	6.3	3.0	24.6

Table 4. Cross-sectional area and weight range relationship of non-fistulae artery. Note. CSA values derived from Lopes-Berkas.

Weight Range (kg)	External Femoral Artery CSA (mm ²)
30-39	19.6 \pm 5.0
40-49	20.4 \pm 6.9

Weight Range (kg)	External Femoral Artery CSA (mm ²)
50-59	24.6 ± 12.8
60-69	27.3 ± 10.1
110-150	43.0 ± 13.7

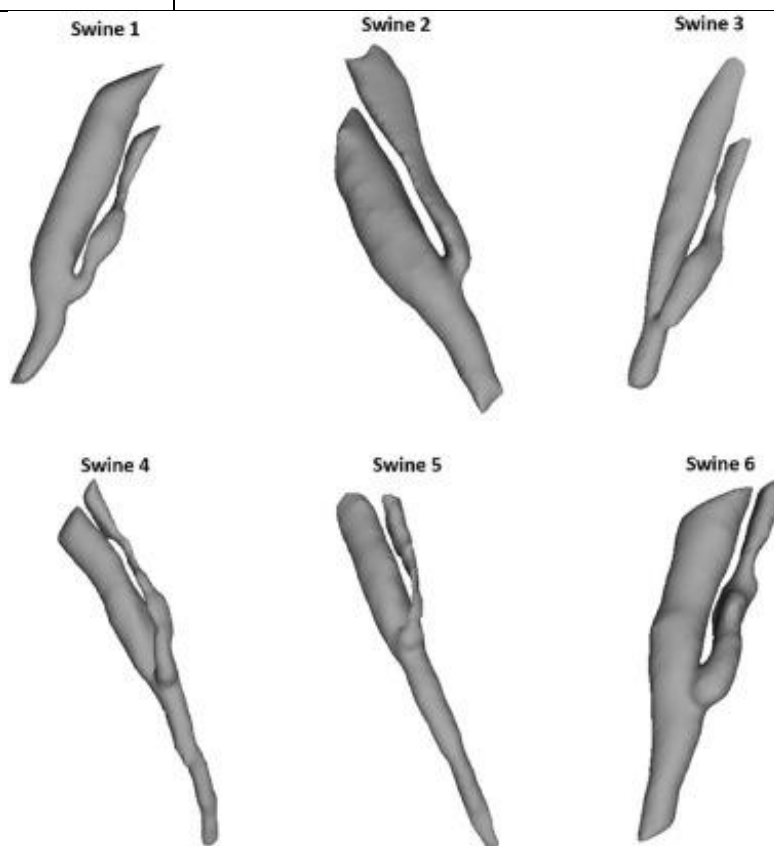


Fig. 7. **Reconstructed 3D models of the fistulae.** 3D models of the fistulas for all six swine.

4. Discussion

Our software accurately identifies the AVF anastomosis plane, segments the femoral artery and the femoral vein, and generates an accurate 3D model of the fistula from non-contrast black blood MR images. In addition, our software automatically quantifies cross-sectional area of the vein, and other possible predictors of AVF maturation such as fistula angle and vein curvature.

We have analyzed six Yorkshire cross domestic swine subjects using our AVF analysis software and have quantified CSA, fistula angle, and vein curvature.

This study shows that even with low surgical variability denoted by small changes in fistula angles and vein curvature, there is significant variability in CSA of the vein which suggests that the pattern of stenosis is likely to be dependent upon hemodynamic profiles. We believe that this is a critically important finding at mechanistic, diagnostic, and therapeutic levels. At a mechanistic level the identification of specific hemodynamic profiles which result in venous segment stenosis could allow us to study the linkages between hemodynamics and venous biology. This could result in the identification of specific molecular shear dependent pathways. At a diagnostic level the early identification of “good” and “bad” hemodynamic profiles could allow us to distinguish AVFs into high and low risk groups, which could then be allocated appropriate and individualized process-of-care pathways. Finally, at a therapeutic level the identification of beneficial flow profiles could allow for the development of devices that could result in these optimal flow profiles with good downstream vasculature. The use of MRI-based CFD modeling has been shown to advance the understanding of the pathobiology of AVF development, specifically in the identification of the hemodynamic conditions that lead to pathologic changes such as stenosis³⁹. The accuracy of the MRI-derived CSA can also be used to determine end points for clinical trials of new therapies.

There are, however, some additional issues that need to be addressed before our technology is transferred into the clinical setting. These include:

- (a) MRI/MRA versus ultrasound: Although we are excited about the potential for the described MRI/MRA software to be able to play a role in the possible future risk stratification of patients, we also recognize that more work needs to be done to identify the exact place for our research, within the larger process of care for AVF maturation. In particular, some of us have been involved in studies that demonstrate the strong predictive ability for successful AVF maturation of 2-week and 6-week ultrasound data⁸. A better predictive and risk stratification ability of MRI/MRA technology will need to be proven in the clinical setting. Overall, we believe that the method proposed in this study, despite the disadvantage of the higher costs associated with MR imaging, offers significant advantages when compared to the standard ultrasound: MR imaging provides highly accurate flow and anatomic data (free of any possible interference derived from the pressure of the transducer or the skin or the skill level of the operator), our software automatically and objectively segments the imaging data and recreates a 3D model that provides a detailed tool for a comprehensive analysis of the AVF configuration. Furthermore, the combination of both, flow and anatomical configuration data, facilitates the generation of computational fluid dynamics, which brings in the possibility of studying and

visualizing flow parameters like wall shear stress and oscillatory shear index that can lead to the early detection of lesion prone regions.

(b) The femoral artery (4mm) and vein (6mm) in our pig model are much larger than the minimum clinical diameters recommended in ESKD patients (1.8 mm artery and 2.5mm vein). We anticipate that the efficacy of our software would not reduce when segmenting smaller vessels. Our algorithms would need to be used in the clinical setting and also compared to ultrasound data as described in (a) above.

(c) The described experiments were conducted in non-uremic pigs, without the endothelial dysfunction and oxidative stress that characterizes the uremic state. While our lab has since developed a uremic pig model, this would not address the myriad of other clinical issues linked to the vasculature in patients with ESKD, such as vessel size, medial calcification and pre-existing needle stick injury. We are confident that the efficacy and usefulness of the software tool developed to segment and generated 3D images of the AVFs is not affected by the presence or absence of renal failure in the animal model used.

We therefore recognize the importance of taking our algorithms into the real-world clinical setting of AVF creation in ESKD patients, ideally in a head-to-head comparison with standard of care duplex doppler ultrasound. Putting together our positive findings, our results suggest that the pattern of stenosis is likely to be dependent upon hemodynamic profiles and could be the first step towards a more precision-based approach to dialysis vascular access dysfunction at both a stratification and mechanistic level. This early stratification of AVF into high and low risk groups using our imaging software could result in an improved process of care and the potential selective use of future maturation therapies. Most importantly, our software algorithms could potentially hasten the adoption of advanced medical imaging into vascular access care at the level of (a) mechanisms, (b) developing novel therapies, (c) conducting clinical research, and (d) clinical risk stratification, all of which would result in added value to vascular access care by improving patient outcomes as well as reducing healthcare-related costs by providing specialized medicine.

Appendix 1. Segmentation of the Arteriovenous Fistula

In the proposed method, the initial step in the AVF segmentation is the identification of the vein and the artery. For cases that have flow information included, a script automatically identifies the different aspects of the fistula based on the following inputs:

1. The Black Blood File
2. The Flow in the Distal Artery
3. The Flow in the Proximal Artery
4. The Side where the Fistula is located.

Next, landmarks are manually placed at the center of the artery throughout the entire region of interest. Once the landmarks are placed at the beginning and the end of the fistula, the landmark is propagated among all the points that were previously selected. This is an automated process and it propagates the landmark for all the image slices that did not have one. Once the landmarks are propagated, a manual check is done to confirm that they accurately represent the center of the artery. Then, the regions are generated automatically across all the frames that have landmarks. Typically, the fistula covers 20-40 frames, depending on the size or on the position of the flow measurements. This phase may require looking at each of the different planes: axial, sagittal, or coronal. When creating a region in one of the view planes, this is drawn in each plane and removes the need for the artery to be imaged in a certain plane. This step takes about 10 minutes. Next, the same step is repeated for the vein adding 10 minutes to the process.

This gives us two sets of regions that may have intersected when automatically generated. Thus, following the generation of the vein, it is necessary to check each frame manually for accuracy. This can take the form of adding points to match more closely a complex geometry, or by moving the existing points. In the regions close to the anastomosis, it may be necessary to split the regions of the vein and artery. This is done by clicking a button (macro) and the regions in a frame are automatically split. After the splitting, it is necessary to manually alter the vein and region to create a more precise segmentation. This part takes around 20 minutes to complete.

Once the entire region of the vein and artery is generated, an image of the segmented fistula is obtained, and this allows to perform a visual quality check. Finally, a 3D model can be generated and saved as a part of the black blood file and as an .stl file. Overall the process for segmenting a fistula and creating the cut image takes approximately 40 minutes.

Acknowledgment and Contributions:

Authors:

José A. Rosado-Toro ^a, Rohit C. Philip ^{a b}, Samuel Thomas Dunn ^{a c}, Diego Celdran-Bonafonte ^d, Yong He ^e, Scott A Berceci ^e, Prabir Roy-Chaudhury ^f, Eleonora Tubaldi

- a) B105 Institute, University of Arizona, Tucson, AZ, USA
- b) Department of Electrical and Computer Engineering, College of Engineering, University of Arizona, Tucson, AZ, USA
- c) Department of Aerospace and Mechanical Engineering, College of Engineering, University of Arizona, Tucson, AZ, USA
- d) University Animal Care Department, The University of Arizona, Tucson, AZ, USA
- e) Department of Surgery, College of Medicine, University of Florida, Gainesville, FL, USA
- f) UNC Kidney Center, College of Medicine, University of North Carolina, Chapel Hill, NC, USA
- g) Department of Mechanical Engineering, University of Maryland, College Park, MD, USA

My contributions to this paper was the following:

- 4. Segmentation of the Fistula
- 5. Troubleshooting of the 3D Mode Generation Protocol
 - a. Identified Failure Modes
 - b. Helped Establish Best Practices
- 6. Figure Generation and Data Processes

3. Chapter 3: Computational Fluid Dynamics (CFD) of Arteriovenous Fistula

3.1 Introduction

In this Chapter, the objective is to perform a longitudinal study examining the hemodynamic parameters at day 3 in the vein's regions that experienced a CSA reduction at day 28. The overarching goal is to determine the flow factors that may contribute to the onset and progression of the stenosis. While geometric parameters such as angle of attachment and curvature influence the fistula maturation, there is still significant variation in end states (i.e., maturation vs failure). Hemodynamic factors, including wall shear stress (WSS) and oscillatory shear index (OSI), that can capture differences in fistulas that have similar geometrical parameters and allow for improved predictions of fistula maturation.

There is a general agreement that flow parameters have impacts on whether stenosis of the vein occurs, although there is no consensus on which factors are leading indicators of AVF failure. This study analyzes three AVF's at two separate time points to allow for a comparison between the flow conditions at the first time point and the CSA reduction/ in the second time point. The hemodynamic parameters of three AVF's are calculated using Computational Fluid Dynamics (CFD) modeling with the solver ANSYS Fluent.

A method is developed for using non-contrast MR Images and phase-contrast images to extract the 3D model of the AVF and to find the velocity profile used for the CFD analyses. From the CFD and the MR images of the AVF, the proposed method calculates the key hemodynamic and geometric parameters to determine markers of fistula maturation.

Particular attention in the analysis is given to the anastomosis region and, specifically, the first 20 mm of the vein, which represents the most critical AVF region in case of failure. To fully characterize this region, the vein CSA is divided up into quadrants and the sub-regions of the vein are investigated to account for localized flow conditions. High OSI in the internal region of the vein (the side closest to the artery) compared to the other vein regions at the same distance from the anastomosis region, appeared to be correlated with AVF stenosis at the later time point. The streamlines of the failed AVF show higher recirculation on the internal region of the vein and a higher flow rate on the external region. In the case of matured AVFs, low levels of OSI were seen in the internal region at day 3.

The potential link between CSA changes and OSI in the internal vein region might shed some light on the development of peripheral vein stenosis and it might be used in the future to develop a functional model to stratify patients into clinically high risk and low risk groups. While this study focused on Yorkshire cross domestic swine (*sus scrofa*), their resemblance to the human vasculature [22–24] potentially allows for rapid translation of our AVF functional analysis protocol to clinical settings

3.2 Methods

Two male Yorkshire Cross domestic swine were purchased from an USDA approved vendor and kept at the University of Arizona Animal Care Center. After 7 days of acclimation to the experimental facilities, AVFs were created between the external femoral artery and femoral vein. Black blood (BB) contrast-free MRIs were performed at 3 days for each pig. Three AVFs were created in total and had MRIs performed at 28 days to quantify neointimal hyperplasia or cross-sectional area [17]. Two AVFs were created in the same swine, while the a the third AVF were created in a second animal. The post-processing tool used to analyze the fistula was MATLAB (Mathworks Inc, Natick, Massachusetts).

MRI acquisition:

Contrast-free coronal BB sequences with spin-echo, segmented k-space, spoiled oversampling phase were acquired on 2 swine using a Siemens 3T Skyra scanner. For the first swine (i.e, swine 1 in Table 1), a CAIPIRINHA [15] variation of the BB sequence was used. All swine were imaged in the feet-first supine position. The BB measurement is taken at two specific locations perpendicular to the Distal and Proximal ends of the artery.

Segmentation:

For the segmentation of the 3 fistulas, the protocol discussed in Chapter 2 was used to create the 3D models of each one at day 3 and day 28, leaving a total of 6 fistulas. With the black blood measurements taken at specific locations on the artery, it is key in this step to segment the vein and artery past the point that the flow planes measurements were taken. After fully segmenting the vein and artery, a Matlab script is used to cut the segmented models. When saving the segmented model, it is saved to black blood file. When cutting the model, the following data is uploaded:

1. The Black Blood File.
2. The Flow in the Distal Artery.
3. The Flow in the Proximal Artery.
4. The Side where the Fistula is located.

The software identifies the coordinate plane that measurement was taken and then cuts the fistula to create open ends at each end of the artery and the end of the vein. After the cut, the ends of the fistula were each extended by 10 mm and capped to make the generated .stl file compatible with the ANSYS software. This extension on both the proximal and distal ends is to ensure the blood flow entering and

exiting the fistula isn't affected by the edge conditions of exiting a pipe flow. In addition to the extension, the model geometry is smoothed. The model was then smoothed and prepared for ANSYS in ICEM Fluent. The capped end was used to create the inlets and outlet for the simulation. Mesh independence was assumed as the protocol follows the outline of previous AVF studies and maintains the same meshing steps [4,37,46,56].

For case that the artery and vein are difficult to distinguish, the script developed in Chapter 2 for identifying the vein can be used. This is important for finding the fistula flow profile. The flow profile of the plane was extracted from the software program Segment. The inlet flow volume of the distal and proximal artery is used to generate the hemodynamic profile. The phase and magnitude images are loaded into the software. A region of interest (ROI) is drawn around the vein, the proximal artery, and the distal artery for each time point in the cardiac cycle. If aliasing exists on the image, then the pixel intensity is corrected. The velocity flow is calculated and used as the initial flow boundary conditions for the CFD.

CFD:

The hemodynamic profile paired with the 3D model are inputs to the generation of the Computational Fluid Dynamic (CFD) simulation. The WSS, OSI, and the streamlines are obtained from the CFD analyses.

The 3D model is imported into ANSYS Fluent, and the model is scaled to the correct dimensions in millimeters. The velocity profile is uploaded for the boundary conditions of the distal artery and proximal artery and are designated the inlets. The fluid velocity entering the proximal and the fluid velocity exiting the distal artery are used as the inlet boundary conditions. The vein is considered the outlet boundary of the simulation and is not imposed by the blood flow.

The fluid is modeled as a viscous-laminar fluid and the type of simulation is set as transient. The blood fluid properties are considered with a density of $1050 \frac{kg}{m^3}$ and the viscosity $0.0035 \frac{kg}{m*s}$.

The high pulsatility of the fluid is considered using the Fluent Second Order Implicit method as the solution method for calculating the Transient Formulation. The Pressure-Velocity Coupling is calculated using the standard SIMPLE algorithm used in Fluent. The Pressure is calculated to Second Order level of accuracy, while the momentum is calculated using a Second Order Upwind method. The Gradient is calculated using the Fluent Least Cells Based method.

The monitor results created were for the Area-Weighted Average of the Wall Shear Stress and the Mass Flow Rate. The step-size used was $\frac{1}{1.5 * (\text{total time in milliseconds})}$. This results in step-sizes that have a $\Delta t < .001$ [4,37,46,56], which is consistent with previous AVF studies.

Post-Processing:

The CFD results were imported into TecPlot (TecPlot Inc., Bellevue, Washington) to generate the WSS, WSSG, OSI for each point in the AV fistulae. The CFD data is imported over the time domain of 0.5-1.5 seconds. This is done to keep the calculations within one cycle, as metrics like OSI are time-averaged. These values are used to produce 3D plots and the data containing the WSS, WSSG, and OSI is exported as a .dat file. This data file is imported into MATLAB.

In MATLAB, the data is processed to show heatmaps of the WSS and OSI for each fistula timepoint. The fistula geometry is used to extract the CSA from the fistula. The CSA for each fistula is plotted for both timepoints. The CSA at 3 Days for each fistula compared with the fistulae CSA measured at 28 Days. A 50% reduction of the CSA is marked as a failed AVF and that stenosis has occurred. The CFD analysis is run at 1.5 cycles, meaning data needed to be clipped and reordered to show results from 1.0-1.5-.5-1.0 to capture the normal cardiac rhythm.

Using the method described in Chapter 2, the anastomosis plane was calculated, along with the angle of attachment for each fistula. For this study, the algorithm for angle determination was refined to account for the curvature of the artery by adding additional points of the arterial centerline. Four quadrants were created for the vein CSA (Figure 12): the *internal region* with respect to the artery, the *external region* with respect to the artery, the *upper region*, and the *down region*. The WSS and OSI values were mapped to the wall of the vein and averaged within the aforementioned regions.

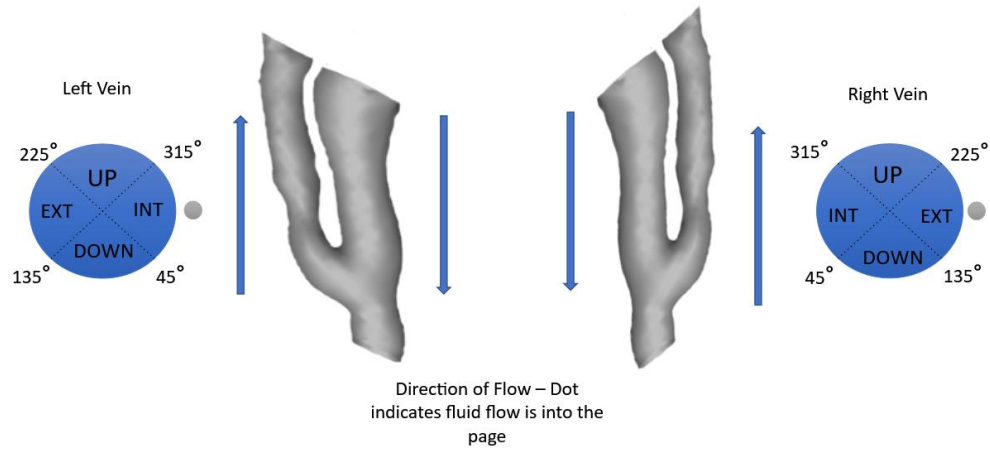


Figure 12: Depiction of vein subregions and the direction of blood flow.

To estimate how the CSA vein values changed over time for a given region, ΔCSA are obtained as follows

$$\Delta CSA = \frac{(Day\ 28\ CSA - Day\ 3\ CSA)}{Day\ 3\ CSA} \quad (7)$$

The OSI at Day 3 for each fistula was compared to the normalized CSA change. The software ANSYS Fluent was used to calculate the streamlines over the entire fistula and the velocity and vorticity values along the vein at 5 mm, 10 mm, and 15 mm distance from the anastomosis plane.

3.3 Results

Swine Fistula	Case 1		Case 2		Case 3	
Time point	Day 3	Day 28	Day 3	Day 28	Day 3	Day 28
Angle (°)	60.9	65.4	37.4	29.3	53.3	58.6
Mean Curvature (κ)	.1121	0.0927	0.0844	0.0681	0.0734	0.0686
Maximum Curvature (κ)	0.2687	0.2666	0.1799	0.1317	0.1171	0.1347
Mean CSA Proximal Artery (mm ²)	19.1450	29.2640	25.4325	63.5813	23.7992	23.5174
Mean CSA Distal Artery (mm ²)	35.2856	61.9172	27.1404	72.5683	22.0683	22.0532
CSA Anastomosis Plane (mm ²)	17.810	23.280	23.920	28.310	25.050	32.980
Minimum CSA Vein (mm ²)	11.4700	14.1400	12.3700	1.2600	8.3000	10.1200
Δ CSA Vein (mm ²)	4.3325		-12.5169		-2.4273	

Table 5: Fistula Data

The AV fistula configuration is an important aspect of how the flow develops. The angles (See Table 4) that are close to 55° seems to align with an increased likelihood of maturation, which is the configuration in Case 1 and Case 3 [41, 42]. As stated earlier, angles lower than 30° tend to require multiple intervention to prevent stenosis from occurring [41]. In Case 2, the angle is 37° and drifts below the lower threshold at 29°. This shift suggests that fistula configurations near the 30° angle are at risk of the geometry shifting and bringing the angle under that threshold [41]. This shift may be due to the vascular remodeling that occur due to the flow conditions. Indeed, the initial angle configuration may contribute to the higher level

of recirculation in the internal region of the vein. This leads to higher fluid velocities flow rate on the outer region of the vein due to how the flow is redirected. Based on the average CSA at day 28, Case 1 and Case 3 have achieved full maturation while Case 2 had significant stenosis occurring with the mean CSA reduction by more than 10 mm^2 seen in Table 5.

The curvature of the three AVF did not have large differences between the three of them. Case 1 had a higher maximum curvature of .269 compared to the other cases, although the average of .112 was much closer to the other two cases' average. Both Case 2 and Case 3 had similar levels of curvature and, interestingly, the vein in all three cases had a reduced curvature at Day 28.

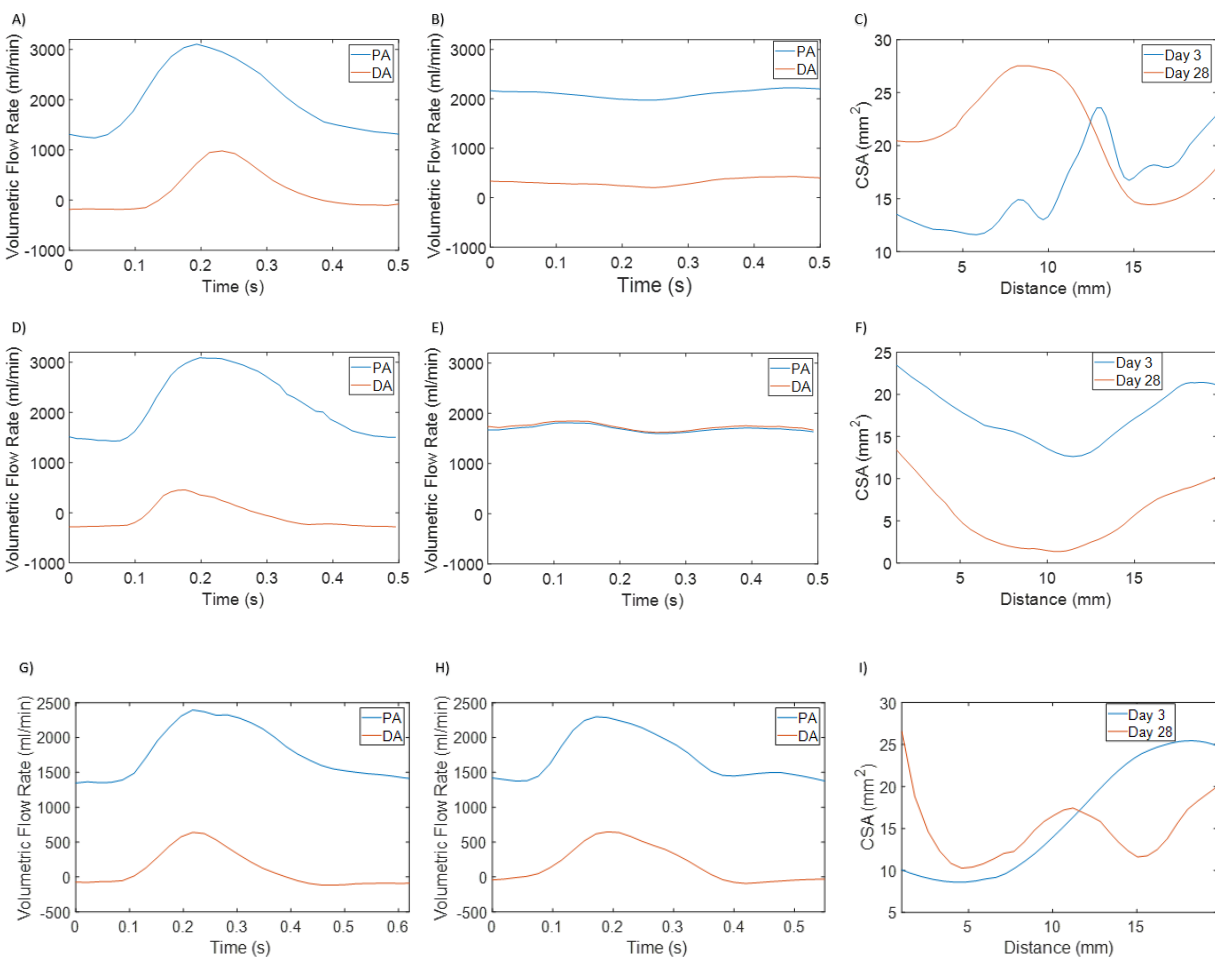


Figure 13: Fistula Flow Rates. Fistula Case 1 A) Volumetric Flow Rate Day 3 B) Volumetric Flow Rate Day 28 C) CSA at Day 3 and Day 28
Fistula Case 2 D) Volumetric Flow Rate Day 3 E) Volumetric Flow Rate Day 28 F) CSA at Day 3 and Day 28
Fistula Case 3 G) Volumetric Flow Rate Day 3 H) Volumetric Flow Rate Day 28 I) CSA at Day 3 and Day 28

A key aspect at the Day 3 timepoint is that most of the blood flow flowed through the vein as it is a low-pressure vessel (Figure 13 A, D, G) implying that all three cases the surgery was successfully performed. Additionally, one of the clear markers of stenosis is when the Distal and Proximal artery volumetric flow rates match, indicating that minimal blood flow is moving through the vein due to CSA reductions. In all the cases, the Distal artery produced a backflow in the artery and into the vein at diastolic pressure. In Figure 13, positive flow through the distal artery means that the blood is exiting at the distal end. At the systolic pressure, that construction holds true. For Case 2, the flow rates had a net negative flow through the distal artery, which means that nearly all the blood is flowing through the vein in this situation. The flow rate is a snapshot of approximately 0.5 seconds, and so it is likely that there is variation between cardiac cycles that would drive a net positive volume of blood through the distal artery at time intervals to allow for there to be a backflow. Having significant intervals of Distal artery net backflow may be a contributing factor to CSA reduction.

Having a higher flow rate through the vein had variable effects on each of the cases and within the cases themselves. In Case 1 and Case 3 (Figure 13 C, I), the CSA had a general increase between the two timepoints over the first 10 mm and Case 1 appears to have a significant CSA increase up to ~12 mm.

In Case 2, the CSA had significant decreases over the entire 20 mm examined and all blood appears to have stopped flowing through the vein altogether and resulted in stenosis. This contrasts with Case 1 and Case 3, which both maintained a high mass flow rate through the vein. At day 28, flow profile in Case 1 more closely resembles that of a vein (Figure 13 B). The low-pressure of the vein appears to have been able to disrupt the typical shape of the cardiac cycle for an artery and had a relatively constant volumetric flow rate. Past the 12 mm distance, the CSA did have a small reduction. But overall, there was an increase in the mean CSA over the length of the vein.

Case 3 managed to maintain a similar profile to day 3. The CSA at Day 3 started at 10 mm^2 and had a large increase at Day 28 near the anastomosis region and had a small increase over next portion of the vein. Over the 10 mm to 20 mm section, there was a reduction of over 50% in the CSA but no region of the vein that dropped below the minimum CSA recorded at day 3 (Figure 13 F). Despite the high reduction in CSA, the CSA did not drop below the Day 3 minimum CSA. With the volumetric flow rate at day 28 staying close to the day 3 rate, the case was considered to have been successful.

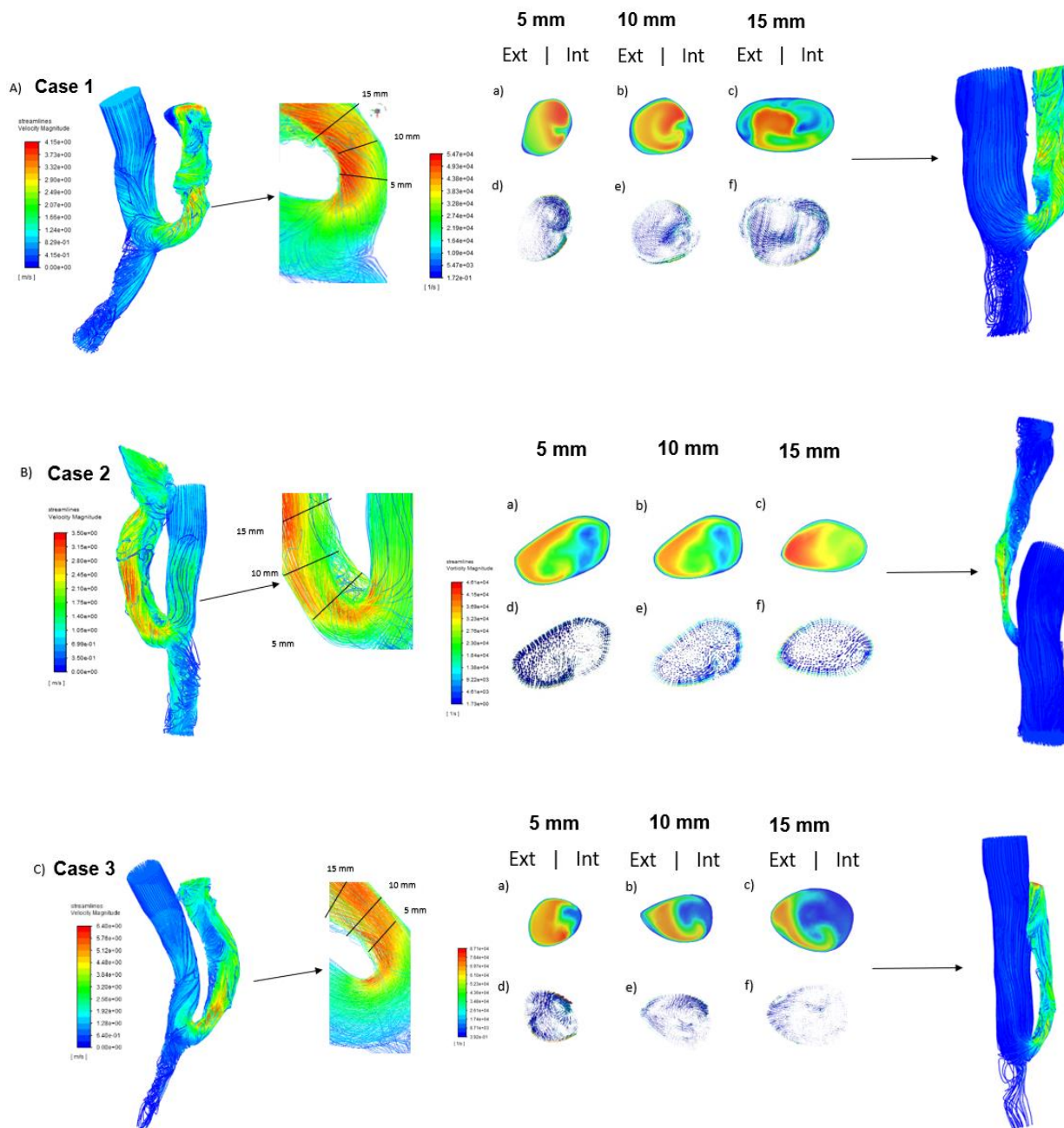


Figure 14: A) Fistula Case 1 with Velocity Streamlines at Day 3 and Day 28 1 A-a) Velocity Heatmap at 5mm A-b) Velocity Heatmap at 10mm A-c) Velocity Heatmap at 15 mm A-d) Vorticity Heatmap at 5mm A-e) Vorticity Heatmap at 10mm A-f) Vorticity Heatmap at 15 mm B) Fistula Case 2 with Velocity Streamlines at Day 3 and Day 28 1 B-a) Velocity Heatmap at 5mm B-b) Velocity Heatmap at 10mm B-c) Velocity Heatmap at 15 mm B-d) Vorticity Heatmap at 5mm B-e) Vorticity Heatmap at 10mm B-f) Vorticity Heatmap at 15 mm C) Fistula Case 3 with Velocity Streamlines at Day 3 and Day 28 1 C-a) Velocity Heatmap at 5mm C-b) Velocity Heatmap at 10mm C-c) Velocity Heatmap at 15 mm C-d) Vorticity Heatmap at 5mm C-e) Vorticity Heatmap at 10mm C-f) Vorticity Heatmap at 15 mm. The velocity heatmaps are oriented with the external region of the vein on the left and the internal region of the vein cross-section on the right. Note: The day 28 arteries have higher velocity magnitudes closer to the arterial centerlines that are not visible due to the angle the fistulae are shown at.

In Figure 14 the vein flow velocity profile at Day 3 is analyzed at three different locations (5 mm, 10 mm, and 15 mm) with respect to the anastomosis plane. In general, the Velocity heatmaps plots (Figure 14 A-a, B-a, C-a) show that the internal region has a reduced flow velocity compared to the average of the cross-section of the flow. The exception was for Case 1 at 5 mm (Figure 14 A-a), the external region has a velocity magnitude that is equal or lesser when compared to the velocity of internal region. The internal region maintained a high velocity with only a small portion of the region having a reduced relative flow. As shown in the vorticity heatmap (Figure 14 A-d), the outer region has little to no recirculation even with the lower velocity magnitude. The internal region seems to present a low level of recirculation but that noticeable portion of the blood does have a slight oscillatory nature to the flow. At the 10 mm section (Figure 14 A-b), Case 1 had an evenly distributed velocity with the vorticity (Figure 14 A-e) remaining low. At 15mm (Figure 14 A-c), recirculation maybe occurring as the velocity around the internal region and the edges is lower, while the vorticity (Figure 14 A-f) is relatively higher in the low velocity regions. Considering the anastomosis region, the velocity streamlines show a steady flow with few occurrences of eddies. The higher curvature of the vein compared to the other cases may have contributed to a more uniform velocity profile.

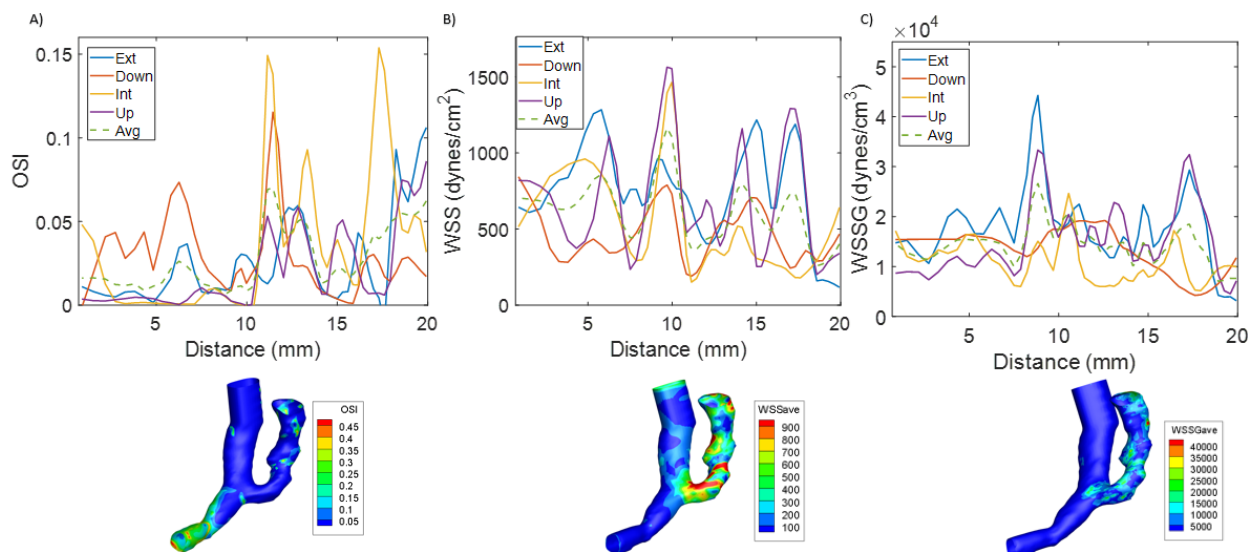
Case 1 that successfully matured presents at 5 mm a more evenly distributed velocity profile when compared to the failure AVF Case 2. For Case 2 at 5mm (Figure 14 B-a), the velocity of the internal region was much lower at the systolic velocity when compared to the external region of the vein. The vorticity plot (Figure 14 B-d) shows that the recirculation is occurring, with a relatively steady rotational aspect to the flow over the entire cross-section with a peak along the wall of the internal region. At 10 mm (Figure 14 B-b), the velocity profile is more evenly distributed but the relative minimum is still along the internal vein region. The vorticity (Figure 14 B-e) is concentrated only along the edge of the vein's wall. At 15mm (Figure 14 B-c), the increase in CSA appears to have led to a lower overall velocity and an increased vorticity (Figure 14 B-f) over the entire section with the peak being along the walls. Examining the streamlines of the internal region (Figure 14 B), the vein appears to have recirculation occurring and a greater mass flow rate along the external edge of the vein.

For Case 3 (Figure 14 C-a, b, c), the velocity profile at each of the three cross-sections have a similar distribution, with the velocity decreasing over the course of the vein as the CSA increases in area. At 5mm (Figure 14 C-d), the vorticity levels are significant over the entire vein with the minimum being near the internal regions. The 10 mm cross-section's vorticity (Figure 14 C-e) is low throughout the vein with

an exception at the upper region of the vein which has a higher level of vorticity. The streamlines of the anastomosis region show a strong flow with little visible recirculation.

By comparing the trends of the three cases, the internal region is the most likely to have a reduced velocity. Vorticity seems to be present in each of the cases, and the areas with lower velocity are likely to have higher levels of vorticity.

When the 15mm distance is reached, the recirculation regions are less dependent on a specific region and any of the subregions has the potential for areas of lower velocities profiles. As the flow develops over the course of the vein, the dominating effect on the flow profile becomes the curvature of the geometry and the variation of the CSA over the length of the vein. For regions with relatively higher flow recirculation, the CSA reduction appears to be more likely.



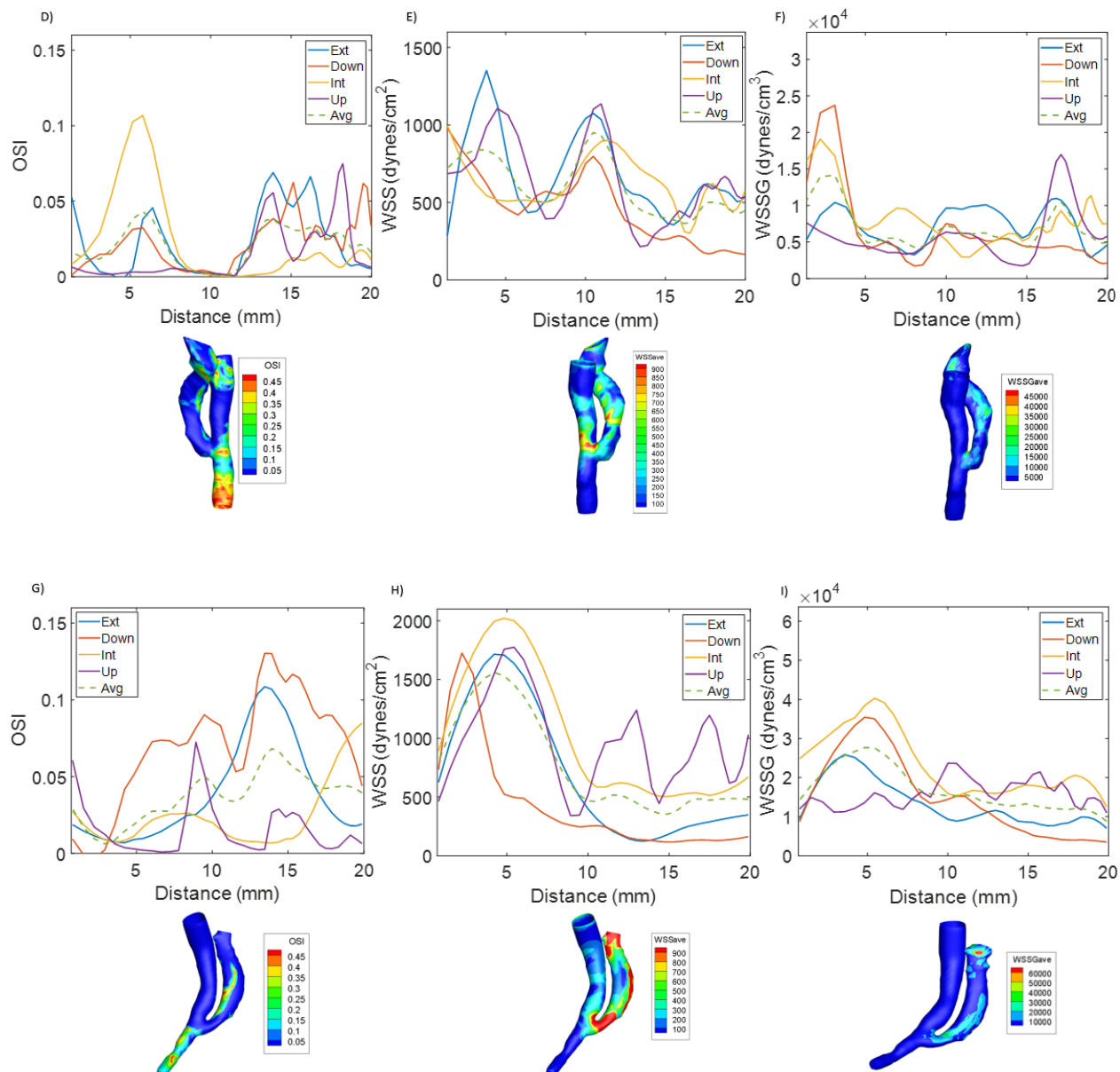


Figure 15: Hemodynamic Parameters at Day 3 with the below fistula displaying the corresponding parameter A) Case 1 OSI B) Case 2 WSS C) Case 1 WSSG D) Case 2 OSI E) Case 2 WSS F) Case 2 WSSG G) Case 3 OSI H) Case 3 WSS I) Case 3 WSSG. The units of the 3D model match the units of the paired plot.

The first 20 mm of each fistula was examined to avoid the edge effects of the extended vein. The veins were divided into four subregions. This was done to avoid averaging out the extremes potentially seen in the vein CSA. By creating smaller regions to average for analysis, the effects of the flow characteristics can be analyzed granularly without creating regions too small that potential outliers from the simulation dominate the averages. *Internal* refers to the region of the vein that is closest to the artery. The *external*

region is the portion of the vein that is farthest from the vein. The “Up” and “Down” regions are the remaining sections of the vein, with the naming convention used to have a consistent reference for the region between the fistulas.

Considering the WSS independently across the three cases, the WSS varied significantly over the length of the vein. In Case 1, the vein WSS (Figure 15 B) maintains the same range of values and behavior over the entire vein. When looking at the vein subregions, the WSS tends to remain lower where the OSI is higher, while the inverse is true with the WSS is lower. Since the OSI is defined based on the WSS, the lower the shear stress, the more directional difference will affect the OSI. The OSI (Figure 15 A) has a clearer trend in comparison. Early in the vein, the average of the OSI is relatively low until the flow passes the 10 mm mark. The “Down” region within the vein has a relative peak with a low WSS. Past the 10 mm point of the vein, the OSI has a large increase in the internal region with the peaks coming at approximately 11 mm and 17 mm. The Down region also sees a peak at the 11 mm point. The WSS is lowest along the internal region of the vein wall and is below the overall average WSS. Thus, the vein is showing a sustained level of high OSI with a low WSS over the region that saw a reduction in CSA. The third parameter examined was the WSSG (Figure 15 C). The WSSG is steady until the 8 mm point, where the average the External and Upper region has a spike. The WSSG for the internal region is low throughout the vein with one spike at 11 mm. The WSSG describes how much change in the shear stress is occurring over the averaged values of the region. The peaks in the WSSG show that there is significant change in WSS along the vein, and the OSI due to its relationship with WSS. Looking at the 3D plots of the parameters, the artery has low OSI over the Proximal end, while seeing a spike near the end of the Distal end. The WSS is reverse scenario, as it is higher prior to the anastomosis plane. Over the length of the artery, the WSSG is constant as the changes in the WSS neighboring locations do not have drastic changes.

In Case 2 (Figure 15 E), the average WSS is decreasing as the flow moves farther along the vein. In the first 7 mm, the External and Upper region have peaks in the WSS, while the Internal and Down regions had relative minimums. After the peak at 11 mm, the WSS for each region decreases. When examining the OSI, the average is below 0.5 over the length of the vein. At the 3 mm to the 8 mm point, the OSI of the internal region has a peak greater than .1. The Internal OSI (Figure 15 D) remains for the remainder of the vein. After 12 mm, the OSI of the other three regions peak and maintains a high level of OSI. This suggests that there is recirculation occurring at high levels over the entire vein. The WSSG (Figure 15 F) for this case has an initial peak, but when it is compared to the other fistulas, the WSSG is low. This

suggests that the variation on the vein's wall are small changes and that the observed averages are adequately describing the behavior. The arterial flow for the proximal side of the fistula has a high WSS and low WSS for the distal end. The OSI is significantly higher when compared to the first case. Due to the low blood flow, there is significant recirculation as the blood moves through the artery. In addition to the low blood flow, the backflow in this fistula likely contributes to the observed OSI. When looking at the WSSG, the artery is relatively low across the entire length of the artery.

In Case 3, the WSS (Figure 15 H) is at its maximum value across all regions, the Down region seeing a drop off at the 3 mm point. After 10 mm, the shear stress decreases across the vein, with the only exception being the Upper region. This decrease corresponds to the increase in CSA and a lowering of the mean velocity. The average OSI (Figure 15 G) remains low for the first 10 mm, with the Down region having a large amount of recirculation. Past the 12 mm mark, the OSI peaks for the fistula in the External and Down region. The average OSI sees an uptick and the internal region reach as maximum at the end of the analyzed range. For the WSSG, there is peak at 5 mm, with it being the largest among the 3 cases. This suggests that the vein is experiencing significant variability across the regions close to the anastomosis region. This variability drops to the same level of the other cases after 10 mm. The arterial flow characteristics follow that of Case 1. The proximal arterial WSS is high prior to the anastomosis plane and low after passing to the Distal end. The OSI sees the reverse effect, with high OSI on the distal end and low on the Proximal side. The WSSG (Figure 15 I) is constant throughout the artery, supporting the notion that the flow conditions for the artery are stable 3 days post-operation.

When comparing the results between the 3 cases, the WSS and WSSG independently do not have clear correlation to when CSA reduction may be at risk of occurring. In regions where there is high OSI, the WSS is lower than average but the WSS itself does not provide a clear indication of future CSA reduction. Although a low WSS tends to occur when the OSI is larger, a low WSS does not mean that a high level of recirculation is occurring. The WSSG results suggest that the part of the vein closest to the anastomosis region has the greatest likelihood of seeing large variations in WSS, as this is where the disruption point of normal arterial flow occurs. The WSSG does not seem to project regions of risk but identify changes where flow conditions are stable. For OSI, the regions that experience high OSI follows CSA reduction at Day 28. Based on fistula configuration, the internal region of the fistula is at the highest risk of having recirculation occurring. In case 2, the high OSI in the internal region appears to indicate a risk of CSA reduction in the first 10 mm. The other cases had low Internal OSI values in the anastomosis range. For Case 1, the Down region OSI value was relatively high compared to the average but was still half of the

peak OSI seen past 10 mm. Past 10 mm, the Internal region peaks with low WSS, and this is the region that does see a downstream reduction in CSA. In Case 3, there is relatively low OSI for most quadrants except for the Down region. In this region, the WSS is still relatively high. When looking at the OSI with respect to the change in CSA, the CSA still increased at Day 28, although the CSA increase was much smaller compared to the change in CSA up to that point. This implies that the flow parameters have downstream effects on the changes in CSA, and that each wall segment is not independent.

In Case 2, the high internal OSI highlights the part of the vein that had the highest CSA reduction, although the entire vein experienced a reduction in CSA. Past 10 mm, any subregion of vein is as likely as another subregion to have a high level or a low level of OSI. Slightly after the drop in OSI near 10mm, the CSA decrease becomes less severe. Then there is an uptick in the overall OSI while the increase levels off.

For each fistula that had reduction in CSA past 10 mm, the average seemed to be as good of an indicator when compared the internal region. Though the internal region had high OSI when reduction occurred, other regions had high OSI and had a higher average. Since reduction appears driven in regions when OSI is high and the flow further down the vein is less directly impacted from the anastomosis region, any region is as likely as the other to have recirculation. In summary, the areas that have high OSI and CSA reduction correspond to regions with low WSS and low WSSG. When the WSSG and WSS are higher, the regions that have relatively higher OSI did not have clear correlation with CSA reduction.

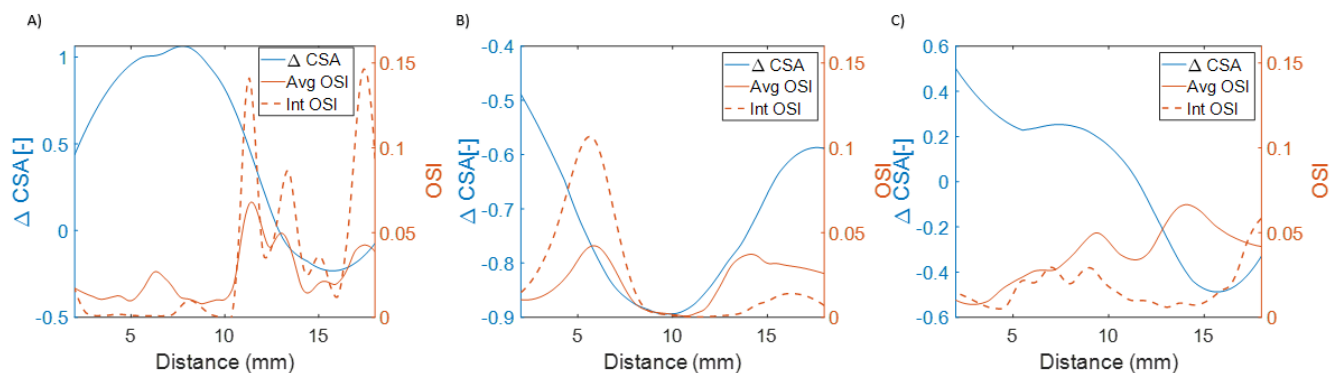


Figure 16: ΔCSA vs Average OSI and the OSI of the internal Subregion A) Case 1 Change in CSA vs OSI B) Case 2 Change in CSA vs OSI C) Case 3 Change in CSA vs OSI

When looking at the Internal OSI and average OSI in directly to the change in CSA (figure 16), there are a few aspects that should be pointed out. There typically is a peak in OSI before the CSA reaches its maximum decrease. When focusing on changes in CSA for Case, there are two key aspects. The first is

that there is low OSI over in the internal region and the whole average where the CSA is at its largest. The second is when the CSA is decreasing, there is a spike in both the average and in the internal OSI. Following this peak, the fistula CSA at Day 28 reduces below where it was at Day 3. As the OSI decreases at the CSA minimum before starting to increase. An important aspect to consider is that change in CSA does not capture the situations where there is an increase in CSA that is larger than an earlier segment. In this situation, there appears to be a CSA decrease when the reality is that the CSA maintained the Day 3 area. Despite the reduction of CSA further down the vein, the original vein segment had a larger CSA at Day 3, which provided buffer for when reduction occurred.

For Case 2 (Figure 16 B), the CSA change is negative over the entire vein and should be considered a total stenosis. The Internal OSI matched the behavior of the average OSI, but with much higher values peaks. The peak in internal OSI occurs just prior to vein CSA change reaching its maximum CSA reduction in the vein. When the OSI reaches a minimum value, the CSA change reaches a maximum reduction, and then reduction lessens. This minimum seems to correlate with where the vein starts to increase in CSA again. Looking at the non-normalized CSA values, the fistula vein after ~12 mm CSA started from a larger CSA. After that 10 mm point, the average OSI increases again and the CSA rate of change decreases again.

In our third case (Figure 16 C), the internal OSI is relatively low over the examined range and there is no CSA reduction until we are past 11 mm. At this point, the average OSI is growing and reached a maximum OSI prior to the point of the highest amount of CSA reduction. The reduction in this case more closely follows the average OSI increase. When looking at the *Down* region of the vein, the OSI peaks follow the CSA reduction closer than the average. One more aspect of the CSA is that at Day 3, the CSA starts low and increases over the entire range. So, although there was a reduction in the CSA, the Δ CSA captures the rate at which the vein CSA converges to a similar value. This implies that the previous CSA segment has an impact on the connected segment downstream.

4. Chapter 4: Conclusion

4.1 Conclusions

This study aims to determine which hemodynamic features of an AV fistula 3 days after surgery can impact the AVF maturation after 28 days. The hemodynamic profile is impacted by a variety of factors, with the primary ones being the vein CSA, velocity profile, the angle of attachment, and the curvature of the vein. The change in CSA from the vein accelerates the blood flow through the vein to maintain conservation of mass and causes a major increase in the WSS. The angle of attachment and the curvature dictate the regions of the vein that experience high velocities magnitudes and which regions experience lower velocity magnitudes. The regions of the vein with a lower blood flow velocities are more prone to recirculation and high levels of recirculation are thought to lead to stenosis. This is captured with flow parameter of OSI.

The results of this study examined three AVFs within the porcine animal model. With high levels of OSI in the internal region of the vein (*i.e.*, towards the artery), there appeared to be a reduction of CSA at Day 28. At the locations of high OSI, the WSS was relatively lower compared to the average. The low WSSG indicated that the hemodynamic profile near the vein wall was similar and directional changes were small. This implies that a region undergoing high levels of recirculation are likely to maintain those high levels of OSI. High levels of WSSG seem to indicate that the local directional changes are significant. The results suggest that of the hemodynamic parameters, OSI in the internal region of the vein might be linked to a CSA reduction that should be explored in further studies. The three parameters likely have impacts on gene expression, wall thickening and stenosis, but more AV fistula experiments are necessary to characterize these effects. With more AV fistula data, direct relationships can ideally be established with maturation and stenosis.

Considering the velocity streamlines and vorticity, the steady flow along the vein walls was important for maturation. The regions with high levels of recirculation at Day 3 corresponded with the regions that had CSA reduction at Day 28, even in the cases that matured. The AV fistula with higher relative curvature had a more uniform velocity profile compared to the straighter configurations in Case 2 and Case 3. The

difference in curvature may have contributed to the differing results seen in Case 1 and Case 2, even though they were created in the same animal.

The other key aspect of the study is the generation of the 3D models from the swine fistulas. With larger vessels being analyzed in the animal study, the transition to human fistulas will be a key challenge to overcome with the current imaging techniques.

With further characterization of hemodynamic profiles in AV fistulas in conjunction with the physical configuration, a risk categorization profile can ideally be generated and provide insight into biomechanical reason for fistula stenosis. With the risk stratification, there hopefully can be an improvement in patient care for end-stage renal failure. With the goal of reducing fistula failure rate and allow for earlier interventions to avoid prolonged patient wait times for safe vascular access.

4.2 Limitations and Future Work

Sample size is a major limitation with this study. With an N of 3 for the CFD study, there were not enough AVF fistulas studied to come to firm conclusions about the role of OSI, WSS, and WSSG in the maturation process. There are many factors that can lead to a failed maturation. Fistula configuration drives the shape of the flow. The curvature of the vein and the angle of alignment both have an impact on future maturation. Gene expression has a major impact on the occurrence of stenosis as well. Wall thickness was a characteristic that was not measured and would have an impact on how the vein would respond to the increased flow. As a result, purely analyzing the hemodynamic parameters helps to build the picture of why stenosis may be occurring. Increasing the number of AV fistulas studied with this technique with multiple configurations would help to begin creating risk categories. In addition, it would be able to help physicians to avoid configurations with adverse outcomes.

Gene expression can drive stenosis as well as mechanical changes as well and is assumed to play a major role in success or failure. The change in mechanical stresses along the cell walls activates protein expression and can either thicken the vein, making the vein more arterial, or drive stenosis. A future study involving blood panel testing would be a first step in understanding how WSS and OSI change the histology of the vein. By characterizing protein expression, there would be two potential pathways to improve fistula maturation rates. The first would be to determine configurations that reduce the expression of pro-thrombotic factors and reduce the stenosis through drug therapies. The second path would be to adjust the AV fistula configurations to determine an alignment that would reduce pro-thrombotic factors and reduce the occurrence of stenosis by adjusting the geometry.

In additional studies, measuring the wall thickness at the initial time point and at the study endpoint would allow for an examination of a few aspects. The first would be how the vein thickness affects the outcome of the procedure. During the surgical procedure, the vein is manipulated to be able to be attached to the artery and to be accessible for cannulation. As result, the vein may be stretched and result in thinner vessel walls. In a second scenario, different vein configurations may require longer veins to be able to achieve intended curvatures. Discovering wall thickness impact may aid in risk classifications of fistulas.

A major drawback of the study is that the pigs that were studied were healthy and were not experiencing kidney failure. Uremia is the condition of having high level of toxins in the kidneys. Kidney

failure affects the blood content. Though pigs are good analogs for human cardiovascular systems, having a uremic model would allow for a closer analog to physiological conditions a patient with end-stage renal failure would experience.

Additionally, how the vein is attached and remodeled for cannulation has an impact on long-term development and is out-of-scope in this study as well. This study only focused on the maturation process of the anastomosis region and the effects of cannulation and repeated needle use impact the long-term success of fistulas.

Applying these methods in clinical settings is ideal for future studies. With the difference in animal models and human cardiovascular systems, eventually proving the method in a clinical setting would hopefully allow for novel treatments for patients enduring end-stage renal failure.

5. Appendix:

The following depicts additional figures that were generated as a part of the analysis:

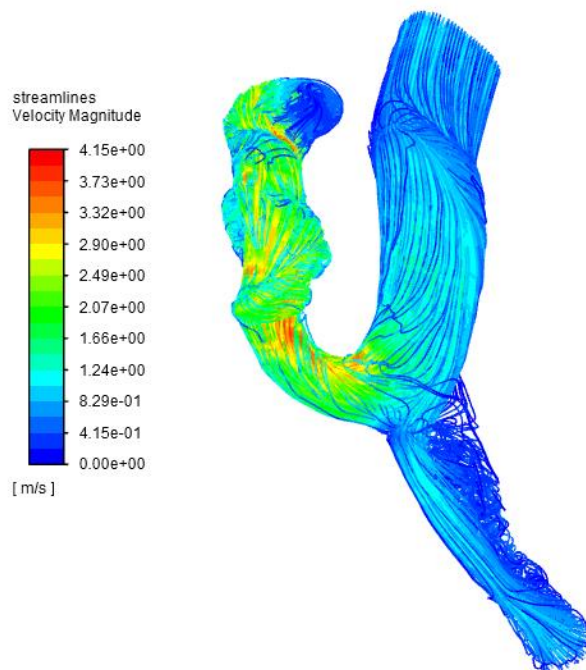
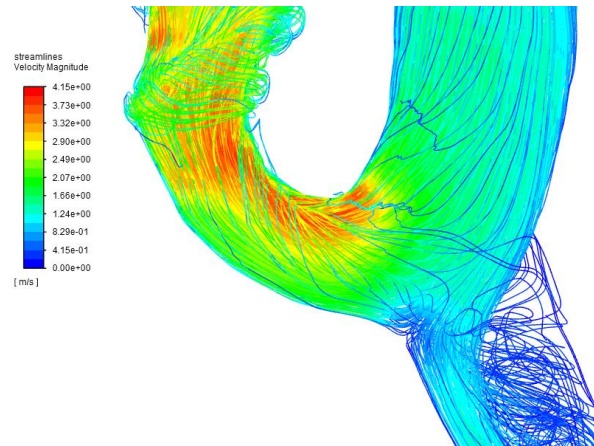


Figure A.1 Alternative Streamline angle for Case 1 Fistula at Day 3



A.2 Alternate Zoomed view of velocity streamlines for Case 1 at Day 3

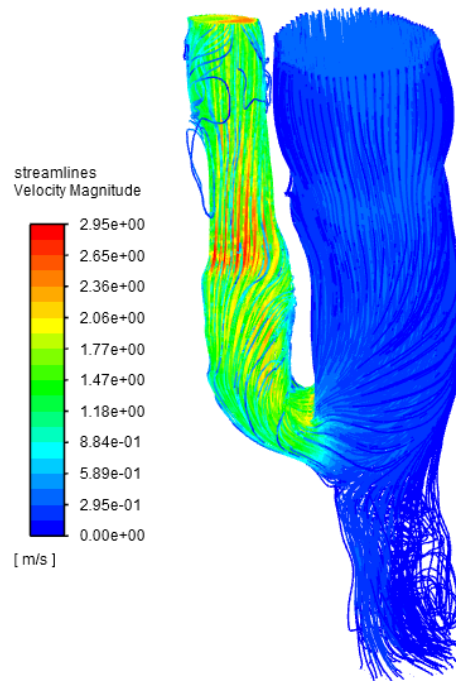


Figure A.3 Alternative Streamline angle for Case 1 Fistula at Day 28.

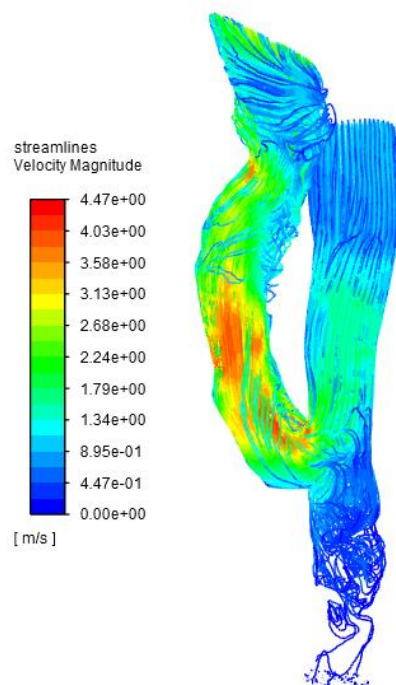


Figure A.4 Alternative Streamline angle for Case 2 Fistula at Day 3

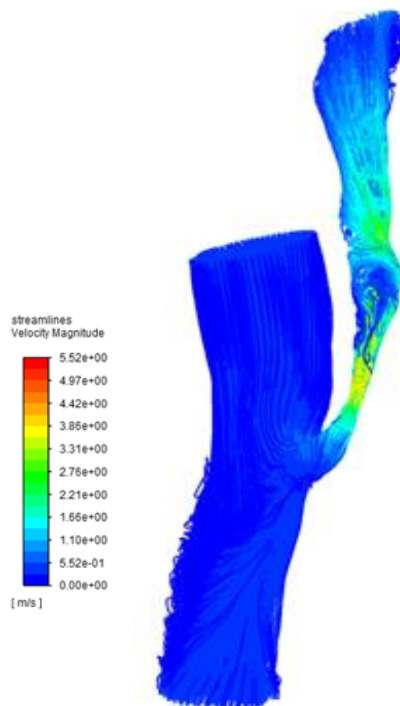


Figure A.5 Alternative Streamline angle for Case 2 Fistula at Day 28

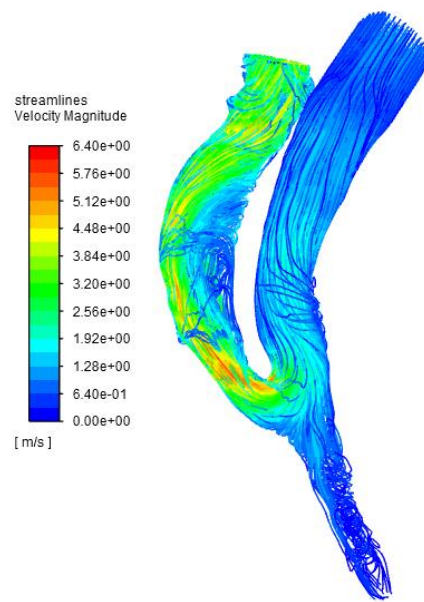


Figure A.6 Alternative Streamline angle for Case 3 Fistula at Day 3

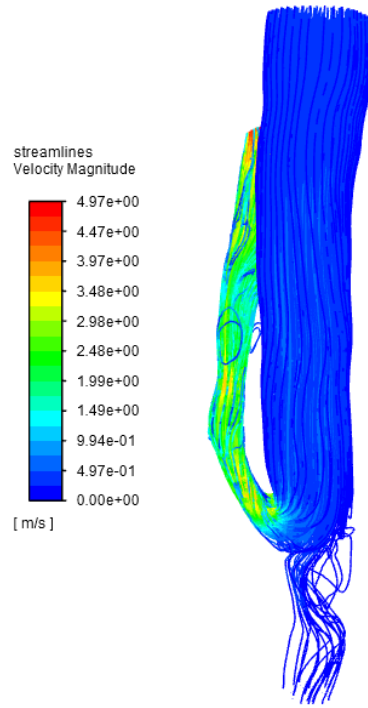


Figure A.7 Alternative Streamline angle for Case 3 Fistula at Day 28

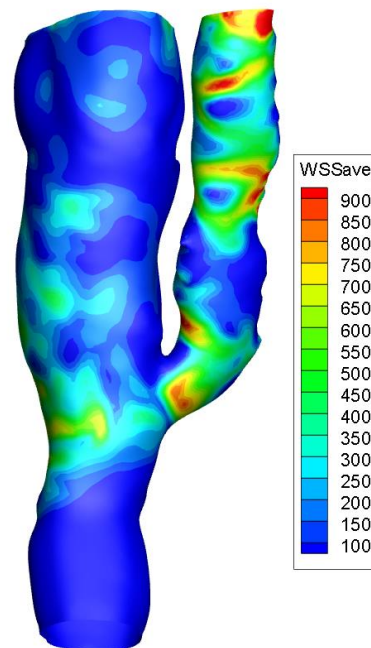


Figure A.8 WSS ($\frac{\text{dynes}}{\text{cm}^2}$) Case 1 Fistula at Day 28

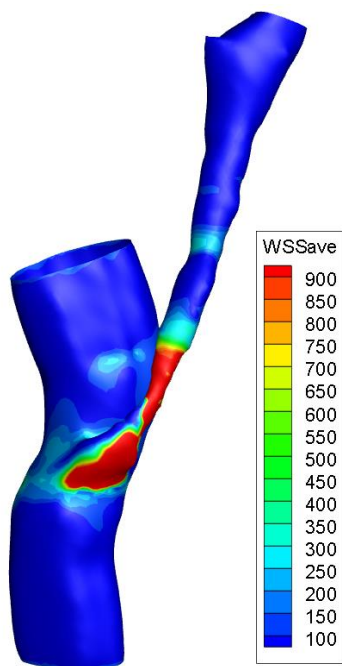


Figure A.9 WSS ($\frac{\text{dynes}}{\text{cm}^2}$) Case 2 Fistula at Day 28

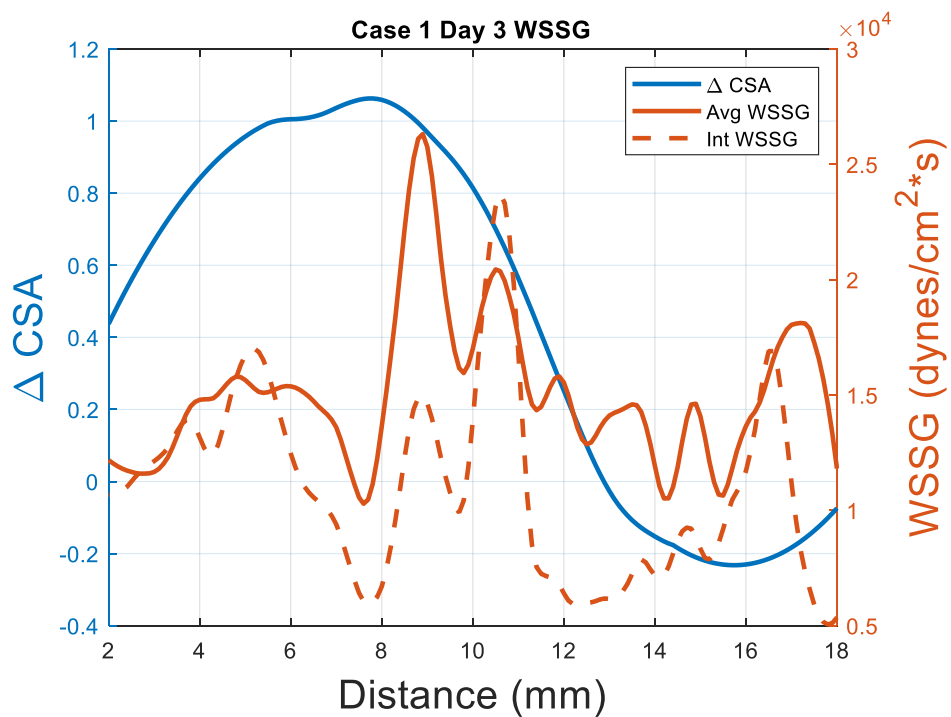


Figure A.10 WSSG ($\frac{\text{dynes}}{\text{cm}^3}$) vs ΔCSA (non-dimensional) Case 1 Fistula at Day 3

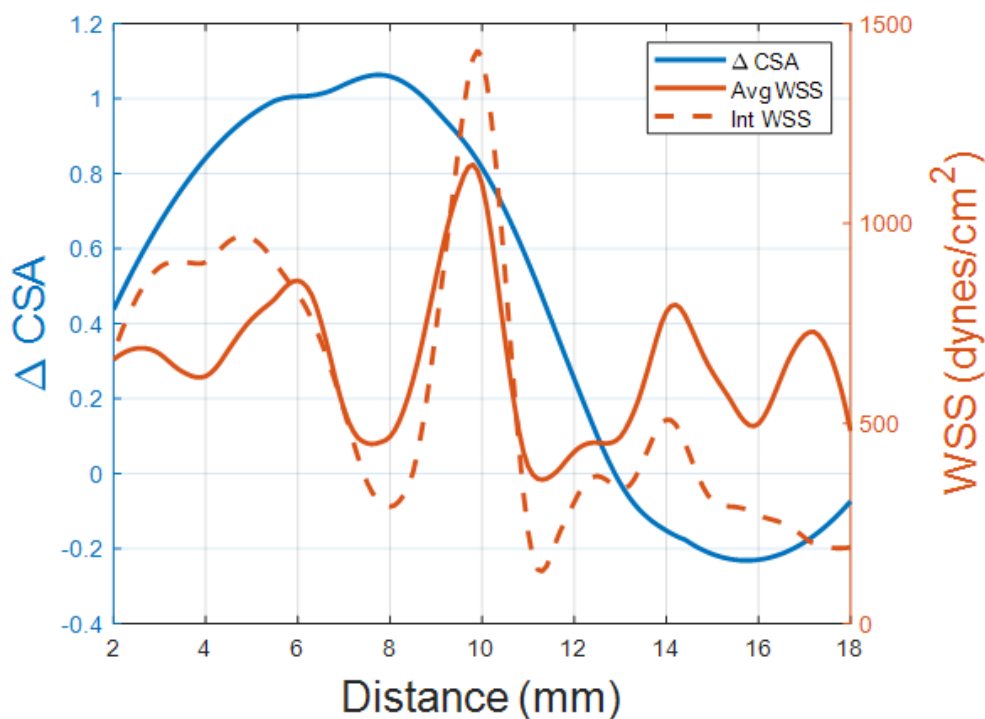


Figure A.11 WSS ($\frac{\text{dynes}}{\text{cm}^2}$) vs ΔCSA (non-dimensional) Case 1 Fistula at Day 3

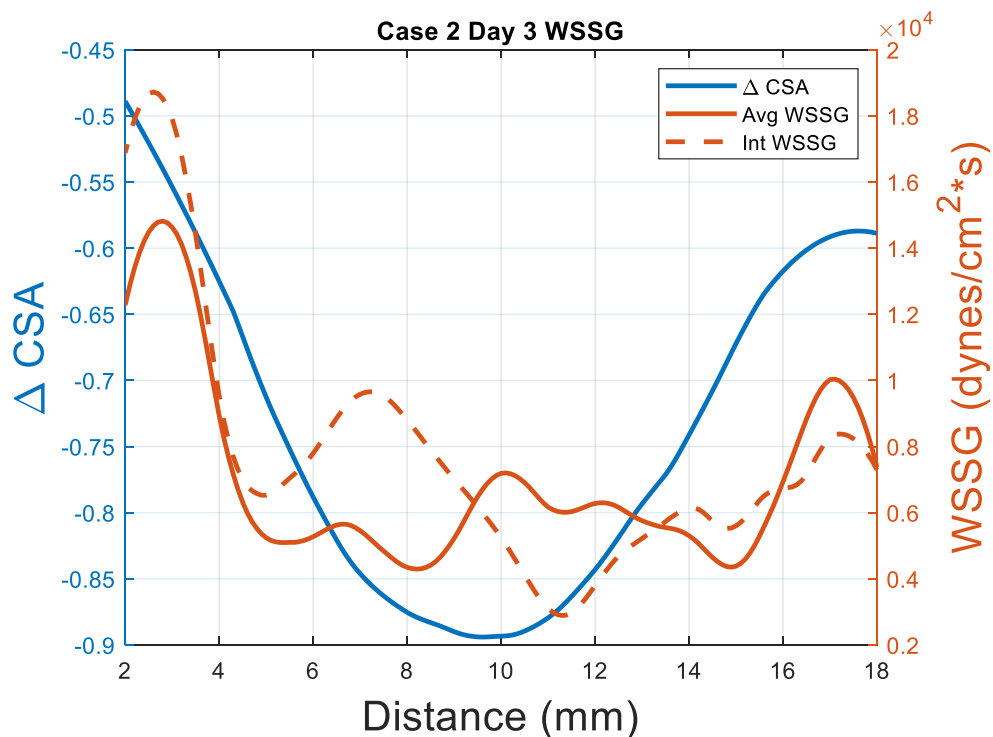


Figure A.12 WSSG ($\frac{\text{dynes}}{\text{cm}^3}$) vs ΔCSA (non-dimensional) Case 2 Fistula at Day 3

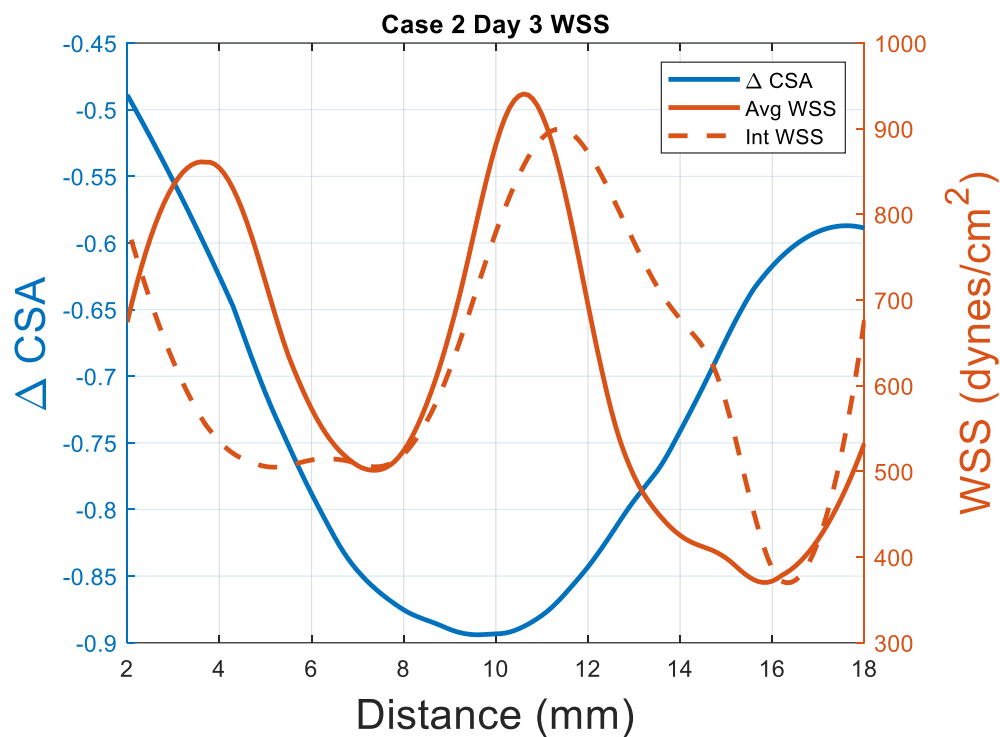


Figure A.13 WSSG ($\frac{\text{dynes}}{\text{cm}^2}$) vs ΔCSA (non-dimensional) Case 2 Fistula at Day 3

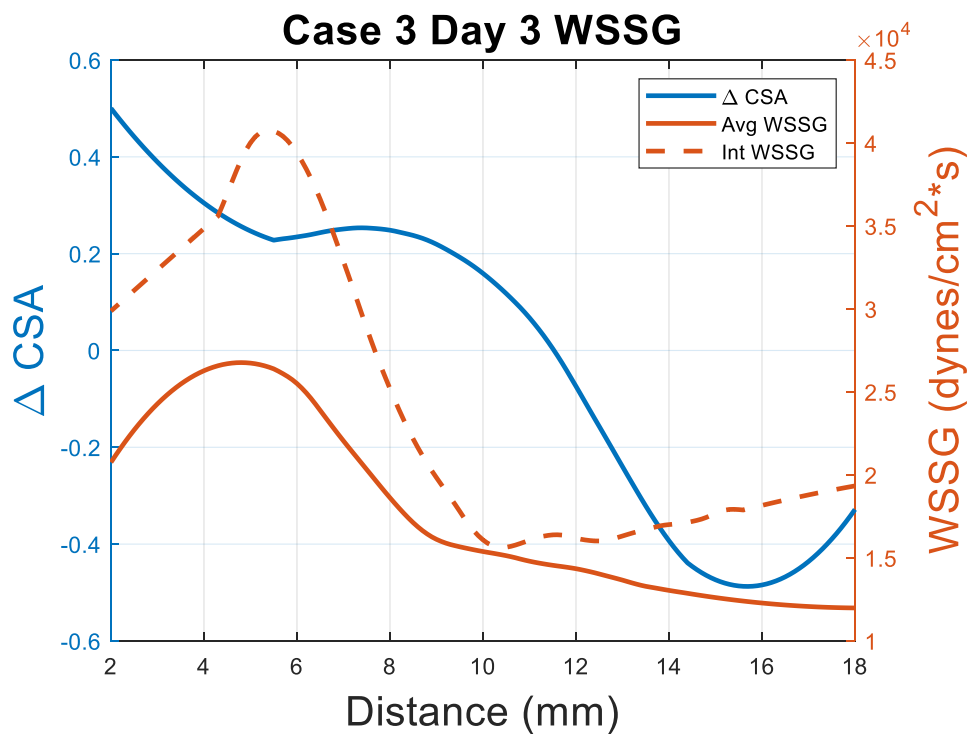
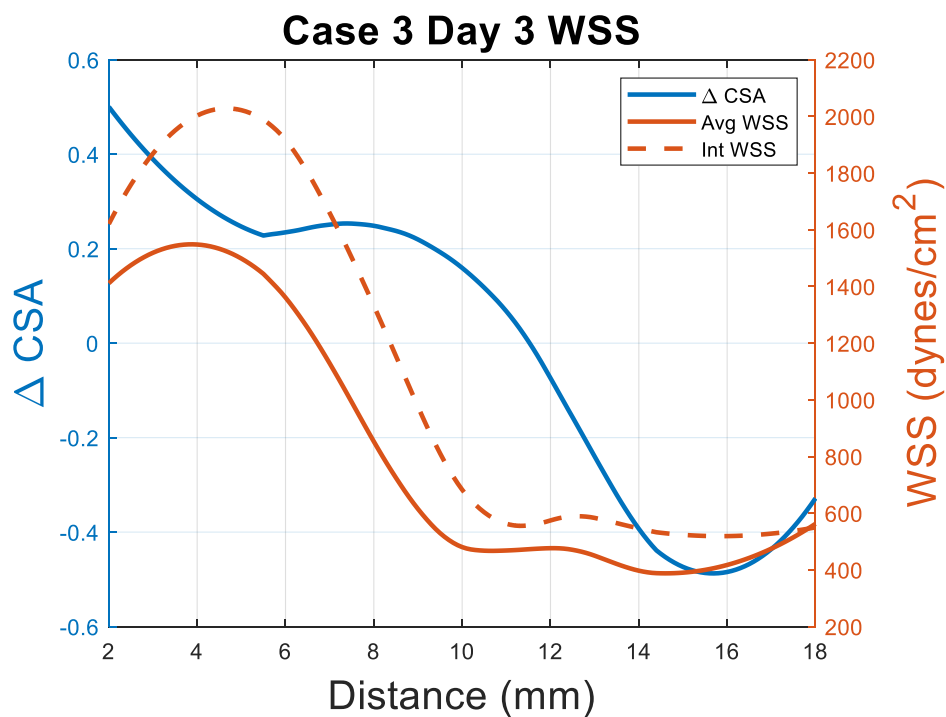
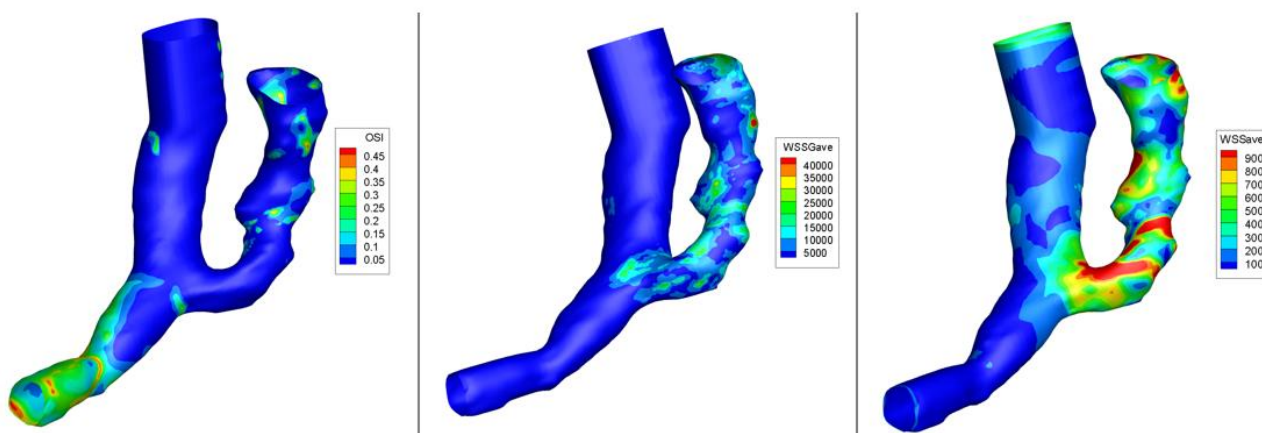
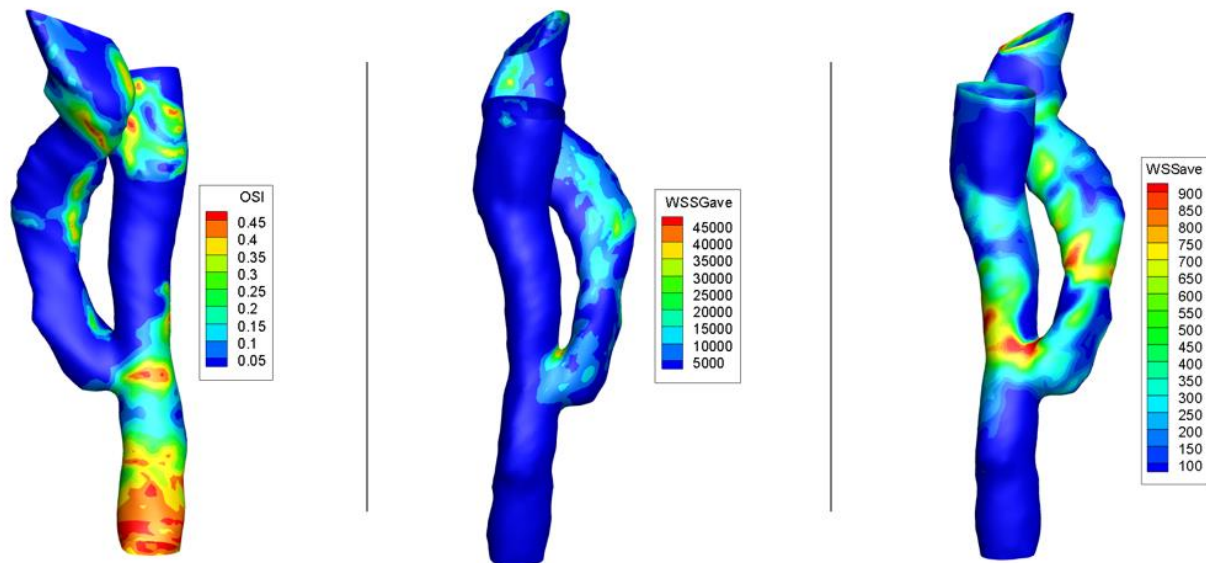
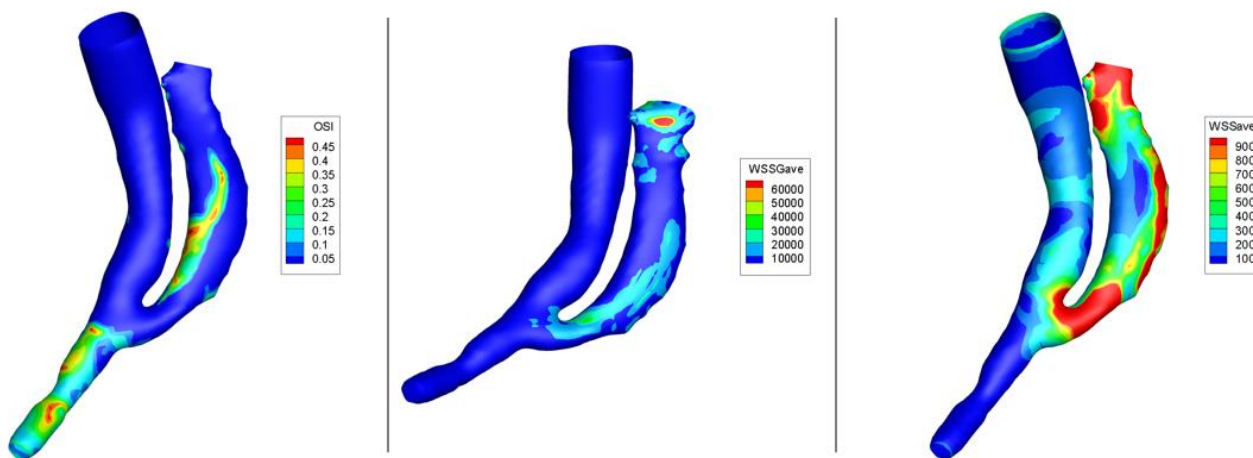


Figure A.14 WSSG ($\frac{\text{dynes}}{\text{cm}^3}$) vs ΔCSA Case 3 Fistula at Day 3Figure A.15 WSS vs ΔCSA Case 3 Fistula at Day 3A.16 Larger View of Case 1 Fistula. OSI is non-dimensional, WSS ($\frac{\text{dynes}}{\text{cm}^2}$), WSSG ($\frac{\text{dynes}}{\text{cm}^3}$).

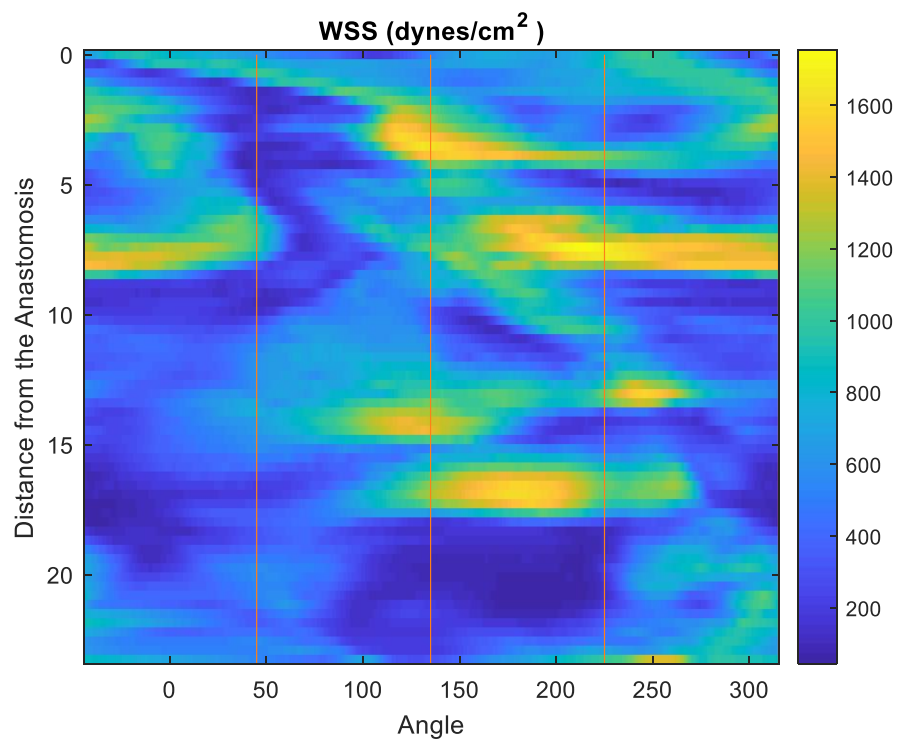


A.17 Larger View of Case 2 Fistula. OSI is non-dimensional, WSS ($\frac{\text{dynes}}{\text{cm}^2}$), WSSG ($\frac{\text{dynes}}{\text{cm}^3}$).

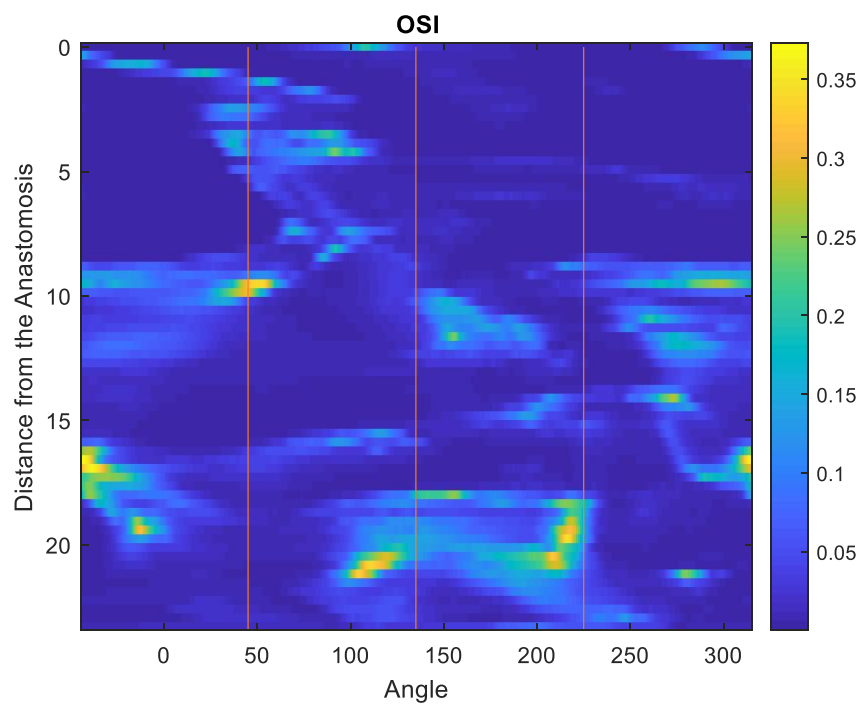


A.18 Larger View of Case 3 Fistula Hemodynamic Parameters. OSI is non-dimensional, WSS ($\frac{\text{dynes}}{\text{cm}^2}$),

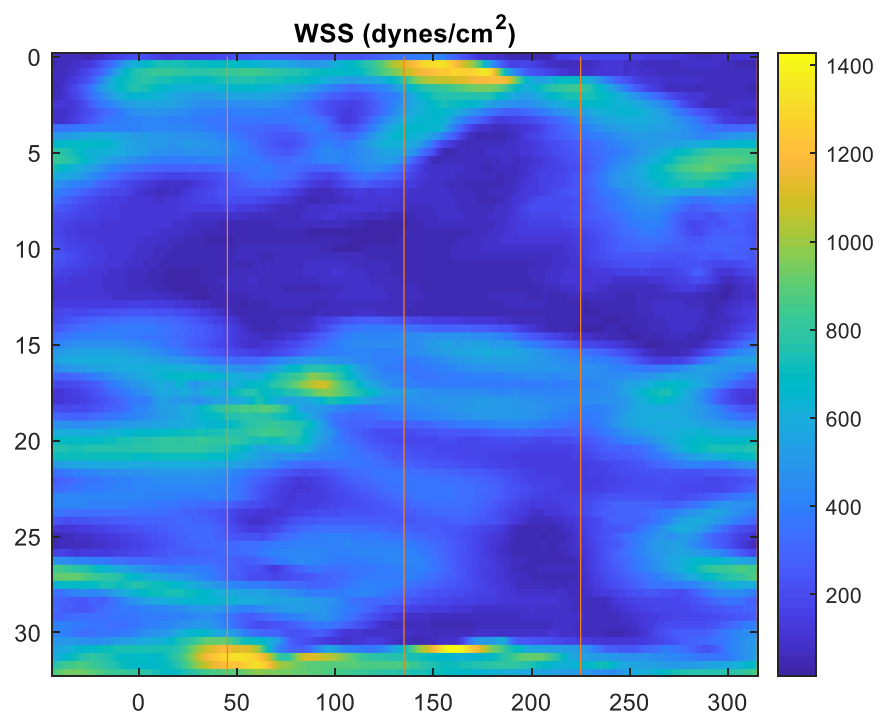
WSSG ($\frac{\text{dynes}}{\text{cm}^3}$).



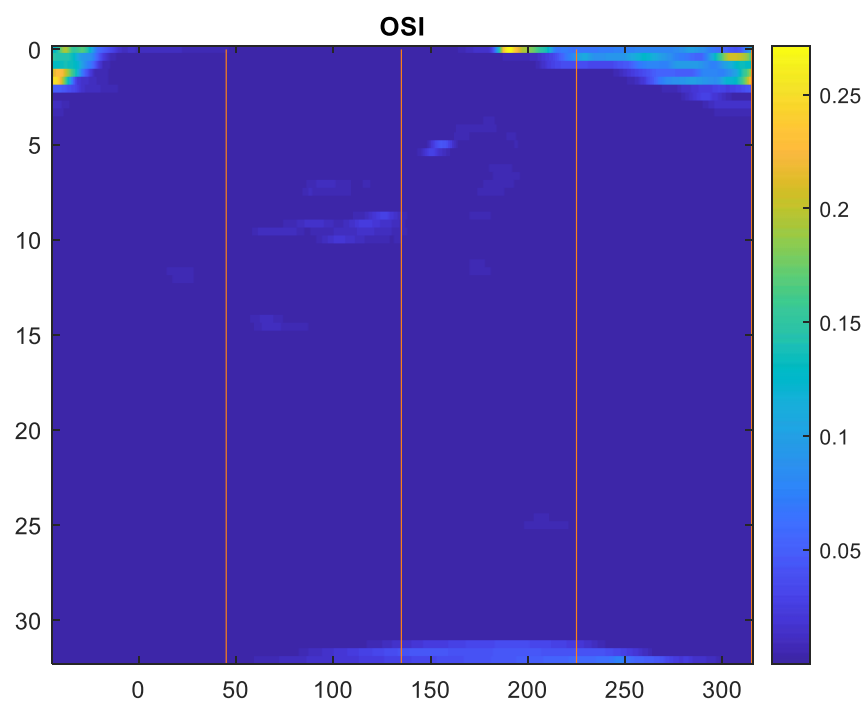
A.19 Case 1 Day 3 WSS Heatmap



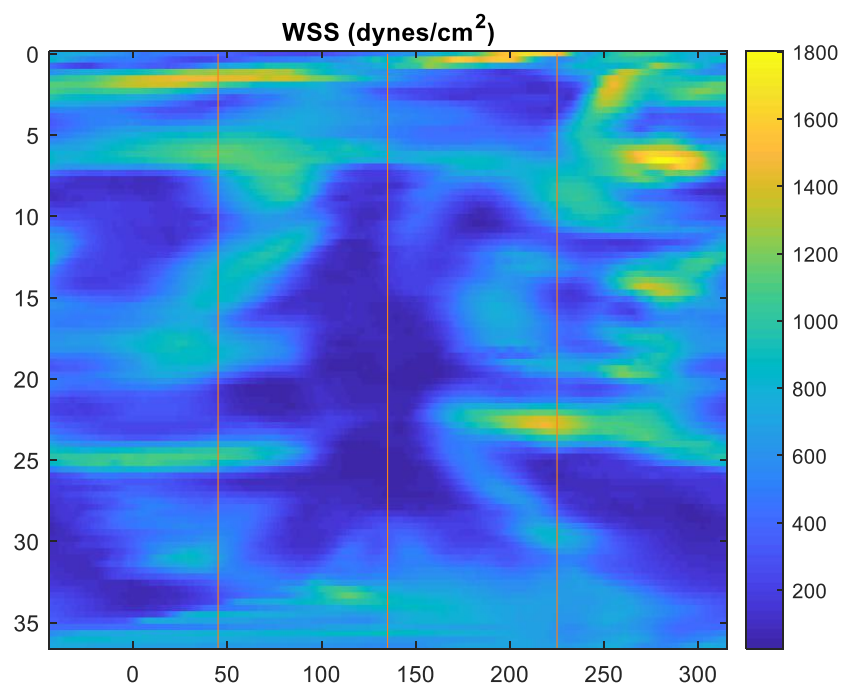
A.20 Case 1 Day 3 OSI Heatmap



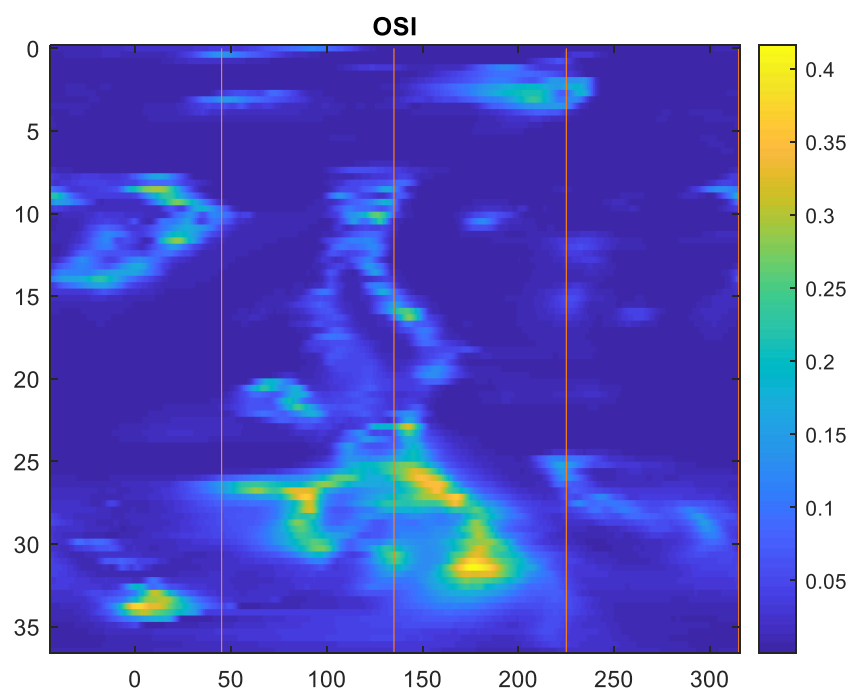
A.21 Case 1 Day 28 WSS Heatmap



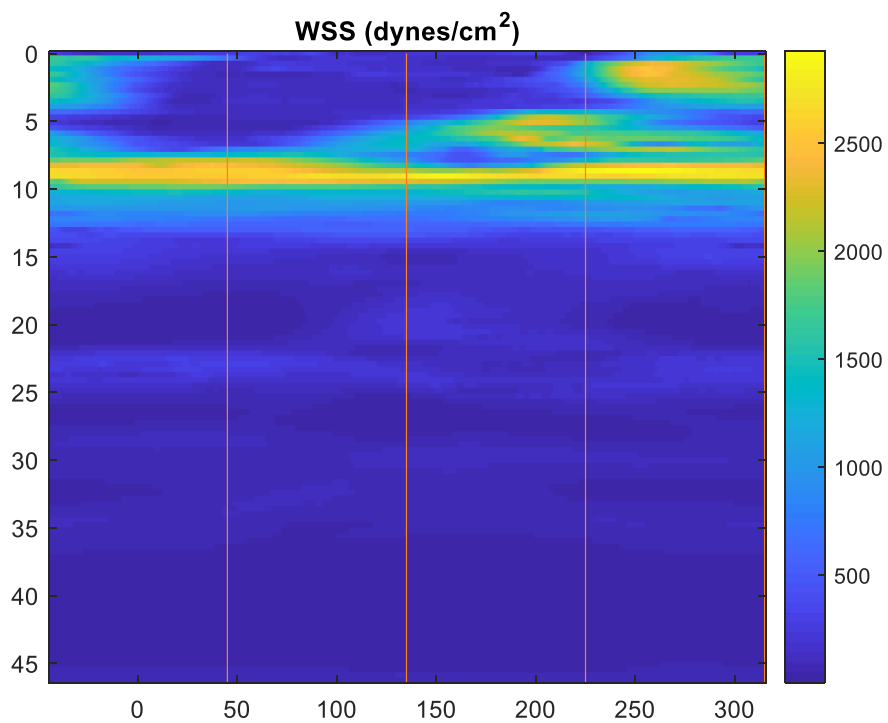
A.22 Case 1 Day 28 OSI Heatmap



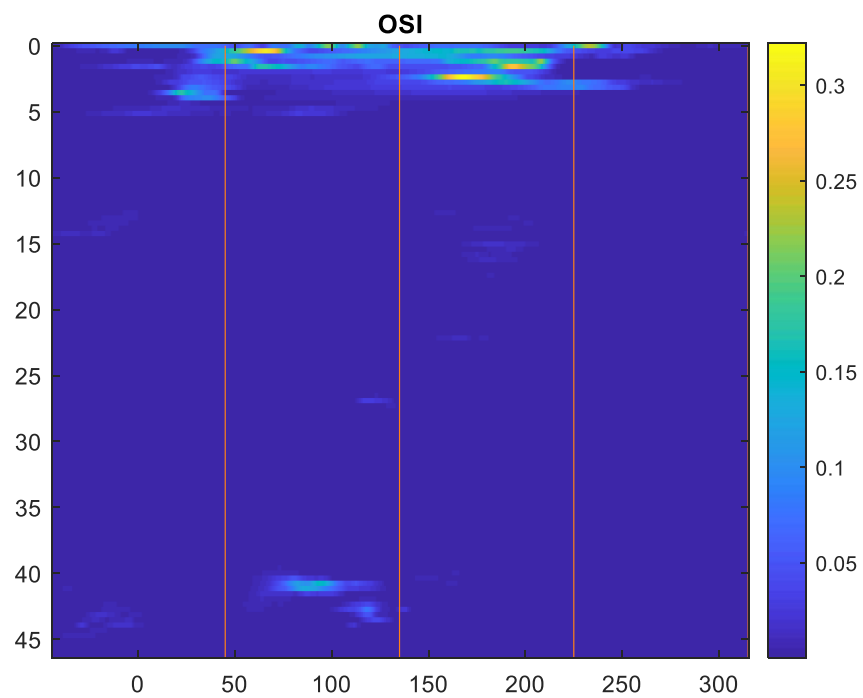
A.23 Case 2 Day 3 WSS Heatmap



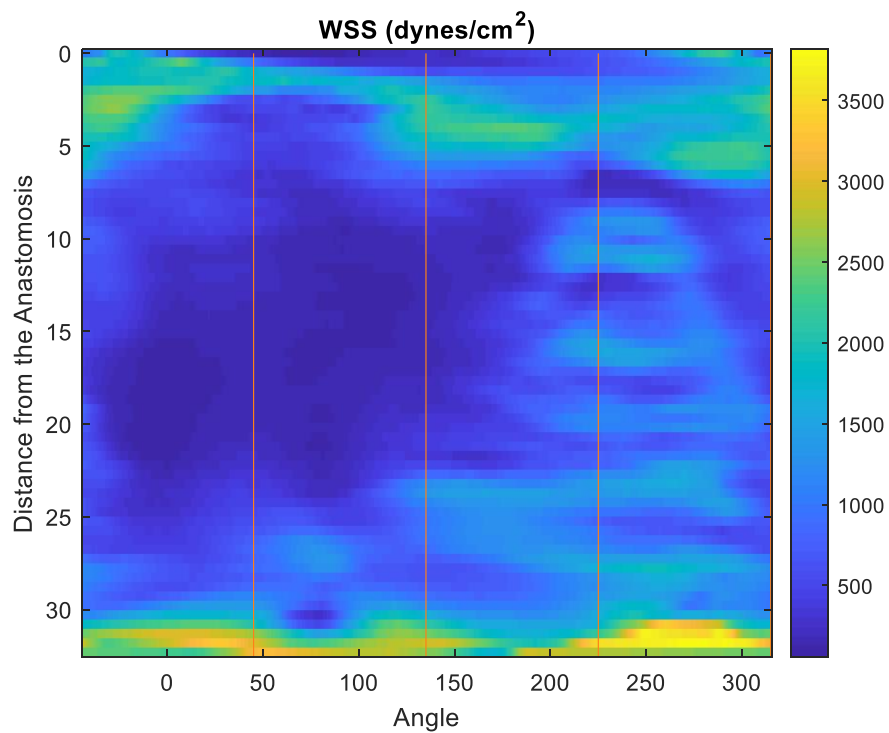
A.24 Case 2 Day 3 OSI Heatmap



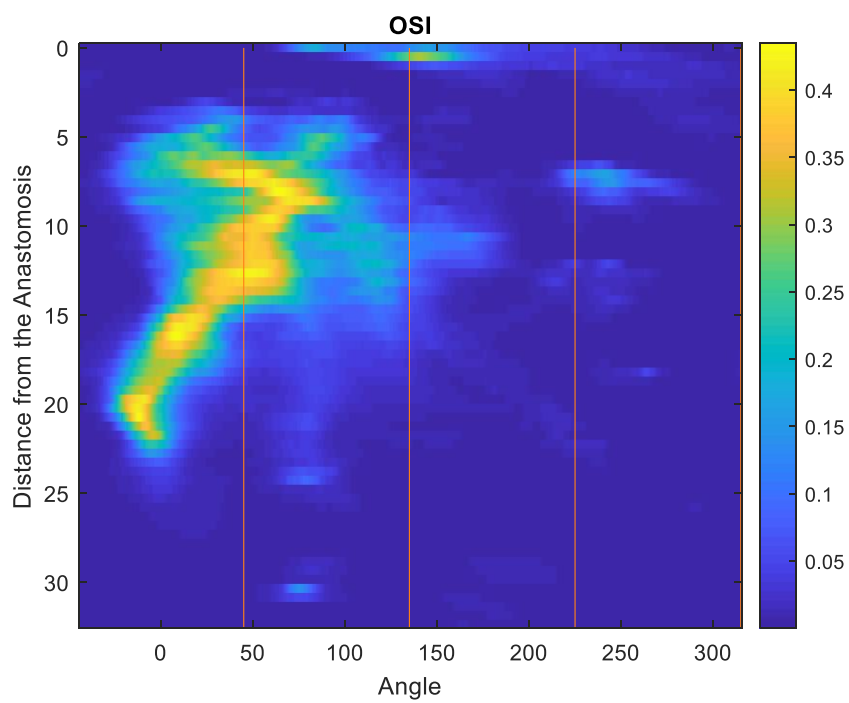
A.25 Case 2 Day 28 WSS Heatmap



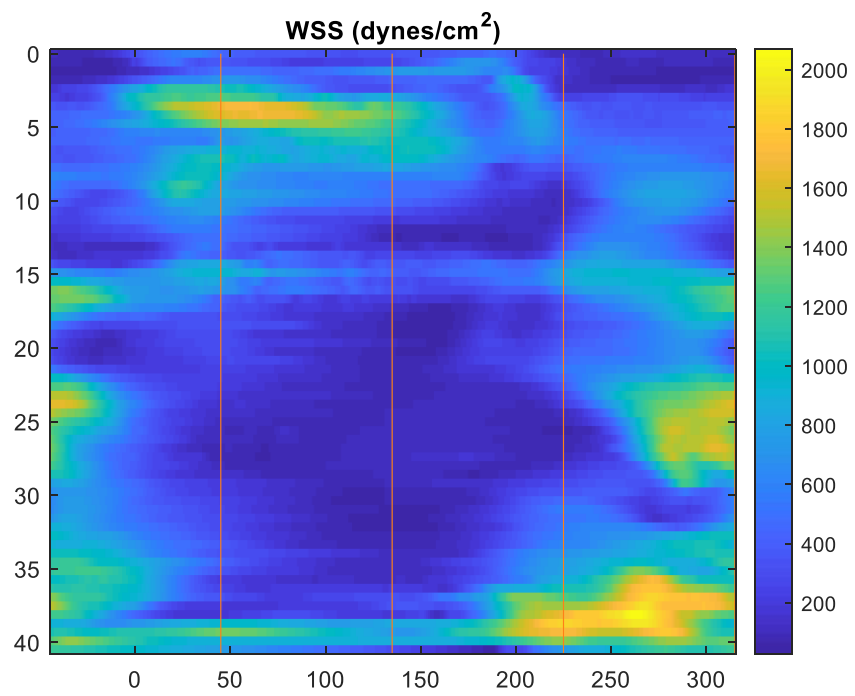
A.26 Case 2 Day 28 OSI Heatmap



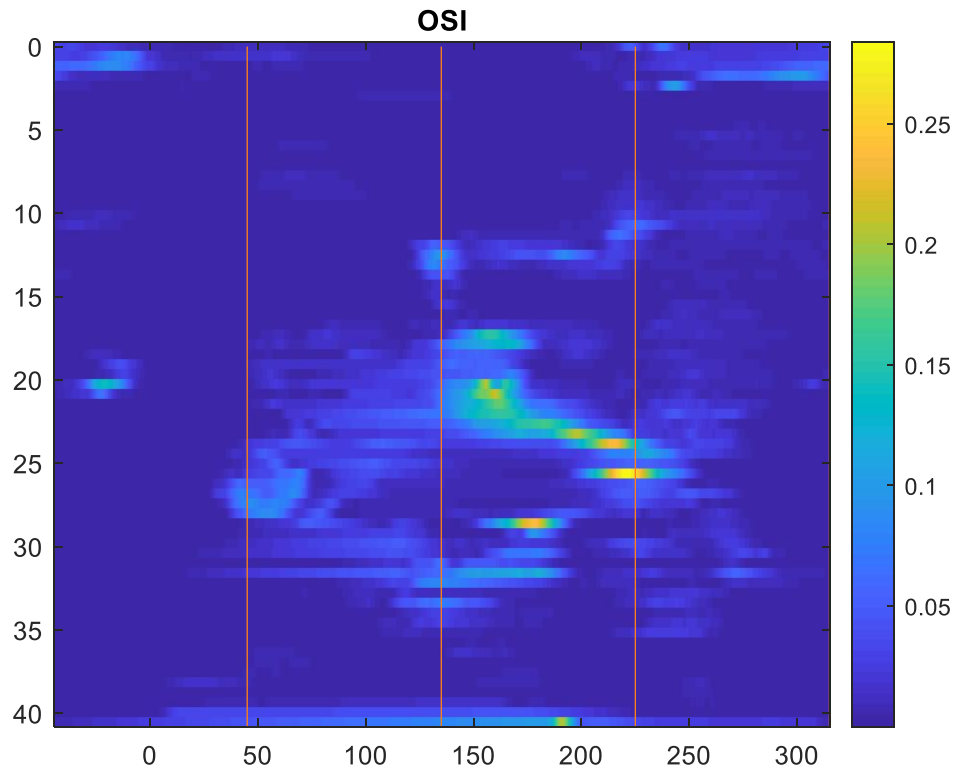
A.27 Case 3 Day 3 WSS Heatmap



A.28 Case 3 Day 3 OSI Heatmap



A.29 Case 3 Day 28 WSS Heatmap



A.30 Case 3 Day 28 OSI Heatmap

6. References

1. McCarley P, Wingard RL, Shyr Y *et al.* Vascular access blood flow monitoring reduced access morbidity and costs. *Kidney Int* 2001; 60: 1164-1172.
2. Allon M, Daugirdas J, Depner TA *et al.* Effect of change in vascular access on patient mortality in hemodialysis patients. *Am J Kidney Dis* 2006; 47: 469-477.
3. Pisoni RL, Arrington CJ, Albert JM *et al.* Facility hemodialysis vascular access use and mortality in countries participating in DOPPS: an instrumental variable analysis. *Am J Kidney Dis* 2009; 53: 475-491.
4. Krishanmoorthy MK, Banerjee RK, Wang Y *et al.* Anatomic configuration affects the flow rate and diameter of porcine arteriovenous fistulae. *Int Soc Nephrol* 2012; 81: 745-750.
5. Lee T, Allon M. Reassessing recommendations for choice of vascular access. *Clin J Am Soc Nephrol* 2017; 12: 865-867.
6. Dember LM, Beck GJ, Allon M *et al.* Effect of clopidogrel on early failure of arteriovenous fistulas for hemodialysis: a randomized controlled trial. *JAMA* 2008; 299: 2164-2171.
7. Dixon BS, Beck GJ, Vazquez MA, Greenberg A, Delmez JA, Allon M, Dember LM, Himmelfarb J, Gassman JJ, Greene T, Radeva MK. Effect of dipyridamole plus aspirin on hemodialysis graft patency. *New England Journal of Medicine*. 2009;360(21):2191-201.
8. Allon M, Imrey PB, Cheung AK, Radeva M, Alpers CE, Beck GJ, Dember LM, Farber A, Greene T, Himmelfarb J, Huber TS. Relationships between clinical processes and arteriovenous fistula cannulation and maturation: a multicenter prospective cohort study. *American Journal of Kidney Diseases*. 2018;71(5):677-89.
9. Woodside KJ, Bell S, Mukhopadhyay P, Repeck KJ, Robinson IT, Eckard AR, Dasmunshi S, Plattner BW, Pearson J, Schaubel DE, Pisoni RL. Arteriovenous fistula maturation in prevalent hemodialysis patients in the United States: a national study. *American Journal of Kidney Diseases*. 2018;71(6):793-801.
10. Roy-Chaudhury P, Arend L, Zhang J *et al.* Hemodialysis vascular access dysfunction: a cellular and molecular viewpoint. *J Am Soc Nephrol* 2006; 17: 1112-1127.
11. Lauvao LS, Ihnat DM, Goshima KR *et al.* Vein diameter is the major predictor of fistula maturation. *J Vasc Surg* 2009; 49: 1499-1504.
12. Migliavacca, F., & Dubini, G. (2005). Computational modeling of vascular anastomoses. *Biomechanics and modeling in mechanobiology*, 3(4), 235-250.
13. Carroll, J., Varcoe, R. L., Barber, T., & Simmons, A. (2019). Reduction in anastomotic flow disturbance within a modified end-to-side arteriovenous fistula configuration: Results of a computational flow dynamic model. *Nephrology*, 24(2), 245-251.
14. He, Y., Northrup, H., Roy-Chaudhury, P., Cheung, A. K., Berceci, S. A., & Shiu, Y. T. (2020). Analyses of hemodialysis arteriovenous fistula geometric configuration and its associations with maturation and reintervention. *Journal of Vascular Surgery*.
15. Gameiro, J., & Ibeas, J. (2020). Factors affecting arteriovenous fistula dysfunction: a narrative review. *The Journal of Vascular Access*, 21(2), 134-147.
16. Lawson, J. H., Niklason, L. E., & Roy-Chaudhury, P. (2020). Challenges and novel therapies for vascular access in haemodialysis. *Nature Reviews Nephrology*, 16(10), 586-602.
17. Cheung AK, Imrey PB, Alpers CE *et al.* Intimal hyperplasia, stenosis, and arteriovenous fistula maturation failure in the hemodialysis fistula maturation study. *J Am Soc Nephrol (JASN)* 2017; 28:3005-3013.
18. Updegrove A, Wilson NM, Merkow J *et al.* SimVascular: an open source pipeline for cardiovascular simulation. *Ann Biomed Eng* 2017; 45: 525-541

19. Arthurs C. J., Khlebnikov R., Melville A., Marčan M., Gomez A., Dillon-Murphy D., ... & Figueroa C. A., CRIMSON: An open-source software framework for cardiovascular integrated modelling and simulation. *PLOS Computational Biology*, 20221, 17(5), e1008881.
20. Bozzetto M, Brambilla P, Rota S *et al.* Toward longitudinal studies of hemodynamically induced vessel wall remodeling. *ESAO* 2018; 41: 714-722.
21. Haneder S, Kucharczyk W, Schoenberg SO *et al.* Safety of magnetic resonance contrast media: a review with special focus on nephrogenic systemic fibrosis. *Top Magn Reson Imag* 2015; 24: 57-65.
22. van Andel CJ, Pisteky PV, Borst C. Mechanical properties of porcine and human arteries: implications for coronary anastomotic connectors. *Ann Thorac Surg* 2003; 76: 58-65.
23. Kelly BS, Heffelfinger SC, Whiting JF *et al.* Aggressive venous neointimal hyperplasia in a pig model of arteriovenous graft stenosis, *Kidney Int* 2002; 62: 2272-2280.
24. Heldman AW, Cheng L, Jenkins M, *et al.* Paclitaxel stent coating inhibits neointimal hyperplasia at 4 weeks in a porcine model of coronary restenosis. *Circ* 2001; 103: 2289-2295.
25. Wang Y, Krishnamoorthy M, Banerjee R, Zhang J, Rudich S, Holland C, Arend L, Roy-Chaudhury P. Venous stenosis in a pig arteriovenous fistula model—anatomy, mechanisms and cellular phenotypes. *Nephrology Dialysis Transplantation*. 2008;23(2):525-33.
26. Breuer FA, Blaimer M, Heidemann RB *et al.* Controlled aliasing in parallel imaging results in higher acceleration (CAIPIRINHA) for multi-slice imaging. *Magn Res Med* 2005; 53: 684-691.
27. Rosado-Toro JA, Abidov A, Altbach MI, *et al.* Segmentation of the right ventricle in four chamber cine cardiac MR images using polar dynamic programming. *Comp Med Imag Graph* 2017; 62: 15-25.
28. Rosado-Toro JA, Altbach MI, Rodríguez JJ. Dynamic programming using polar variance for image segmentation. *IEEE Trans Imag Proc (TIP)* 2016; 25: 5857-5866.
29. Desbrun M, Meyer M, Schröder P *et al.* Implicit fairing of irregular meshes using diffusion and curvature flow. *Proc 26th Annual Conf Comput Graph Interact Techn* 1999; 317-324.
30. Sethian JA. A fast-marching level set method for monotonically advancing fronts. *Proc Nat Acad Sci* 1996; 93: 1591-1595.
31. Peyré G. The numerical tours of signal processing. *IEEE Comput Sci Eng* 2011; 13: 94-97.
32. http://nipy.org/nibabel/dicom/dicom_orientation.html
33. Weisstein EW, Point-plane distance. From MathWorld—A Wolfram Web Resource. <http://mathworld.wolfram.com/Point-PlaneDistance.html>.
34. Desbrun M, Meyer M, Schröder P *et al.* Implicit fairing of irregular meshes using diffusion and curvature flow. *Proc 26th Annual Conf Comput Graph Interact Techn* 1999; 317-324.
35. Rosado-Toro JA, Altbach MI, Rodríguez JJ. Dynamic programming using polar variance for image segmentation. *IEEE Trans Imag Proc (TIP)* 2016; 25: 5857-5866.
36. Soille, P. Morphological image analysis: principles and applications, Springer-Verlag, 1999, pp. 173-174.
37. Krishnamoorthy M, Banerjee R, Wang Y *et al.* Hemodynamics wall shear stress profiles influence the magnitude and pattern of stenosis in a pig AV fistula. *Int Soc Nephrol* 2008; 74:1410-1419.
38. Lopes-Berkas V, Jorgenson M. Measurement of peripheral arterial vasculature in domestic Yorkshire swine by using quantitative vascular angiography. *J Am Assoc Lab Animal Science (JAALAS)* 2011; 50:629.
39. Pike D., Shiu, Y. T., Somarathna, M., Guo L., Isayeva T., Totenhagen J., & Lee T. High resolution hemodynamic profiling of murine arteriovenous fistula using magnetic resonance imaging and computational fluid dynamics. *Theoretical Biology and Medical Modelling*, 2017; 14(1), 1-17.

40. Fitts M., Pike D., Anderson K., Shiu Y. Hemodynamic Shear Stress and Endothelial Dysfunction in Hemodialysis Access. *Open Urol Nephrol J.* 2014; 7(Supple 1 M5): 33-44.
41. Prouse G., Stella S., Vergara., Quarteroni A., Engelbergr S., Canevascini R., Giovannacci L, Computational Analysis of Turbulent Hemodynamics in Radiocephalic Arteriovenous Fistulas to Determine the Best Anastomotic Angles. *Annals of Vascular Surgery.* 2020; 68: 451-459.
42. Hull J., Balakin B., Kellerman B., Wrolstad D. Computational fluid dynamic evaluation of the side-to-side anastomosis for arteriovenous fistula. *Journal of Vascular Surgery.* 2013; 58: 187-193.
43. Papachristou E., Vasquez-Paldrón R. From basic anatomic configuration to maturation success. *Kidney International.* 2012; 81: 724-726.
44. Mayo Clinic. (2021, Aug.). Hemodialysis. [Online]. Available: <https://www.mayoclinic.org/tests-procedures/hemodialysis/about/pac-20384824>
45. Rosado-Toro J., Philip R., Dunn S., Celdran-Bonafonte D., He Y., Berceli S., Roy-Chaudhury P., Tubaldi E. Functional analysis of arteriovenous fistulae in non-contrast magnetic resonance images. *Computer Methods and Programs in Biomedicine.* 2022; 222, 106938.
46. Krishnamoorthy M., Banerjee R., Wang Y., Zhang J., Roy A., Khoury S., Arend L., Rudich S., Roy-Chaudhury P. Hemodynamic wall shear stress profiles influence the magnitude and pattern of stenosis in a pig AV fistula. *International Society of Nephrology.* 2008; 74, 1410-1419.
47. Formaggia L., Quarteroni A., Veneziani A. Cardiovascular Mathematics: Modeling and Simulation of the Circulatory System. Springer-Verlag Italia, Milano: Springer Science & Business Media, 2010.
48. Stella S., Vergara C., Giovannacci L., Quarteroni A., Prouse G. Assessing the Disturbed Flow and the Transition to Turbulence in the Arteriovenous Fistula. *Journal of Biomechanical Engineering.* 2019; 141:10101.
49. Mayo Clinic. (2021, Oct.). Hemodialysis. [Online]. Available <https://www.mayoclinic.org/diseases-conditions/end-stage-renal-disease/symptoms-causes/syc-20354532>
50. Reneman R., Hoeks A. Wall shear stress as measured in vivo: consequences for the design of the arterial system. *Med Biol Eng Comput.* 2008; 46:499-5077.
51. Colley E., Simmons A., Varcoe R., Thomas S., Barber T. Arteriovenous fistula maturation and the influence of fluid dynamics. *Engineering in Medicine.* 2020; 234:1197-1208.
52. Allon, M. Dialysis catheter-related bacteremia: treatment and prophylaxis. *Am. J. Kidney Dis.* 44: 779–791 (2004).
53. Rajabi-Jagahrg E., Krishnamoorthy M., Roy-Chaudhury P., Succop P., Wang Y., Choe A., Banerjee R. Longitudinal Assessment of Hemodynamic Endpoints in Prediction Arteriovenous Fistula Maturation. *Seminars in Dialysis.* 2012.
54. Cleveland Clinic. (2022, Apr). [Online]. <https://my.clevelandclinic.org/health/articles/17060-how-does-the-blood-flow-through-your-heart>
55. Guggenberger K., Krafft A., Ludwig U., Vogel P., Elsheik S., Raithel E., Forman C., Dovi-Akue P., Urbach H., Bley T., Meckel S. High-resolution Compressed-sensing T1 Black-blood MRI. *Clinical Neurology.* 2021; 31:207-216
56. He Y., Terry C., Nguyen C., Berceli S., Shiu Y., Cheung A. Serial analysis of lumen geometry and hemodynamics in human arteriovenous fistula for hemodialysis using magnetic resonance imaging and computational fluid dynamics. *Journal of Biomechanics.* 2012